Deanship of Graduate Studies

Al-Quds University

Spectroscopic Investigations of Anesthetic Drugs (Pentobarbital and Propofol) Interaction with Human Serum Albumin

Sawsan Eid Hamed Abu sharkh

M.Sc. Thesis

Jerusalem - Palestine

1431 / 2010

Spectroscopic Investigations of Anesthetic Drugs (Pentobarbital and Propofol) Interaction with Human Serum Albumin

Prepared by:
Sawsan Eid Hamed Abu sharkh

B.Sc. Physics, Al-Quds University, Palestine

Supervisor: Dr. Saker Darwish
Co-supervisor: Prof. Mahmoud Abu hadid

"A thesis Submitted to the Faculty of Science and Technology, Al-Quds University in Partial Fulfillment of the Requirements for the Degree of Master of Science in Physics"

1431 / 2010

Al-Quds University
Deanship of Graduate Studies
Physics Department

Thesis Approval

Spectroscopic Investigations of Anesthetic Drugs (Pentobarbital and Propofol) Interaction with Human Serum Albumin

Prepared by: Sawsan Eid Hamed Abu Sharkh
Registration No.: 20714236

Supervisor: Dr. Saker Darwish
Prof. Mahmoud Abu hadid

Master thesis submitted and accepted, Date: / / 2010
The names and signatures of the examining committee members are as follows:

1-Head of Committee: …….. Signature ……

2-Internal Examiner: …… . Signature……

3-External Examiner: …… Signature ……

4-Committee member: …….. Signature…….

Jerusalem – Palestine

1431 / 2010

Dedication

I dedicate this thesis to all of my wonderful family members who have supported me throughout my life and allowed me to achieve my goals: to my father Eid, who helped in making my educational decisions and sent me on the path to my graduate career; to my mother Riad; who raised me to be the person I am today, she has been with me on every step of the way, through good times and bad. Thank you for all the unconditional love, guidance, and support that you have always given me, helping me to succeed and instilling in me the confidence that I am capable of doing anything I put my mind to, to my husband Sami for his encouragement and support; to my supporting brothers; to my nice sisters; to my daughter Rawand who gave me more reasons to succeed; and to any future child…I just don't know who you are yet. Thank you for everything. I love you!

Sawsan Eid Hammed Abu sharkh

Declaration:

I certify that this thesis submitted for the degree of master is the result of my own research, except where otherwise acknowledged, and that this thesis (or any part of the same) has not been submitted for a higher degree to any other university or institution.

Signed: _____

Sawsan Eid Hamed Abu sharkh

Date: / / 2010

Acknowledgements

At first and at last; my great commendation and thanks to Allah, who gave me the ability to accomplish this work, and created such nice supporting people.

I would like to thank all those people who deserve my gratitude and made this thesis possible and an enjoyable experience for me.

First of all, I wish to express my sincere gratitude to my supervisor Dr. Saqer Darwish not only for the support he gave me during my research, but most of all for providing the ability to work in a stimulating environment eager of discovery and continuous learning. He has instilled good scientific values by being a leading example and an excellent teacher for his pastoral heart, wisdom, patience, encouragement, positive criticism and assistance in bringing this work to completion. You patiently guided me towards an interesting and workable project. Your experience, your insight, and your openness to my ideas made the pages that follow possible. I will strive with my future students to be the kind of supervisor that you have been to me. I sincerely thank you.

I gratefully acknowledge Prof. Mahmoud Abu hadid my co supervisor for his interest in this work and for providing many details and valuable comments. I convey special acknowledgement to my best teacher Dr. Musa Abu Teir, he has been a source of motivation and strength during moments of despair and discouragement. Also I would like to express my deepest gratitude to Dr. Mukhles sowwan who contributed to the success of this work.

Special thanks to my dear husband who has unwavering encouragement, kindness, incorporeal support to me and to be with me in achieving my dream of obtaining a master degree. Where would I be without my family? My parents deserve special mention for their inseparable support and prayers. My father, in the first place is the person who put the fundament my learning character, showing me the joy of intellectual pursuit ever since I was a child. My mother, is the one who sincerely raised me with her caring and gently love. Thank you.

ABSTRACT

The interaction of anesthetic drugs pentobarbital and propofol with HSA has been investigated by using UV-absorption, fluorescence spectroscopy, and Fourier transform infrared (FTIR) spectroscopy. The binding constants of pentobarbital and Propofol have been determined by both UV- absorption, and fluorescence spectroscopy. The values of the binding constants calculated at 293k are 1.812×10^{4} M^{-1} for pentobarbital and $2.55x10^{3}$ M^{-1} for propofol. The Stern–Volmer quenching constant values were found to be 3.875×10^{7} $L.mol^{-1}$ pentobarbital and $9.686x10^{6}$ L mol^{-1} propofol. The UV-absorption intensity of HSA-drug complexes has increased with increasing of pentobarbital and propofol concentration.

The fluorescence data reveals a decrease in HSA-drug emission intensity with the increase of pentobarbital and propofol concentration. This decrease of intensity indicates that both of pentobarbital and propofol have a strong ability to quench the intrinsic fluorescence of HSA through a static quenching mechanism.

FTIR spectroscopy with Fourier self-deconvolution technique and second derivative resolution enhancement, as well as curve-fitting procedures were applied in the analysis of the amide I,II, and III regions to determine the effects on protein secondary structure and drug binding mechanisms. All peak positions in the three amide regions (amid I, amide II and amide III) have been assigned and any effects due to concentration changes have been investigated. The FTIR spectra measurements indicate a change in the intensity of absorption bands due to change in the drug concentrations. In addition, a larger intensity decrease in the absorption band of the α-helix relative to that of β-sheets has been observed. This variation in intensity is related indirectly to the formation of H-bonding in the drug HSA complexes, which accounts for the different intrinsic propensities of α-helix and β-sheets in HSA.

It was found that the (carbonyl groups and N-H groups) and the hydroxyl group which are substituted on aromatic ring of pentobarbital and propofol respectively play an important role in the protein's secondary structure changes. The analysis supports that propofol with the lower binding constant has a faster sedation time than pentobarbital.

Table of contents

List of tables

List of figures

List of abbreviations:

Symbol	Abbreviation representation
HSA	Human Serum Albumin
UV	Ultraviolet
FTIR	Fourier transform infrared
CNS	Central nervous system
FDA	Food and drug administration
Trp	Tryptophan
CD	Circular dichroism
NMR	Nuclear magnetic resonance
Tyr	Tyrosine
Phe	Phenylalanine
nm	Nanometer
KDa	Kilodalton
LED's	Light emitting diodes
DTGS	Deuterated triglycine sulfate
MCT	Mercury cadmium telluride

List of symbols:

Symbol	description
E_{total}	Total energy of a molecule
E_{tran}	Translational energy
E_{rot}	Rotational energy
E_{vib}	Vibrational energy
E_{el}	Electronic energy
ν_i	vibrational frequency
V(r)	Potential energy
r	distance between the atoms
n_i	quantum number of the ith mode
E_v **(0, 0, 0…)**	zero point energy
E_v	Total vibrational energy
h	Plank's constant
ν_e	Harmonic frequency
T	Transmittance
A	Absorbance
I_0	intensity of the incident light
I	intensity of the transmitted light
K	force constant of the spring(Binding constant)
λ	wavelength
f **(t)**	radiant power
θ	Path difference (retardation)
$I(x)$	intensity for an ideal Michelson interferometer
$(\bar{\nu})$	wavenumber of the radiation in gas or vacuum
$I(\bar{\nu})$	intensity of the radiation
R	reflectance of the beam splitter
$A(\bar{\nu})$	spectral intensity
K_{sv}	Stern-Volmer quenching constant
k_q	Bimolecular quenching constant
τ_0	Unquenched lifetime
Q	Quencher concentration
ε	Beer's law molar absorptivity coefficient (or extinction coefficient)
b	Path length
C	Sample concentration
A_0	initial absorption of protein
A_∞	Final absorption of the ligated-protein
F_0	Fluorescence intensities without quencher
F	Fluorescence intensities with quencher

Chapter ONE

Introduction

Chapter one

INTRODUCTION

1.1 Pentobarbital

Pentobarbital is a short-acting barbiturate (Fig.1.1) that was first synthesized in 1928 (Donald, 2003). Pentobarbital was long used as anxiolytic and hypnotic (Whitlock, 1975). Barbiturates were substituted pyrimidine derivatives in which the basic structure common to these drugs is barbituric acid, a substance which has no central nervous system (CNS) activity, CNS activity is attained by substituting alkyl, alkenyl, or any groups on the pyrimidine ring. Barbiturates act as central nervous system depressant, and they produce a wide spectrum of effects, from mild sedation to anesthesia. Pentobarbital is approved for human uses by the FDA for seizure and preoperative sedation. Pentobarbital has a variety of effects, including motor impairments, in both humans and animals (Hetzer et al, 1999). Pentobarbital is capable of having a profound effect on brain function; it is known to depress cerebral glucose utilization and electrical activity(Hodes et al, 1985).

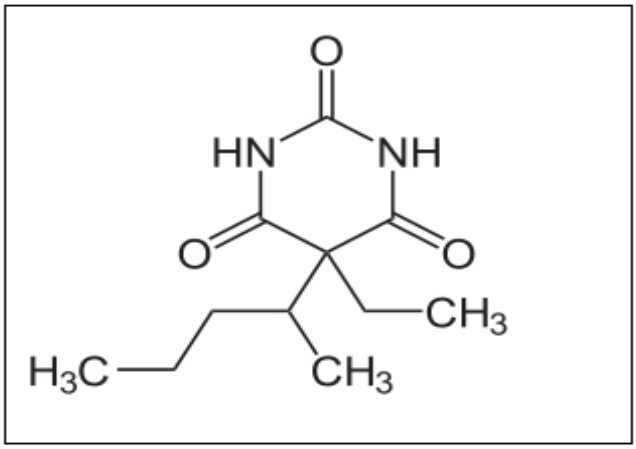

Figure 1.1: Chemical structure of pentobarbital.

1.2 Propofol

Propofol (2, 6-diisopropylphenol) is an ultra–short-acting, non barbiturate, sedative-hypnotic agent (Fig.1.2) (Edward Morgan et al, 1995) with an arm-brain circulation time of 90 to 100 seconds. It is administered as a bolus for the induction of anesthesia and as an infusion for maintenance of anesthesia or for sedation (Bryson et al, 1995). A rapid and complete recovery (Mandsager et al, 1995) is a major advantage of this drug, which is attributable to extensive biotransformation of the parent compound. It has rapid redistribution and clearance account for its brief sedation effect and the need for repeated boluses or continuous infusion to maintain the level of anesthesia and sedation (Smith et al, 1994; Fulton et al, 1995; Bryson et al, 1995). Propofol induces dose- dependent central nervous system depression (Hannallah et al, 1991). Also at subhypnotic doses, propofol induces sedation, amnesia, and antiemetic activity (Reves et al, 2000).

The rapid titrability, brief pharmacologic effect, and maintenance of spontaneous ventilation make intravenous propofol an ideal agent for deep sedation. It is preferred for the shorter-duration computed tomography studies (Pershad et al, 2006). This highly lipophylic drug crosses promptly the cellular membrane and takes about 2-4 minutes for establishing blood-brain balance, causing a rapid induction of anesthesia. It is metabolized in liver to form glucuronid and sulfate conjugates (Muñoz-Cuevas et al, 2005; Padrid, 2000; Schuttler et al, 2000).

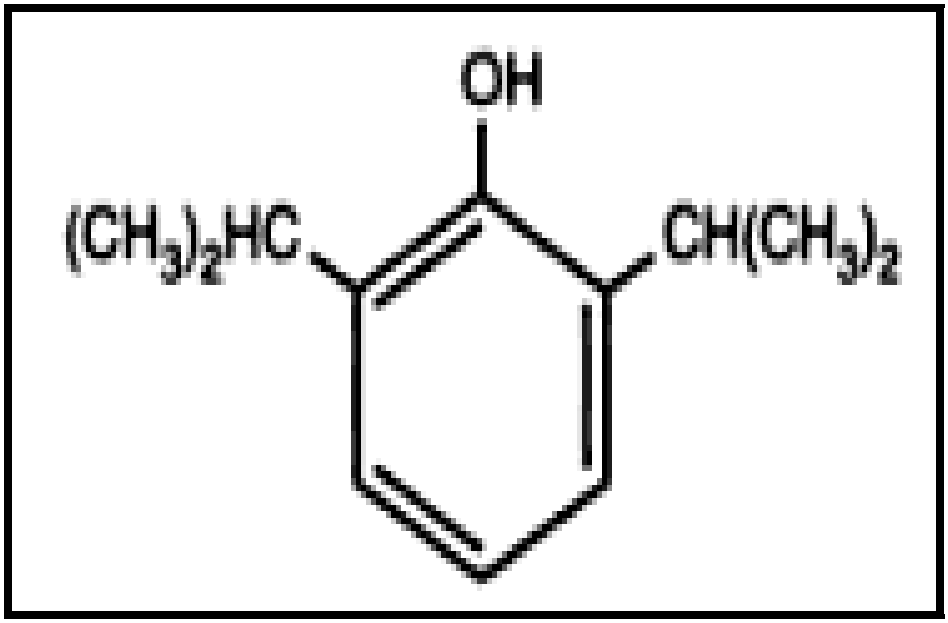

Figure 1.2: Chemical structure of propofol.

1.3 Human serum albumin (HSA)

HSA is the major circulating plasma protein, which is synthesized in the liver. It is present in all body fluids, for example its blood concentration is about 40 $mgmL^{-1}$ (~0.6 mmol L^{-1}) (Curry et al, 1998). HSA is a single-chain protein containing three albumin domains characterized by six disulfide bridges. The three dimensional structure of the entire serum albumin has 585 amino acids in complex with fatty acids. For example polyunsaturated arachidonic acid was determined by X-ray diffraction (Schaller et al, 2008). HSA consists of three homologous domains (labeled as I, II and III), each of which is divided into two subdomains, A and B, having six and four α-helices, respectively (Curry et al, 1999). HSA exhibits a heart-shaped structure characterized by a high content α-helices and β-strands.

HSA has a good binding capacity for different types of compounds: water, ions (Ca^{+2}, Na^{+}, K^{+}) and heavy metal ions (Cu^{+2}, Zn^{+2}), fatty acids, hormones, synthetic drugs and many other compounds. Because of its high concentration in plasma (35–50 g/l) and its excellent binding capacity, HSA is the major transport protein in plasma; it regulates and maintains the colloidal

osmotic pressure in blood, which is essential for the distribution of body fluids between intravascular compartments and tissues, so helping in the regulation of body temperature. Furthermore, HSA is by far the most important protein contributing to the acid/base balance in plasma. Its plasma concentration is a marker for good nutrition and longevity and a decline of this concentration is a negative acute-phase marker of illness, trauma and infection (Schaller et al, 2008).

The primary function of HSA is to interact with other molecules. This requires the polypeptide chain to fold in one phase and unfold in the next phase allowing for additional bonding. The importance of serum albumin in anaesthesia derives from its high concentration in the circulatory system and from its ability to bind an extraordinarily diverse range of anesthetic drugs (Curry et al, 1999). It has been shown that distribution, free concentration, and metabolism of various drugs can be significantly altered as a result of their binding to HSA (Kragh-Hansen et al, 1981).

The binding properties of albumin depend on the three dimensional structure of its binding sites, which are distributed all over the molecule. Strong binding can decrease the concentrations of free drugs in the plasma, whereas weak binding can lead to a short lifetime or poor distribution. Investigating the interaction of drugs to HSA can elucidate the properties of drug–protein complex, as it may provide useful information of the structural features that determine the therapeutic effectiveness of drugs. Therefore, it has become an important research field in life sciences, chemistry, and clinical medicine (Ruhl et al, 2003; Cui et al, 2004).

Multiple drug binding sites have been reported for HSA by several researchers (Oettl et al, 2007; Kragh-Hansen et al, 2002; Sudlow et al, 1975; Shin-ichi et al, 2008; Ulrich et al, 2006; Bhattacharya et al, 2000; Simard et al, 2006). The principle regions of ligand binding sites of HSA are located in hydrophobic cavities in sub-domains IIA and IIIA, which are corresponding to site I and site II, respectively. Site I is dominated by strong hydrophobic interaction with most neutral, bulky, heterocyclic compounds, while site II mainly by dipole–dipole, van der Waals, and/or hydrogen-bonding interactions with many aromatic carboxylic

acids. HSA contained a single intrinsic tryptophan residue (Trp 214) in domain IIA and its fluorescence is sensitive to the ligands bounded nearby (Krishnakumar et al, 2002; Il'ichev et al, 2002). Therefore, it is often used as a probe to investigate the binding properties of drugs with HSA.

The modes of binding include complex formation with metal like copper, hydrophobic and electrostatic interaction in high affinity binding and covalent binding to different amino acids. Several binding sites are distributed over the molecule according to different marker molecules (Kragh-Hansen et al, 1990). For fatty acids alone, seven binding sites have been described (Simard et al, 2006). For anesthetic drugs several cases reported more than 50% of a clinically administered general anesthetic will be bound to serum albumin.

The molecular interactions are often investigated by a spectroscopic technique including fluorescence, UV-absorption, circular dichroism (CD), Fourier transform infrared spectroscopy (FT-IR), and nuclear magnetic resonance (NMR). These methods have been used to study the interaction of small molecule substances and protein and clarify the conformational change of protein (Nahar et al, 1997; Filyasova et al, 2001; Bertucci et al, 1995; Zsila et al, 2003; Jiang et al, 2003), because of high sensitivity, rapidity and ease of implementation (Cui et al, 2004; Cui et al, 2006; Cui and Wang et al, 2006).

In recent years, many researches on the binding of drugs to protein were carried out (He et al, 2005; Deepa et al, 2005; Kandagal et al, 2006; Zhao et al, 2006; Xie et al, 2005). However, none of these investigations have examined in detail the effects of anesthetic drugs (pentobarbital and propofol) on HSA binding constants, binding mechanisms, and the effects of pentobarbital and propofol on the protein secondary structure.

In this thesis, chapter two includes the theoretical background to provide the readers with latest developments in this research area. In chapter three, the experimental part will describe the materials and the spectroscopic techniques which are used to study the interaction between HSA and the anesthetic drugs. Chapter four will describe results and discussions of the

binding interaction of HSA with the two drugs by several techniques. Finally chapter five will include the main conclusions and future work of this research.

Chapter TWO

Background and Theoretical Considerations

Chapter Two

Background and Theoretical Considerations

We begin this chapter with a brief review of using physical techniques such as spectroscopy to provide information about the structural conformation of proteins, electromagnetic radiation, electromagnetic spectrum and energy levels of the molecule. In section three, information about the vibrational motions of a molecule, normal modes and the types of bond vibrations is given. Section four explains the theory of infrared spectroscopy. Section five gives information about the principles of Fourier transform infrared spectroscopy. Section six and section seven discuss the theory of fluorescence and UV-visible spectroscopy, respectively. Finally section eight explains the secondary structure of proteins.

2.1 Electromagnetic radiation

Electromagnetic radiations consist of transverse waves of both electric and magnetic fields which oscillate in a perpendicular fashion to each other and to the direction of the propagation. These waves cover a wide range of wavelengths, from low-energy radio wave to high-energy γ-ray radiation as shown in (Fig.2.1), which also indicates the processes that may occur in an atom or molecule exposed to the radiation.

When electromagnetic radiation falls on a particular sample, molecular excitations may result, when the energy of the radiation corresponds to the separation of two energy levels of the molecule. If the energy of the radiation does not correspond to the separation of two energy levels, the radiation will be either transmitted or scattered by the sample (Leslie et al, 1993).

The interaction of electromagnetic radiation with matter is more common through the electric field component. Therefore the plane of polarization is conventionally taken to be the plane containing the direction of electric field of strength E and that of propagation.

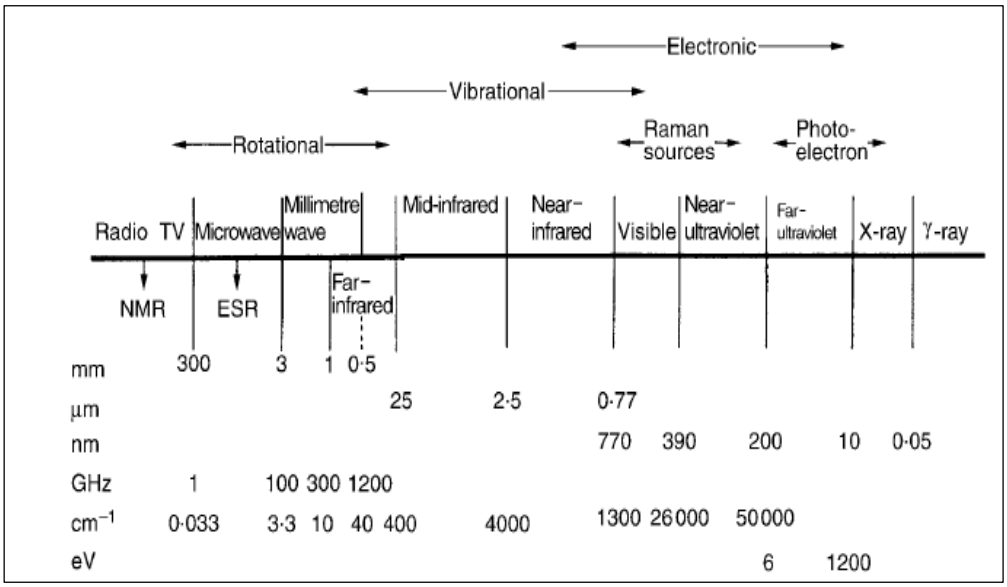

Figure 2.1: Regions of the electromagnetic spectrum.

A molecule may undergo rotational, vibrational, electronic or ionization processes, as a result of increasing energy .Also a molecule may scatter light in a Raman process, and the light source for such an experiment is usually in the visible or near-ultraviolet region .When an atom has no rotational or vibrational degrees of freedom, it may undergo only an electronic transition or ionization (Michael Hollas, 2004).

Let us consider an isolated molecule in space. It has different forms of energy depending on its different types of motion and intermolecular interactions. The total energy of a molecule is expressed as the sum of the constituent energies, that is,

$$\mathbf{E_{total} = E_{tran} + E_{rot} + E_{vib} + E_{el} + \ldots} \qquad \mathbf{2}$$

Where $\mathbf{E_{tran}}$ is translational energy due to the motion of the molecule as a whole, $\mathbf{E_{rot}}$ **is** rotational energy due to the rotation of molecule around the axis passing through the molecule center of gravity, $\mathbf{E_{vib}}$ is vibrational energy due to the periodic displacement around the equilibrium positions of their atoms, and $\mathbf{E_{el}}$ is electronic energy due to the constant motion of the electrons that are associated with each atom and bond (Sathyanarayana, 2004).

In general, the spectrum gives information about the spacing of energy levels of the molecule, which helps to determine the structure of the molecule. In some types of spectroscopy there are only a few, well-separated energy levels. In these cases, only a very narrow range of wavelengths is absorbed by the molecule which is excited from its lowest energy state to some higher energy state, thus giving an absorption line. In many cases, each energy state has a number of energy sublevels with a number of closely spaced wavelengths being absorbed. The lines are so close together, therefore they cannot be resolved and the absorption appears as a band or a broad peak as shown in (Fig.2.2) (Britlain et al, 1970).

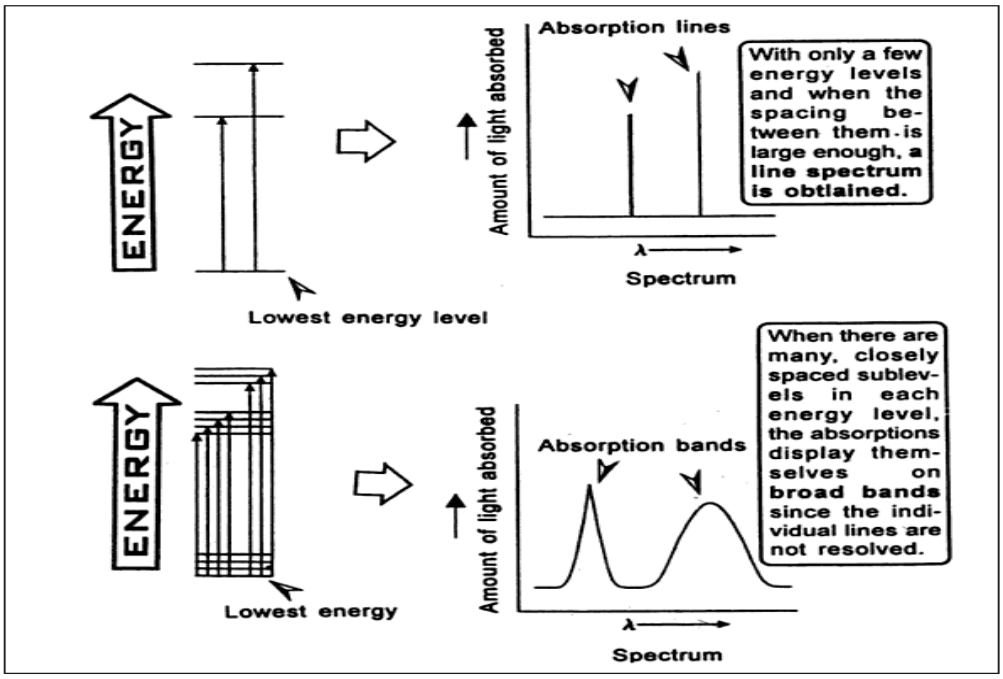

Figure 2.2: Absorption lines and absorption bands.

2.2 Historical developments of spectroscopy

Biological materials have been studied by an array of physical techniques, including many types of spectroscopy. Vibrational spectroscopy offers many advantages over other spectroscopic techniques: First, the accessibility of experiment, specific functional groups provide information about the structural conformation of biological molecules. Second, vibrational spectroscopic data are obtained in a non-invasive manner, i.e vibrational spectroscopy does not require extrinsic probe molecules such as fluorescent probes. Third, there is no limit to the size thus high molecular weight biomaterials can be studied. Fourth, the molecular movements that are monitored by the vibrational spectroscopic method are atomic motions on the picoseconds scale, and provide all the molecular conformation. There is no line broadening in the vibrational spectroscopy due to the investigation of biological materials (Lehninger, 1975).

The history of infrared spectroscopy goes back 200 years, when William Herschel discovered the infrared region of the electromagnetic spectrum in 1800 (Coblentz, 1951). "Infrared and Raman Spectra of Polyatomic Molecules" was the first publication by Gerhard Herzberg in 1945, and from that date, vibrational spectroscopy became an important research tool (Herzberg, 1945).

The knowledge of the infrared spectra of various types of straight, branched, and cyclic hydrocarbons helped the Allied Forces in the Second World War. After the war, commercial infrared spectrometers became readily available; all these infrared spectra led to the creation of the very useful concept of "*group frequency*" and culminated in many published works. In 1954, Bellamy published a papers entitled "Infrared Spectra of Complex Molecules" (Bellamy, 1954), Norman Jones and Camille Sandorfys published "The application of Infrared and Raman Spectroscopy to the Elucidation of Molecular Structure" in 1956 (Jones et al, 1956).Early infrared spectra of biological materials were published in the 1950s.

Proteins are the most numerous and versatile of biomaterials. The vibrational spectroscopy of proteins provides information at different levels of structural system: (a) assessment of protein

secondary structure from an analysis of the amide bands, and (b) Mechanistic information about protein structure and protein ligand bindings at the level of individual functional groups.
The first use of infrared spectroscopy of the conformational structure of proteins and polypeptides was in 1950 by Elliot and Ambrose (Elliott et al, 1950). They suggested that a correlation exists between the position of certain bands in the infrared spectra of proteins and the conformation or structure of the polypeptide backbone. Sam Krimm and co-workers confirmed this correlation by theoretical calculations of the amide normal modes (Krimm et al, 1986).

In 1970s, Fourier transform infrared instrumentation became widely available in the field of biological systems. FTIR is particularly important for protein solutions. It offers not only increased accuracy and reproducibility, but also improvement in the achievable signal to noise ratios and the ability to perform measurements with strongly absorbing samples. In 1982, Heino was the first to learn about Fourier self-deconvolution and other band-narrowing procedures (Theophanides, 1984). Heino and Michael started applying this methodology to the analysis of the amide bands in proteins (Susi et al, 1983).

2.3 Molecular vibrations

When the frequencies of infrared light and the frequency of vibration coincide, the infrared light is absorbed by a molecular vibration. The vibration frequency and absorption probability depend on the strength and polarity of the vibrating bonds, which are also influenced by intra- and intermolecular effects (Vladimir et al, 2007).
The vibrational motions of a molecule can be considered classically, as being a set of balls representing the nuclei, of various masses, connected by Hooke's law springs which are representing the various forces acting between the nuclei. As an example of this model consider H_2O model, which is illustrated in (Fig. 2.3).

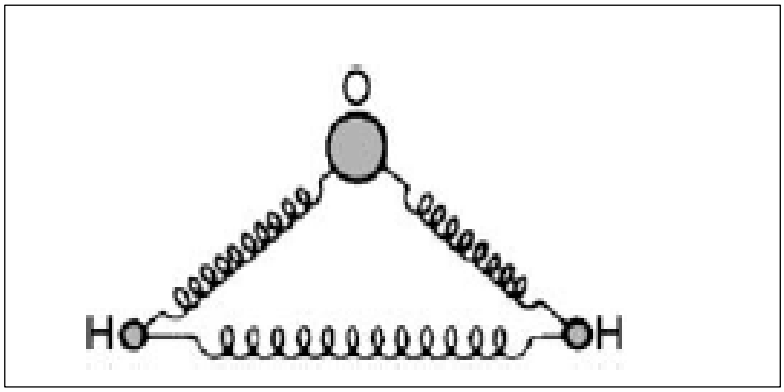

Figure 2.3: Classical model (Ball-and-spring model) of H_2O.

This figure shows that the stronger forces between the bonded O and H atoms are represented by strong springs which provide resistance to stretching the bonds. The weaker force between the non-bonded hydrogen nuclei is represented by a weaker spring which provides resistance to an increase or decrease of the HOH angle (Michael Hollas, 2004).

In general, each atom has three degrees of freedom, corresponding to the motions along any of the three Cartesian coordinate axes (x, y, z). Consider a molecule with N atoms have 3N degrees of freedom, three of which represent translational motion in mutually perpendicular directions (x, y, and z axes) and three represent rotational motion about the x, y, and z axes. The remaining degrees of freedom represent 3N - 6 (3N - 5) vibrations of a nonlinear (linear) molecule, and give the number of ways that the atoms in a nonlinear (linear) molecule can vibrate (i.e., the number of vibrational modes), the so-called normal modes of vibration. The remaining degrees of freedom that produce a net change in the dipole moment may result in an IR activity (Peter et al, 2007).

2.3.1 Normal modes of vibration

A normal mode of vibration is one in which all the atoms undergo harmonic motion (Schermann, 2008). In each normal mode atoms oscillate in-phase and with the same frequency, but generally with different amplitudes. In vibrational spectroscopy, the frequency has a sensitive dependence on the forces acting on the individual atoms and on their respective masses. These forces do not only result from the chemical bonds connecting the individual atoms but also include contributions from nonbonding interactions within the molecule and with the molecular environment (Siebert et al, 2008).

The form of the normal modes may be obtained from the bond lengths and angles and of the bond-stretching and angle-bending force constants, which are a measure of the strengths of the various springs in the ball-and-spring model as shown in the (Fig. 2.3).

The normal modes tend to be localized in a particular group of atoms which is called group vibrations, when there is a chain of atoms in which the force constant between two of them is different from those between other atoms in the chain. A number of group vibration wavenumbers for bond-stretching and angle-bending vibrations are listed in (Table 2.1) (Davies, 1963).

Table 2.1: Typical bond-stretching and angle-bending group vibration wavenumbers ω (Michael Hollas, 2004).

Bond-stretching		Bond-stretching		Angle-bending	
Group	ω/cm^{-1}	Group	ω/cm^{-1}	Group	ω/cm^{-1}
≡C–H	3300	–C≡N	2100	≡C–H	700
=C(H)–	3020	>C–F	1100	=C(H)–H	1100
except: O=C(H)–	2800	>C–Cl	650	–C(H)(H)–H	1000
>C–H	2960	>C–Br	560	>C(H)–H	1450
–C≡C–	2050	>Cl–I	500	C≡C–C	300
>C=C<	1650	–O–H	3600[a]		
>C–C<	900	>N–H	3350		
>Si–Si<	430	>P=O	1295		
>C=O	1700	>S=O	1310		

Whenever a molecule absorbs infrared light, the absorbed light energy is converted into atomic bond vibrations. The atomic bond vibrations are classified as either stretching or bending vibrations. Stretching vibrations are categorized as being either symmetrical (movement in the same direction) or anti symmetrical (movement in opposite directions). Symmetrical stretching requires lower energy than anti-symmetrical stretching. Bending vibrations are classified as scissoring, rocking, twisting, or wagging. The number of stretching vibrations is equal to the number of valance bonds that exist in the molecule and the remaining vibrations are termed as deformation modes. Each vibration is described in terms of internal coordinates which is defined as increments in bond length, bond angle or dihedral angle (Sathyanarayana, 2004).

For example, the non linear triatomic water molecule has three fundamental vibrational modes as shown in (Fig. 2.4).The O-H bonds may vibrate in phase with each other to form symmetric

stretching vibration, or they may vibrate out of phase to form anti symmetric stretching vibration. The H-O-H bond angle can change in a bending vibration (Kalsi, 2004).

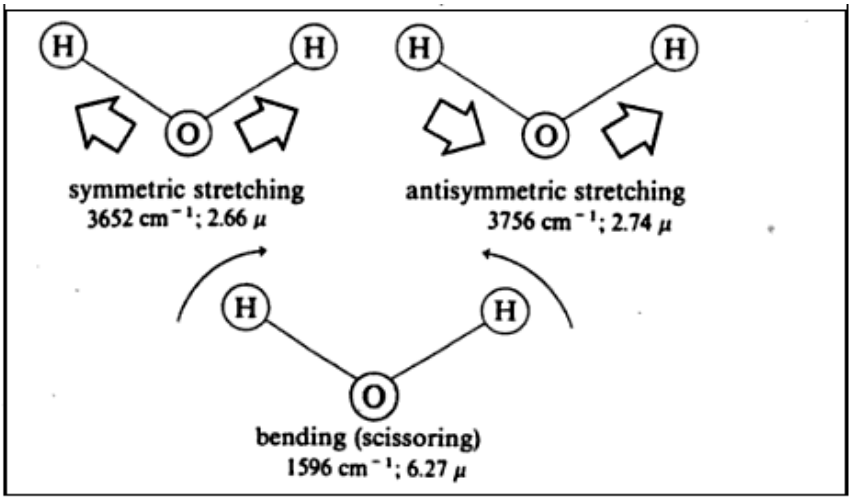

Figure 2.4: Stretching and bending vibrations of H_2O molecule (Kalsi, 2004).

2.3.2 Normal modes of harmonic oscillator

The vibrations of atoms in a molecule can be treated by using the harmonic oscillator model. In each normal mode, the atoms have approximately harmonic displacements from their equilibrium positions; all the atoms vibrate at a certain characteristic frequency, ν_i for each mode, i. The potential energy, V(r), of a harmonic oscillator as a function of the distance between the atoms (r) is represented by the dashed line, and the actual variation of the potential energy as a function of the displacement of the atoms from their equilibrium positions is represented by solid line, as shown in (Fig. 2.5).

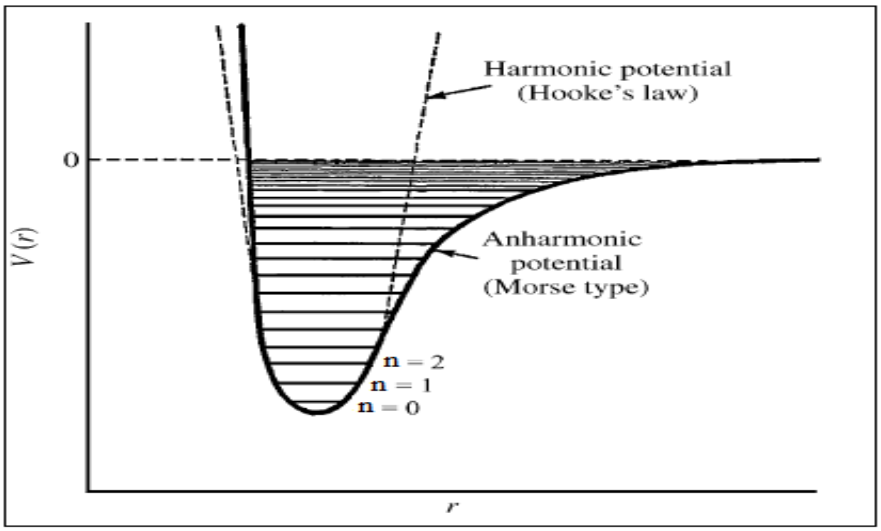

Figure 2.5: Potential energy of a diatomic molecule as a function of the atomic displacement during a vibration for a harmonic oscillator (dashed line) and an anharmonic oscillator (solid line) (Peter et al, 2007).

For any mode in which the atoms vibrate with simple harmonic motion (i.e., obeying Hooke's law), the vibrational energy states, $\mathbf{E_{vib}}$ is given by the equation,

$$\mathbf{E_{vib} = h.\ \nu_i\ (n_i + ½)} \qquad \mathbf{(3)}$$

where ν_i is the fundamental frequency of the particular mode, n_i the vibrational quantum number of the ith mode (n_i = 0, 1, 2 . . .), and h is Planck's constant. The energy difference for transitions between the ground state (n_i = 0) and the first excited state (n_i =1) of most vibrational modes corresponds to the energy of radiation in the mid-infrared spectrum (400 to 4000 cm^{-1}). From (Fig. 2.5), it can be seen that equation 3 is valid only for low values of the vibrational quantum number and is not valid when n_i is large. In practice, $\mathbf{E_{vib}}$ must be described using an anharmonic (Morse-type) potential function. This potential energy is given to a first approximation by the expression,

$$\mathbf{E_{vib} = h.\ \nu_i\ (n_i + ½) + h.\ \nu_i\ .x_i\ (n_i + ½)^2} \qquad \mathbf{(4)}$$

where x_i, the anharmonicity constant, is dimensionless and typically has values between -0.001 and -0.02, depending on the mode. For many normal modes, only a few atoms have large displacements and the rest of the molecule is almost stationary. The frequency of such modes is characteristic of the specific functional group in which the motion is centered and is minimally affected by the nature of the other atoms in the molecule. Thus, the observation of spectral features in a certain region of the spectrum is often indicative of a specific chemical functional group in the molecule (Peter et al, 2007; Gordon et al, 2005).

2.3.3 Vibrational energy levels and transitions

Consider an N-atom molecule. Its vibrational energy is characterized by a set 3N-6 vibrational quantum numbers n_1, n_2, n_3,…$n_{3N-6.}$ The corresponding vibrational level when all the vibrational quantum numbers are equal to zero is the ground state vibrational level. Its energy, referred to as zero point energy, E_v (0, 0, 0…) is not zero. For a poly atomic molecule, the energy level is referred to as a fundamental or a first harmonic level if only one vibrational quantum number n_k =1 is not zero. Each of their 3N-6 vibrational quantum numbers is independently excited from the ground state to the fundamental level. In addition each of these represent a fundamental transition giving rise to a normal mode of vibration.

For 3N-6 vibrations, the total vibrational energy of a polyatomic molecule is written as the sum of individual energies ($E_1 + E_2$…$+ E_{3N-6)}$, that is

$$E_v = \sum_{i=1}^{3N-6} \left(\mathbf{n}_i + \frac{1}{2} \right) h\nu_i \qquad \textbf{(5)}$$

Where n_i is vibrational quantum numbers, h is planck's constant, and ν_i is normal vibrational frequencies.

For an N-atom molecule, the zero point energy E_v (0, 0, 0…) is,

$$E_{\nu}^{0} = (1/2)\sum_{i=1}^{3N-6} h\nu_i \qquad \textbf{(6)}$$

The vibrational energy of a polyatomic molecule with inclusion of the anharmonicity correction is

$$E_{vib} = \sum_{i=1}^{3N-6}\left(\mathbf{n}_i + \frac{1}{2}\right) h\nu_{e,i} + \sum_{i\geq k}\sum_{k}^{3N-6} hx_{ki}\left(\mathbf{n}_k + \frac{1}{2}\right)\left(\mathbf{n}_i + \frac{1}{2}\right) + hG_0$$

(7)

Where G_0 is a constant term usually omitted since it is small. The ν_e are the harmonic frequencies (Gans, 1971; Howarth, 1973; Barrow, 1962; Whiffen, 1972; Chang, 1971).

2.4 Infrared spectroscopy

Spectroscopy is an experimental method which is concerned with the absorption, emission or scattering of electromagnetic radiation by atoms or molecules (Michael Hollas, 2004). Also it is one of the important experimental techniques which can determine the electronic structure of atoms and molecules (Sathyanarayana, 2004). Vibrational spectra were first studied in the form of absorption bands in the infrared region, which was discovered, as the first non-visible region of the electromagnetic spectrum, by the astronomer Sir William Herschel in 1800 (Herschel, 1800).

2.4.1 Infrared regions

Infrared (IR) spectroscopy is defined as the absorption measurement of different IR frequencies by a sample positioned in the path of an IR beam. The main goal of IR spectroscopic analysis is to determine the chemical functional groups in the sample where different functional groups absorb characteristic frequencies of IR radiation, and it is an

important and popular tool for structural elucidation and compound identification (Blitz et al, 1994; Shaw et al, 1993).

The infrared range of the electromagnetic spectrum is divided into three regions due to their location relative to visible spectrum; the near- infrared, mid- infrared, and far- infrared region. The near-infrared, approximately 14000-4000 cm^{-1} (2.5-0.8 μm), lies adjacent to the visible region has high energies to excite overtone or harmonic vibrations. The mid-infrared, approximately 4000-400 cm^{-1} (30-2.5 μm), may be used to study the fundamental vibrations and associated rotational-vibrational structure. The far-infrared, approximately 400-10 cm^{-1} (1000-30 μm), lies adjacent to the microwave region, and has low energy so it may be used for rotational spectroscopy *(*Colthrup et al, 1990*).*

2.4.2 Infrared absorption process

The infrared absorption process is a quantized process where any molecule absorbs only selected frequencies (energies) of the infrared radiation. The absorption of infrared radiation corresponds to changes of energy on the order 8 to 40KJ/mole. In this energy range, the radiation corresponds to the range encompassing the stretching and bending vibrational frequencies of the bands in most organic molecules. In the absorption process, the frequencies of infrared radiation that match the natural vibrational frequencies of the molecule are absorbed, and the energy absorbed serves to increase the amplitude of the vibrational motions of the bonds in the molecule. However, not all the bonds in a molecule absorb the infrared energy. Only those bonds which have changes of the dipole moment as a function of time are capable of absorbing infrared energy (Nakanishi et al, 1977). Therefore In the infrared spectrum the intensity of absorption due to a particular vibration depends on the change of dipole moment during the vibration. For example, the stretching vibration of the strongly polar C=O bond gives a strong absorption band, whereas that of the C=C bond gives a weak band (Duxbury, 1999).

IR absorption is generally presented in the form of a spectrum showing wavelength or wavenumber versus transmittance or absorption intensity. The Transmittance, T, is the ratio of

radiant power transmitted by the sample (I) to the radiant power incident on the sample (I_0). Absorbance (A) is the logarithm to the base 10 of the reciprocal of the transmittance (T) as shown in the equation,

$$A = \log_{10}(1/T) = -\log_{10} T = -\log_{10} T = -\log_{10} I/I_0 \quad (8)$$

The transmittance spectra provide better contrast between intensities of strong and weak bands because transmittance ranges from 0 to 100% *T* whereas absorbance ranges from infinity to zero (Blitz et al, 1994).

2.4.3 Infrared spectroscopy and bond properties

The infrared absorption frequency is usually affected by the bond strength and the masses of the bonded atoms. Let us consider a simple heteronuclear diatomic molecule (two different atoms) as two vibrating masses connected by a spring. When this spring is stretched or compressed beyond the equilibrium distance of the bond, the potential energy of the system increases. When a bond vibrates, as for any harmonic oscillator, its energy of vibration is continuously and periodically changing from kinetic to potential energy.

The total energy of the bond is proportional to the frequency of the vibration, as follows

$$E_{osc} \propto h.\nu_{osc} \quad (9)$$

This total energy for a harmonic oscillator is determined by the force constant of the spring *(K)*, and the masses (m_1 and m_2) of the two bonded atoms. The natural frequency of vibration of a bond is given by the equation, which is derived from Hooke's Law for vibrating springs.

$$\bar{\nu} = \frac{1}{2\pi c}\sqrt{\frac{K}{\mu}} \quad (10)$$

where μ is the reduced mass of the system, is given by

$$\mu = \frac{m_1 m_2}{m_1 + m_2} \qquad (11)$$

The force constant K varies from one bond to another. The force constants for triple bonds are three times those of single bonds, and the force constants for double bonds are twice those of single bonds. From the last two equations, it is shown that the stronger bonds have a larger force constant K and vibrate at higher frequencies than the weaker bonds. And the bonds between atoms of higher masses (larger μ) vibrate at lower frequencies than bonds between atoms of lower masses. In general, bending motions occur at lower energy (lower frequency) than the typical stretching motions because the bending force has lower value for the bending force constant K. For example, C-H stretching occurs at ~ 3000 cm^{-1}, while C-H bending occurs at ~ 1340 cm^{-1} (Nakanishi et al, 1977; Bellamy, 1975).

The vibrational motion is quantized, so it must follow the rules of quantum mechanics, and the only transitions which are allowed are given by equation 3. From this equation, the lowest energy level is E_0= ½ h.ν, and the next highest is E_1=3/2h.ν. According to the selection rule Δn= ±1, only transitions to the next energy level are allowed; therefore molecules will absorb an amount of energy equal to (3/2 – ½) h.ν or h.ν.

As the interatomic distance increases, the energy reaches a maximum, for anharmonic oscillator, as seen in (Fig. 2.6). Also the energy levels become more closely spaced with increasing interatomic distance in the anharmonic oscillator. The allowed transitions, h.ν, become smaller in energy. Therefore, overtones (Δn= ±2, ±3) can be lower in energy than predicted by the harmonic oscillator theory (Ferraro et al, 1979).

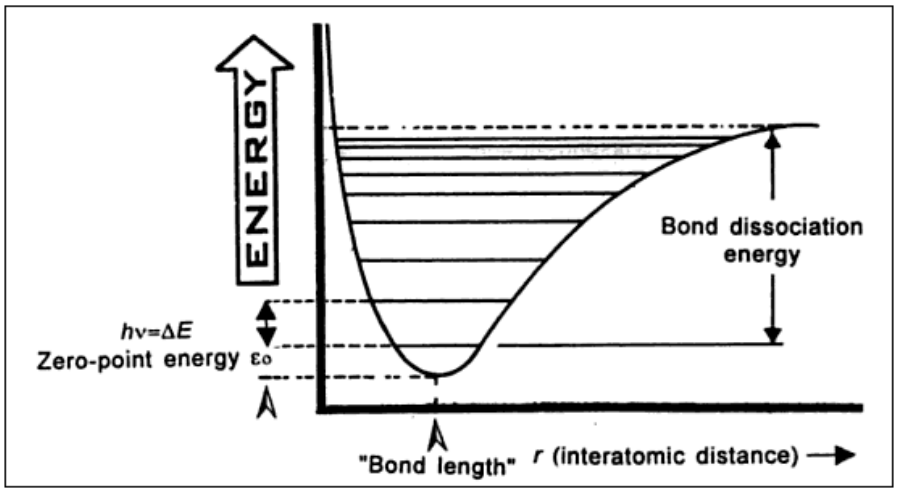

Figure 2.6: Energy curve for an anharmonic oscillator showing the vibrational levels for a vibrating bond. The horizontal lines represent the various vibrational energy levels (Ferraro et al, 1979).

2.4.4 Infrared spectra

Infrared spectra used for qualitative analysis may be obtained from a pure liquid, the solid, embedded in a KBr disk, or a solution using a non-polar solvent. The reason for using non-polar solvents, because polar solvent may affect both group vibration and band intensities and may be involved in hydrogen-bonding with the solute. Each dip in infrared spectrum is called peak or band, which represents the absorption of radiation at certain frequency by the sample *(*Herzberg, 1989*).*

The infrared spectrum has an important use to determine structural information about a molecule. The absorptions of each type of bond such as N-H, C-H, O-H, C=O, C-O, C-C, C=C, C=N, and so on, occur only in certain small portions of the vibrational infrared region. It is known that any absorption in the range 3000 ±150 cm^{-1} is almost always due to the presence of a C - H bond in the molecule; any absorption in the range 1715 ± 100 cm^{-1} is normally due to the presence of a C=O bond (carbonyl group) in the molecule (Herzberg, 1991).

2.5 Fourier transform infrared spectroscopy

An Infrared spectrometer which determines the absorption spectrum for a compound come in two types: one of them is Fourier transform infrared FTIR instrument that provides spectra of compounds in the common range of 4000 to 400 cm^{-1}, and the other is Dispersive infrared spectrometer.

2.5.1 Theory of FTIR

Fourier transform Infrared (FTIR) is the most modern infrared spectrometer which has the design of the optical pathway produces interference signals, which contain infrared spectral information called interferogram. The interferogram (a time domain spectrum displaying intensity versus time) is converted by a mathematical operation known as Fourier transformation to the final IR spectrum, which is the frequency domain spectrum showing intensity versus frequency (Donald, 2001).

The principle of Fourier transform infrared spectroscopy is the simple interference of radiations. When two radiation beams with the same amplitude and wavelength λ interfere in phase with each other, the interference is constructive and the resultant amplitude will be twice as high. If the two beams are out of phase by **(1/2) (2n+1) λ**, the interference will be destructive and the beams will cancel each other. The amplitude at intermediate phase differences is given by the following term,

$$\left(\frac{1}{2}\right)(1 \pm \cos 2\pi\theta/\lambda) \qquad \textbf{(12)}$$

Where θ is the path difference (retardation).The amplitude of the interference pattern of two beams with different wavelengths is given by the expression,

$$\left(\frac{1}{2}\right)\left[\sum_{n=1,2}(1.0+\cos 2\pi\theta/\lambda_n)\right] \qquad \textbf{(13)}$$

The interferogram, which is a plot of the intensity (amplitude) versus path length difference (phase) for the interference of two beams is shown in (Fig. 2.7).

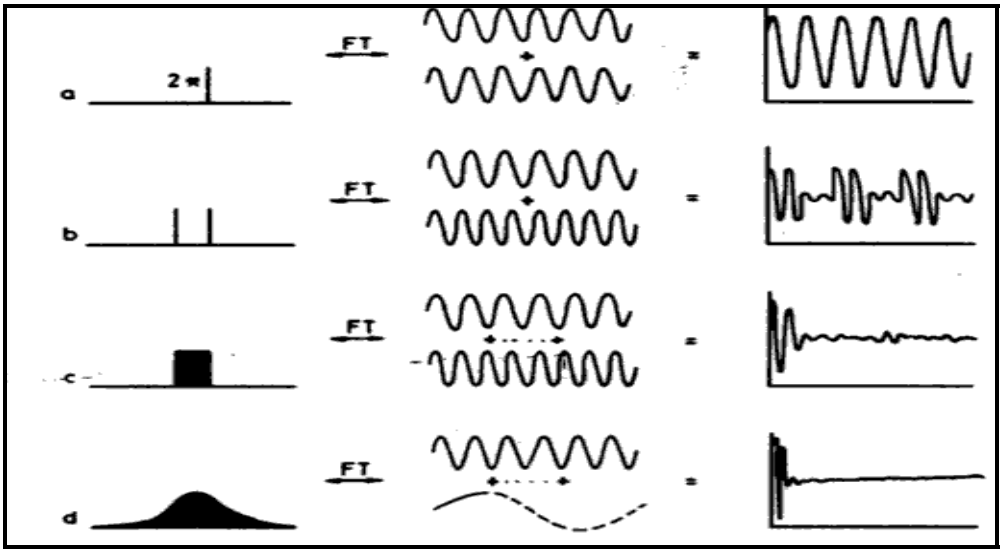

Figure 2.7: Typical interferograms for (a) two beams of identical frequency (b) beams of two different frequencies, (c) two narrow band radiation sources with constant amplitude and (d) two broad band radiation sources with different amplitude.

In a Fourier transform spectrometer, the time domain plot in which the changes in the radiant power *f* (t) are recorded as a function of time t is converted into a frequency domain spectrum. The Fourier transform of the function *f* (t) and the inverse relation is defined by the two equations respectively,

$$G(\nu)=\frac{1}{\sqrt{2\pi}}\int_{-\infty}^{\infty} f(t)e^{i\omega t}\,dt \qquad \textbf{(14)}$$

$$f(t) = \frac{1}{\sqrt{2\pi}} \int_{-\infty}^{+\infty} G(v) e^{-ivt} dv \qquad (15)$$

where ω is the natural frequency. The above equations are said to form a Fourier transform pair (Griffiths et al, 1986).

2.5.2 Intensity

The intensity for an ideal Michelson interferometer *I(x)* of a monochromatic radiation and a poly chromatic radiation which are travelling towards the detector at the optical retardation *x* is given by the given equations, respectively,

$$I(x) = \int_0^\infty 2IRT(1 + 2\cos 2\pi\bar{\nu}x)d\bar{\nu} \qquad (16)$$

$$I(x) = (1/2)\int_0^\infty I(\bar{\nu})(1 + \cos 2\pi\bar{\nu}x)d\bar{\nu} \qquad (17)$$

Where $(\bar{\nu})$ is the wavenumber of the radiation in gas or vacuum in the interferometer ($\nu \text{ in Hz} = c\bar{\nu}$ $(\bar{\nu} \text{ in } \text{cm}^{-1})$), $I(\bar{\nu})$ is the intensity of the radiation of wavenumber $(\bar{\nu})$ incident on the beam splitter, R is the reflectance of the beam splitter and T is the transmittance of the beam splitter as summing beam splitter efficiency to be 100%.

The interferogram function *F(x)* which is the varying part of the interferogram is given by the equation,

$$F(x) = I(x) = I(\infty) = \int_0^\infty A(\bar{\nu})\cos 2\pi\bar{\nu}x \, d\bar{\nu} \qquad (18)$$

This equation shows that the intensity *I(x)* is known for infinitely small increments of retardation *x* and shows that retardation varies from zero to infinity. Since *I(x)* and $A(\bar{\nu})$ are

Fourier transform pairs, the spectral intensities $A(\bar{\nu})$ are obtained through the Fourier transform theorem,

$$A(\bar{\nu}) = 2\int_{-\infty}^{\infty} F(x)\cos 2\pi\bar{\nu}x \, dx \qquad \textbf{(19)}$$

The interferogram can't have infinite length as shown by the above equation (Ferraro et al 1979), it must be truncated at $x = \pm X$, so the above equation must be modified to

$$I(\bar{\nu}) = 2\int_{-x}^{x} F(x)\cos 2\pi\nu x \, dx \qquad \textbf{(20)}$$

2.6 Fluorescence spectroscopy

Luminescence is the emission of light from a substance, and occurs from electronically excited states. Luminescence is divided into two categories: fluorescence and phosphorescence depending on the nature of the excited state. In excited singlet states, the electron in the excited orbital is paired (by opposite spin) to the second electron in the ground-state orbital. Consequently, return to the ground state is spin allowed and occurs rapidly by emission of a photon. The emission rates of fluorescence are typically10^8 s^{-1}, so that a typical fluorescence lifetime (time between excitation and return to the ground state) is near 10 ns (10 x 10^{-9} s). Phosphorescence is the emission of light from triplet excited states, in which the electron in the excited orbital has the same spin orientation as the ground-state electron. Transitions to the ground state are forbidden and the emission rates are slow (10^3 to 100 s^{-1}), so that phosphorescence lifetimes are typically milliseconds to seconds (Berlman, 1971).

Fig.(2.8) illustrates the processes that occur between the absorption and emission of light. The singlet ground, first, and second electronic states are depicted by S_0, S_1, and S_2, respectively. At each of these electronic energy levels the fluorophores can exist in a number of vibrational energy levels, depicted by 0, 1, 2, etc. The transitions between states are depicted as vertical lines to illustrate the instantaneous nature of light absorption (Szudy, 1998). Also this figure

reveals that the energy of the emission is typically less than that of absorption. Fluorescence typically occurs at lower energies or longer wavelengths. This phenomenon was first observed by Sir.G.G. Stokes in 1852 at the University of Cambridge (Stokes, 1852).

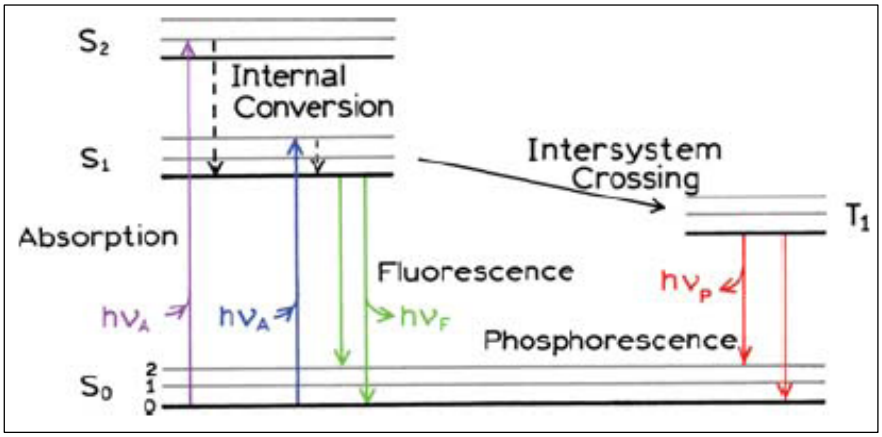

Figure 2.8: One form of a Jablonski diagram (Lakowicz, 2006).

Fluorescence is a phenomenon whereby a material absorbs light of one wavelength and then emits it of a longer wavelength (lower energy). The fluorescence lifetime and quantum yield are the most important characteristics of a fluorophore. Quantum yield is the number of emitted photons relative to the number of absorbed photons. The lifetime determines the time available for the fluorophore to interact with or diffuse in its environment, and hence the information available from its emission.

It is clear that fluorescence is the result of an energy process that occurs in a molecule called fluorophore. The wavelength in nanometer is determined by the spectral properties of the fluorophores. Fluorophores are divided into two main classes: (1) Intrinsic fluorophores are those that occur naturally, such as aromatic amino acids. (2) Extrinsic fluorophore are added to the sample to provide fluorescence when none exists, or to change the spectral properties of the sample. Intrinsic fluorescence protein originates with the aromatic amino acids tryptophan (trp), tyrosine (tyr), and phenylalanine (phe) (Fig. 2.9). The tryptophan residues are the dominant source of UV absorbance and emission in proteins (Houck et al, 2006).

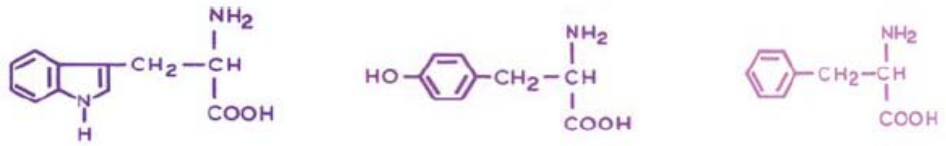

Figure 2.9: Structures of Tryptophan, Tyrosine, and Phenylalanine respectively (Szudy 1998).

The intensity of fluorescence is decreased by a variety of processes. This decrease in intensity is called quenching. Quenching can occur by different mechanisms. Collisional quenching occurs when the excited-state fluorophore is deactivated upon contact with other molecule in solution, which is called the quencher. The decrease in intensity of collisional quenching is described by the well-known Stern-Volmer equation:

$$\frac{F_0}{F} = 1 + K_{sv}[Q] = 1 + k_q \tau_0 [Q] \qquad \textbf{(21)}$$

where K_{sv} is the Stern-Volmer quenching constant, k_q is the bimolecular quenching constant, τ_0 is the unquenched lifetime, and $[Q]$ is the quencher concentration. The Stern-Volmer quenching constant K_{sv} indicates the sensitivity of the fluorophore to a quencher. A fluorophore buried in a macromolecule like a protein is usually inaccessible to water soluble quenchers, so that the value of K_{sv} is low. Larger values of K_{sv} are found if the fluorophore is free in solution or on the surface of a biomolecule. Fluorescence quenching can occur by a variety of other processes. Fluorophores can form nonfluorescent complexes with quenchers. This process is referred to as static quenching since it occurs in the ground state and does not rely on diffusion or molecular collisions. Quenching can also occur by a variety of trivial, i.e., non-molecular mechanisms, such as attenuation of the incident light by the fluorophore itself or other absorbing species (Lakowicz, 1991).

2.7 UV- visible spectroscopy

The Ultraviolet (UV) and visible radiation comprise only a small part of the electromagnetic spectrum, which includes such other forms of radiation as radio, infrared (IR), cosmic, and X rays (Owen, 2000).

In UV-Vis spectroscopy, the low-wavelength UV light has the highest energy. The interaction of UV or visible light with matter exhibits electronic excitation in the molecule. Any change in the electron energy level involves a corresponding change in the energy of the molecule. This change in energy is called *a transition*. In general molecules and atoms exist in the ground state at room temperature. The transition consists of the excitation of the electron from an occupied molecular level (non-bonding *p*, or bonding π-orbital) to the higher energy orbital (anti-bonding, π* or σ*), the promotion of an electron from π-bonding orbital to an anti bonding orbital (π*) is denoted (π → π*). The transition (n→ π*) requires less energy compared to π → π* or σ→ σ* transition as shown in (Fig. 2.10) (Clark et al, 1993).

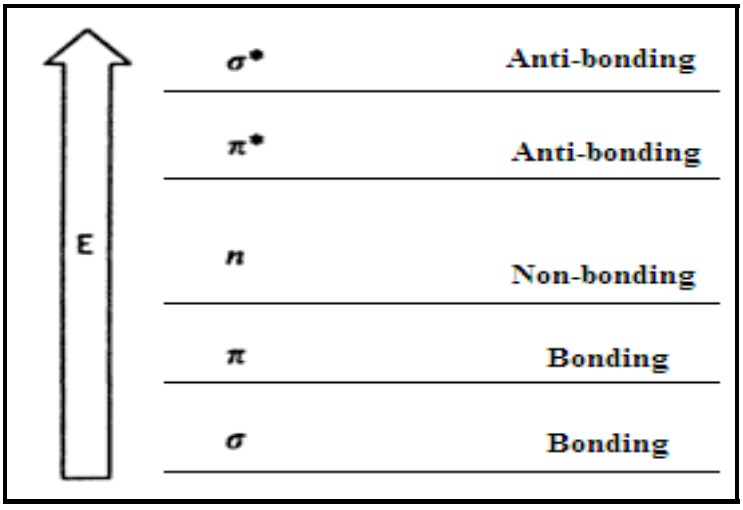

Figure 2.10: Electronic energy levels.

The absorption spectra are characterized by their shape, maximum wavelength and the peak height or molar extinction coefficient. However, the position of the absorbance maximum is

not fixed but depends partially on the molecular environment of the chromophore (molecular group usually containing a π bond) and on the solvent in which the sample may be dissolved. Other parameters, such as pH and temperature, also may cause changes in both the intensity and the wavelength of the absorbance maxima.

UV-visible absorption spectroscopy played an important role in studies of protein structure and functions. The application of ultraviolet spectroscopy in protein studying was provided by Wetlaufer in 1962 (Wetlaufer, 1962), which remains a valuable source of information about the technique. Proteins are colorless to the human eye and show their spectral characteristics when viewed in the UV range. UV spectra of proteins result largely from the presence of the aromatic amino acids tryptophan, tyrosine, and phenylalanine. The absorbance at short wavelength (< 240 nm) is due to peptide amide. A protein at room temperature has a specific tertiary structure or conformation that in turn creates a specific electronic environment for the aromatic amino acids. If the protein is heated it will, at a certain temperature, unfold or melt and lose its structure. In this process, the electronic environment of the aromatic amino acids changes, which in turn results in spectral changes or shifts (Robinson et al, 2005).

2.8 Protein structure

The first structures of proteins at an atomic resolution were determined in the late 1950's (Kendrew et al, 1958). Proteins are a particular type of biological molecules that can be found in every living o on Earth. Also proteins are linear biological polymers for which the monomeric units are amino acids as shown in (Fig. 2.11).Twenty different amino acids are used to make proteins, each distinguished by the identity of the "R" group. The amino acids are linked to form a polymer by linking the amino group on one amino acid with the carboxylic group on another amino acid to form an amide bond(also it is called peptide bond). When many amino acids are linked together by an amide bond, they formed a polypeptide, which consists of a backbone and sidechains. The backbone of polypeptide comprises the amide nitrogen, the alpha carbon and the carbonyl carbon that are contributed by each amino acid unit. The sidechains of polypeptide comprise the "R" groups (Byler et al, 1986).

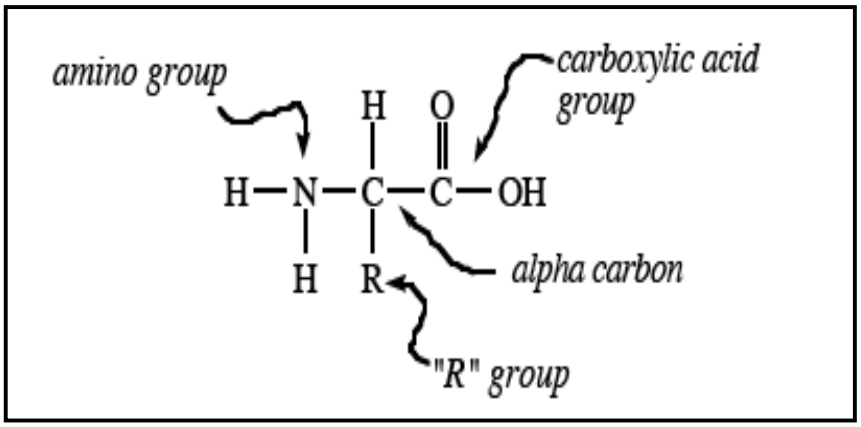

Figure 2.11: The structure of an amino acid; the basic building block for making proteins.

The number of amino acids residues they contain in the protein and the identity and sequential order of the amino acids are used to distinguish proteins from one another (Surewicz et al, 1988).

2.8.1 Structure levels of proteins

Protein exhibits four levels of structure: primary, secondary, tertiary and quaternary structure. Primary structure of protein is the sequence of amino acids; Secondary structure is highly regular sub-structures that describe the local conformation of the amino acids in the protein chain. It is stabilized by hydrogen bonds between the amino-groups which carry a partial positive charge and keto-groups of the peptide bonds which carry a partial negative charge as shown in the (Fig. 2.12). Each hydrogen bond has only relatively small bond energy, but the sum of the bond energies over all hydrogen bonds in a protein is considerable. Tertiary structure describes the way in which the elements of protein secondary structure are arranged in space and Quaternary structure describes how several polypeptide chains come together to form a single functional protein.

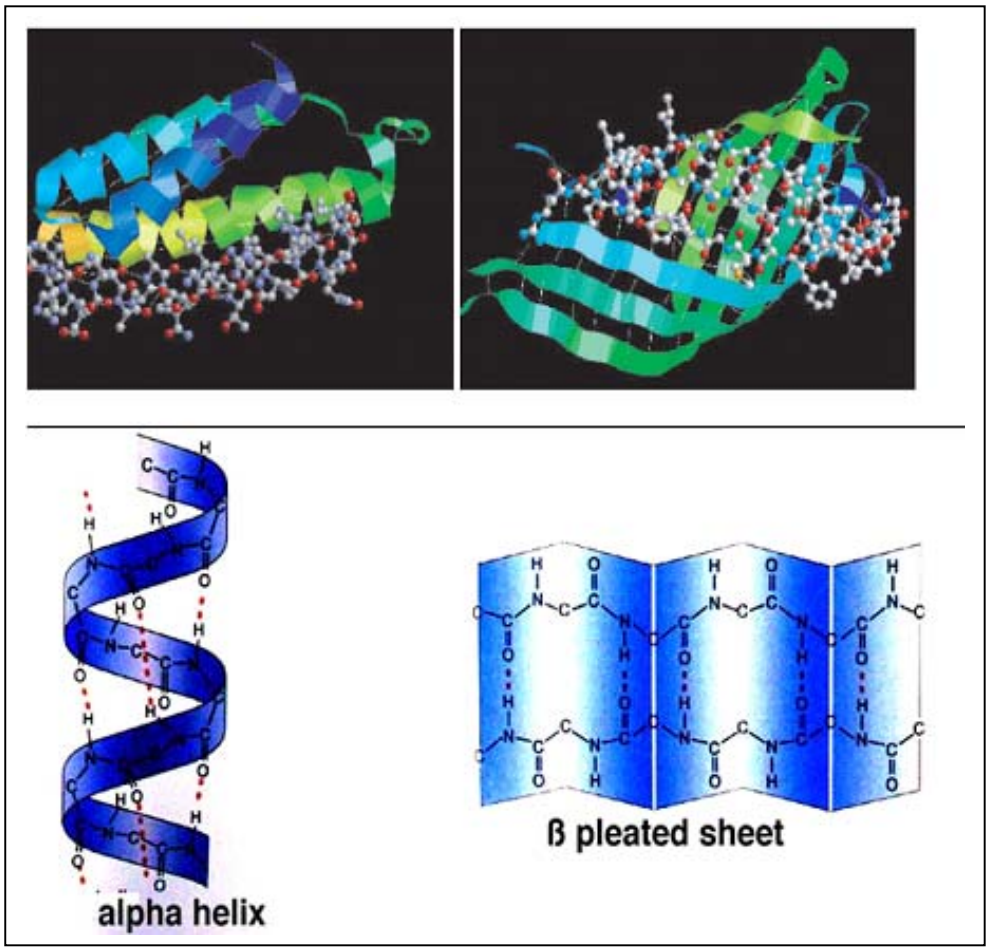

Figure2.12: Hydrogen bonding in α-helix (left) and β-sheets (right). In α-helix all hydrogen bonds between keto groups and amino groups in the protein backbone occur between neighboring amino acids of the same helix. In β-sheets all such hydrogen bonds occur between amino acids in different strands, alternating between the right and left neighbor.

2.8.2 Protein structural motives

The secondary structure of proteins includes four particularly common structural motives: first α-helix, where the polypeptide backbone is coiled in a right-handed helix and the hydrogen bonding occurs between successive turns of the helix. Second β-sheets, the strands of polypeptide are stretched out and lay either parallel (all carboxy-terminal ends are at the same side) or antiparallel to one another, where the hydrogen bonds form between the strands. α-helices and β-sheets are periodic structures allow the amides to hydrogen bond very efficiently

with one another. The other elements of secondary structure include β-turns and unordered structure. β-turns are sharp turns which connect the adjacent strands in an antiparallel β-sheet. The unordered structure is generally loops which form near the surface of proteins and join the other elements of secondary structure, also these areas have an important function, because they add flexibility to the protein and allow for conformational changes (Surewicz et al, 1988; Richardson 1981).

In our work we aim to study and analyze the binding properties between pentobarbital or propofol and HSA including binding mechanism, binding constant, and the main sorts of binding force at 293 K by using fluorescence spectroscopy, and UV-absorption spectroscopy. Another goal of this work was to check the effect of pentobarbital and propofol on HSA secondary structure changes using FTIR spectroscopy.

Chapter Three

Experimental Part

Chapter Three

Experimental Part

This chapter contains three sections. In the first section, information about the samples and their preparation for experiments is given. The second section describes briefly the UV-VIS spectrophotometer (NanoDrop ND-1000), Fluorospectrometer (NanoDrop 3300), and Bruker IFS 66/S spectrophotometer that are used in my study. And the third section deals with the experimental procedures which used in this work.

3.1 Materials and sample preparations

Human serum albumin (HSA) (fatty acid free), was used without further purification. Its molecular weight is 66.5 KDa. 4 % (wt/v), pentobarbital with a chemical formula ($C_{11}H_{18}N_2O_3$) and a molecular weight 226.3 $g.mol^{-1}$, propofol (2, 6-Diisopropylphenol) with a chemical formula ($C_{12}H_{18}O$) and a molecular weight 178.3 $g.mol^{-1}$, and phosphate buffer saline is used to prepare the sample. All above chemicals were purchased from Sigma Aldrich Co. Optical grade silicon windows (NICODOM Ltd) are used as spectroscopic cell windows. The optical transmission is high with little or no distortion of the transmitted signal. The 100% line of a NICODOM silicon window shows that the silicon bands in the MIR region do not exhibit total absorption and can be easily subtracted. These windows were purchased from Sigma Aldrich Company.

The measurements were carried out using several samples in the form of thin films of HSA, pentobarbital mixed with HSA, and propofol mixed with HSA.

3.1.1 Phosphate buffer saline solution

Phosphate buffer saline was directly prepared by dissolving one foil pouch in one liter double distilled water.

Human serum albumin stock solution

Human serum albumin was dissolved in phosphate buffer saline (pH=7.4) at (80 mg/ml).

3.1.2 Pentobarbital stock solutions

The molar concentration of stock pentobarbital solution is 0.265M. The desired concentrations acheived by using the molarity dilution equation ($M_iV_i=M_fV_f$). The follwowing concentrations of pentobarbital (0.96, 0.48, 0.24,0.12, 0.06, 0.03, and 0.015 mM) were prepared in phosphate buffer solution (pH=7.4).

3.1.3 Propofol stock solutions

The density of propofol is 962 gL^{-1}, and the molecular weight is 178.28 $g.mol^{-1}$, by dividing the density over the molecular weight; a molarity of (5.396 $mol.g^{-1}$ = 5.396 M) is obtained. Different concentrations of propofol (1.92, 1.44, 0.96, 0.48, and 0.24 mM) were prepared in phosphate buffer solution(pH=7.4) by using the molarity dilution equation.

3.1.4 HSA-pentobarbital solutions

The final concentration of HSA-drug solutions were prepared by mixing equal volume of protein and pentobarbital solution. HSA concentration in all samples is 40mg/ml. However, the concentration of pentobarbital in the final protein drug solutions is 0.48, 0.24, 0.12, 0.06, 0.03, 0.015, and 0.0075 mM.

3.1.6 HSA-propofol solutions

The final concentration of HSA-drug solutions were prepared by mixing equal volume of protein and propofol solution. HSA concentration in all samples is 40mg/ml. However, the concentration of propofol in the final protein drug solutions is 1.92, 1.44, 0.96, 0.48, and 0.24 mM.

3.1.7 Thin film preparations

50 µL of each sample were applied on silicon window.Then evaporated to complete dryness over night before measurements.

3.2 Instruments

The following instruments have been used in taking the required measurements.

3.2.1 UV-VIS spectrophotometer

UV-VIS spectrophotometer (NanoDrop ND-1000) is used to measure the spectrum of the samples in the range between 220-750nm, with high accuracy and reproducibility. 1-2 µL samples are sufficient to ensure accurate and reproducible results when measuring the sample solutions. It is critical that the liquid column be formed so that the gap between the upper and lower measurement pedestals is bridged with sample, and the light path is completely covered by the sample. ND-1000 has the capability to measure highly concentrated samples without dilution. The excitation is done on 210 nm and the emission occurs at 280nm.

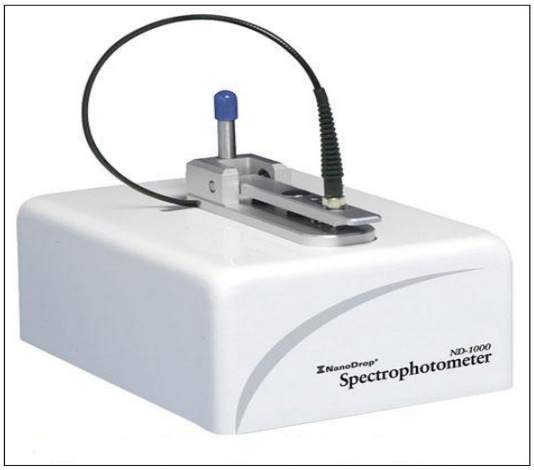

Apparatus of NanoDrop ND-1000

3.2.2 Fluorospectrometer

Fluorospectrometer (NanoDrop 3300) is used to study fluorescent measurements. The uniquely clean optics of the retention system (surface tension), combined with proprietary signal processing for the White LED applications, enables measurements across a wide range of wavelengths using sample volumes of 1–2 µL without cuvettes and costly filter changes. The excitation source comes from one of three solid-state light emitting diodes (LED's), which are oriented 90° to the detector. The excitation source options include: UV LED with maximum excitation 365 nm, blue LED with excitation 470nm, and white LED from 500-650 nm excitation. A 2048-element CCD array detector covering 400 – 750 nm is connected by an optical fiber to the optical measurement surface. The excitation is done at the wavelength of 360 nm and the maximum emission wavelength is at 443 nm. The spectrometer is configured with a cut filter to eliminate light transmission below 395 nm. The image below lists some of common fluorophores that can be measured using the NanoDrop 3300 along with the most appropriate excitation LED.

Apparatus of NanoDrop 3300

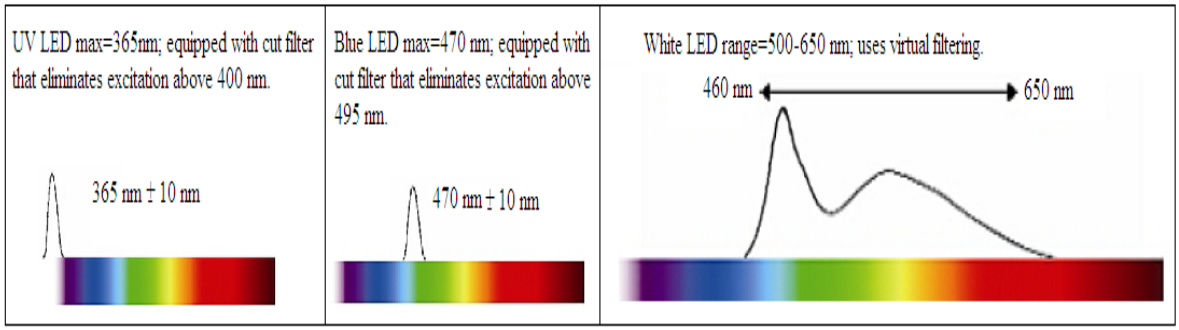

3.2.3 Fourier Transform Infrared Spectroscopy

The FTIR measurements were obtained on a Bruker IFS 66/S spectrophotometer equipped with a liquid nitrogen-cooled MCT detector and a KBr beam splitter. The spectrometer was continuously purged with dry air during the measurements.

There are three basic spectrometer components in an FT system: radiation source (Infrared radiation), interferometer (Michelson interferometer), and detector. The Michelson interferometer, which produces interference signals, that contain infrared spectral information generated after passing through a sample, and measured as a function of optical path difference by a detector, consists of three active components fixed mirror, moving mirror, and a beamsplitter as shown in (Fig. 3.1). The two mirrors are perpendicular to each other, and the beamsplitter is a semi reflecting device which is often made by depositing a thin film of germanium onto a flat KBr substrate.

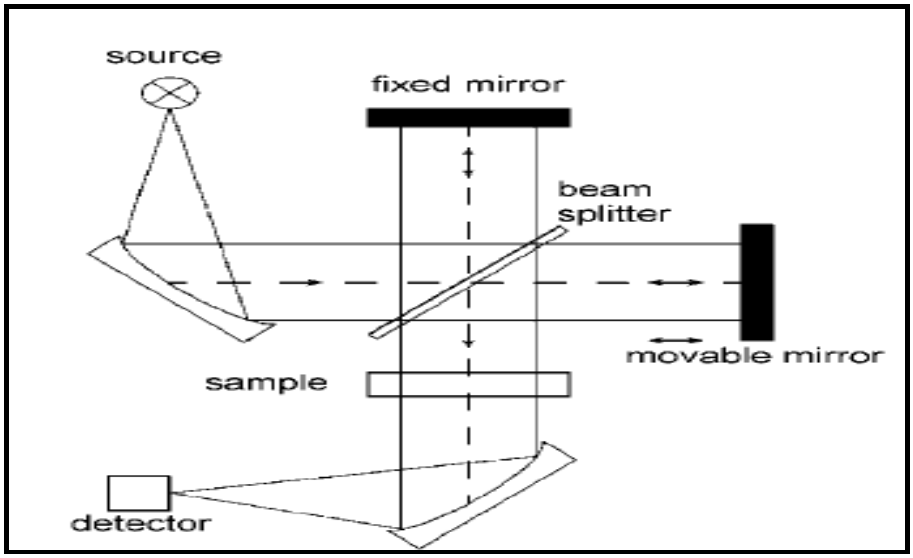

Figure3.1: Optical layout of Michelson interferometer in Fourier transforms infrared spectrometer.

Radiation from the broadband infrared source is collimated and directed into the interferometer, and impinges on the beamsplitter. Half of the infrared beam is transmitted to the fixed mirror and the remaining half is reflected to the moving mirror, at the beamsplitter. Then the reflected beams from the two mirrors are recombined at the beamsplitter. An interference pattern (interferogram) is generated due to changes in the relative position of the moving mirror to the fixed mirror. The resulting beam then passes through the sample and is eventually focused on the detector. The interferogram contains information over the entire Infrared region to which the detector is responsive. Finally a mathematical operation known as Fourier transformation converts the interferogram (The time domain spectrum displaying intensity versus time within the mirror scan) to the final Infrared spectrum, which is the frequency domain spectrum showing intensity versus frequency. The two most popular detectors for a FTIR spectrometer are deuterated triglycine sulfate (DTGS) which is pyroelectric detector that delivers rapid responses because it measures the changes in temperature rather than the value of temperature, and mercury cadmium telluride (MCT) which is a photon (or quantum) detector that depends on the quantum nature of radiation and

also exhibits very fast responses. Whereas DTGS detectors operate at room temperature, MCT detectors must be maintained at liquid nitrogen temperature (77 °K) to be effective.
Other equipment such as Digital balance, pH meter, vortex, plate stirr, and micropipettes were used. Volumetric flasks, beakers, test tubes, petrideshes, and apendroffes were used in sample preparations.

3.2 Experimental procedures

3.3.1 UV-VIS Spectrophotometer procedure

A 1 µL sample is pipetted onto the end of a fiber optic cable (the receiving fiber). A second fiber optic cable (the source fiber) is then brought into contact with the liquid sample causing the liquid to bridge the gap between the fiber optic ends. The gap is controlled to a 1mm path. A pulsed xenon flash lamp provides the light source and a spectrometer utilizing a linear CCD array is used to analyze the light after passing through the sample. The instrument is controlled by special software run from a PC, and the data is logged in an archive file on the PC.
The main steps of measuring samples are:

1. Open the sampling arm and, a small quantity (1 µL) of the sample solution was pipetted onto the lower measurement pedestal.

2. Close the sampling arm and 1initiate a spectral measurement using the operating software on the PC. The sample column is automatically drawn between the upper and lower measurement pedestals and the spectral measurement made.

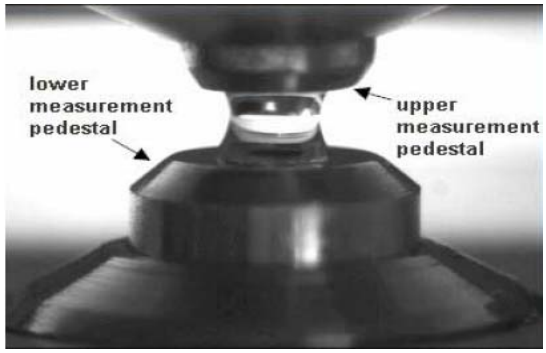

3. When the measurement is complete, open the sampling arm and wipe the sample from both the upper and lower pedestals using a soft laboratory wipe.

Upon completion of each sample measurement, wiping the sample from the upper and lower pedestals is sufficient to prevent sample carryover and avoid residue build up. However, after measuring a large number of samples, it may be necessary to clean the areas around the upper and lower pedestals thoroughly. It is best to use a precision pipettor (0-2 μL) with precision tips to assure that sufficient sample (1-2 μL) is used.

The A280 method is applicable to purified proteins exhibiting absorbance at 280nm. This module displays the UV spectrum, measures the protein's absorbance at 280 nm (A280) and calculates the concentration (mg/ml).

When the NanoDrop ND-1000 spectrophotometer is blanked, a spectrum is taken of a reference material (blank) and stored in memory as an array of light intensities by wavelength. When a measurement of a sample is taken, the intensity of light that has transmitted through the sample is recorded. The sample intensities along with the blank intensities are used to calculate the sample absorbance according to the following equation:

$$\textbf{Absorbance} = -\log\left(\textbf{Intensity}_{\textbf{sample}} / \textbf{Intensity}_{\textbf{blank}}\right)$$

Thus, the measured light intensity of both the sample and of the blank are required to calculate the absorbance at a given wavelength.

The Beer-Lambert equation is used to correlate the calculated absorbance with concentration: **A= ε.b.L** where **A** is the absorbance represented in absorbance units (A), **ε** is the molar

absorptivity coefficient (or extinction coefficient) with units of $Lmol^{-1}cm^{-1}$, **b** is the path length in cm, and **L** is the sample concentration in moles/liter or molarity (M).

3.3.2 Fluorospectrometer procedure

A 1-2 µL sample is pipetted onto the end of the lower measurement pedestal (the receiving fiber). A non-reflective "bushing" attached to the arm is then brought into contact with the liquid sample causing the liquid to bridge the gap between it and the receiving fiber. The gap, or pathlength, is controlled to 1mm. Following excitation with one of the three LEDs, emitted light from the sample passing through the receiving fiber is captured by the spectrometer. The NanoDrop 3300 is controlled by software run from a PC.
The main steps for making a measurement are:

1. Open the sampling arm and a small quantity (1 µL) of the sample solution was pipetted onto the lower measurement pedestal.

2. Close the sampling arm and initiate a measurement using the operating software on the PC. The sample column is automatically drawn between the upper bushing and the lower measurement pedestal and the measurement is made.

3. When the measurement is complete, open the sampling arm and blot the sample from both the upper bushing and the lower pedestal using low lint laboratory wipe.

Blotting the sample from the upper bushing and lower pedestal upon completion of each sample measurement is usually sufficient to prevent sample carryover and avoid residue buildup. Although generally, 2 µl water aliquots can be used to clean the measurement surfaces to ensure no residual sample is retained on either the pedestal or the bushing.

3.3.3 Fourier transform infrared spectroscopy procedure

The absorption spectra for silicon window alone, phosphate buffer saline, free HSA, pentobarbital, and propofol on silicon window in the wave number range of 4000 – 400 cm^{-1} are obtained as background spectra and these spectra are shown in (Figures 3.2-3.6).

Each spectrum is taken as an average of 60 scans to increase the signal to noise ratio, and the spectral resolution was at 4 cm^{-1}. The aperture used in this study was 8 mm, since we found that this aperture gives best signal to noise ratio. Baseline correction, normalization and peak areas calculations were performed for all the spectra by OPUS software (optics user software). The peak positions were determined using the second derivative of the spectra.

The infrared spectra of HSA, pentobarbital–HSA complex, and propofol-HSA complex were obtained in the region of 1800–1000 cm^{-1}. The FTIR spectrum of free HSA was acquired by subtracting the absorption spectrum of the buffer solution from the spectrum of the protein solution. For the net interaction effect, the difference spectra {(protein and pentobarbital/propofol solution) – (protein solution)} were generated using the featureless region of the protein solution 1800-2200 cm^{-1} as an internal standard (Surewicz et al, 1993).

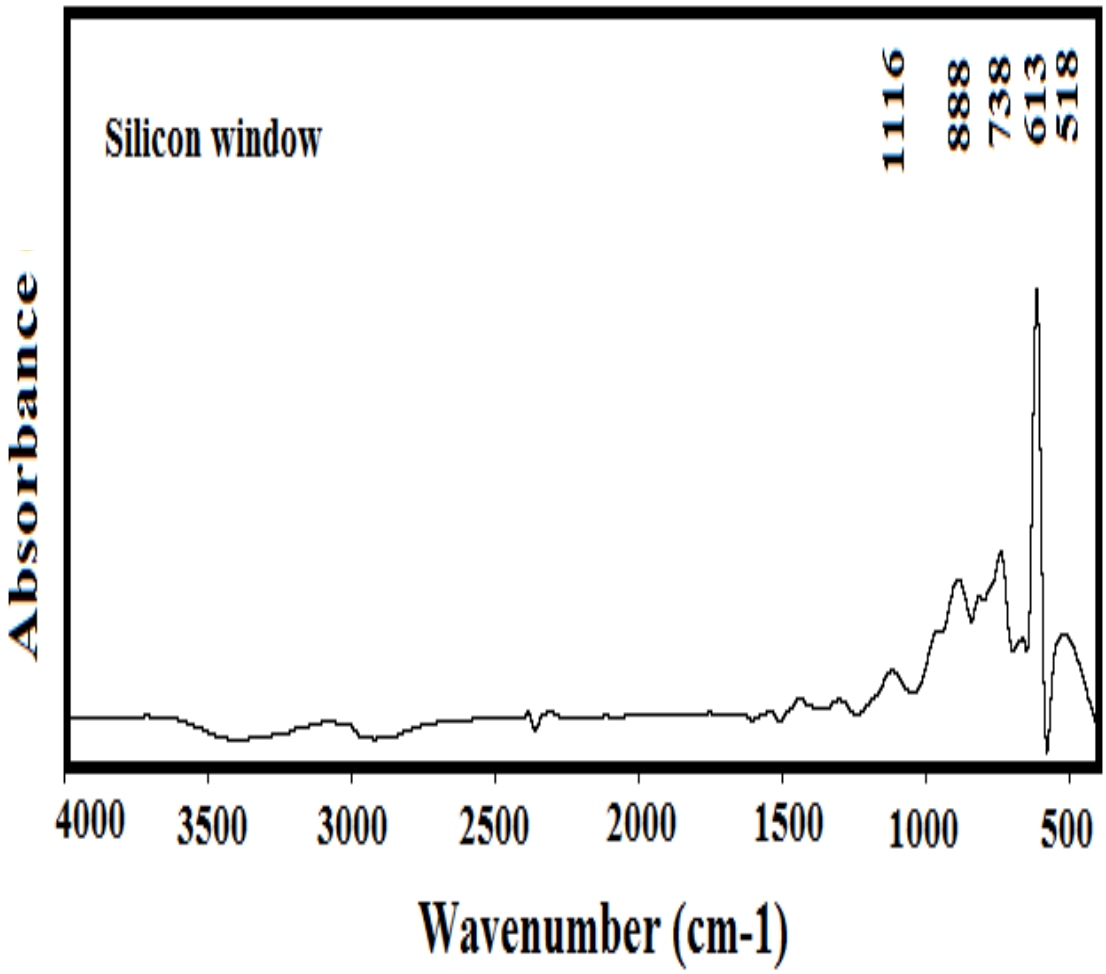

Figure 3.2: FTIR spectra of silicon window in the region of 4000-400 cm^{-1}.

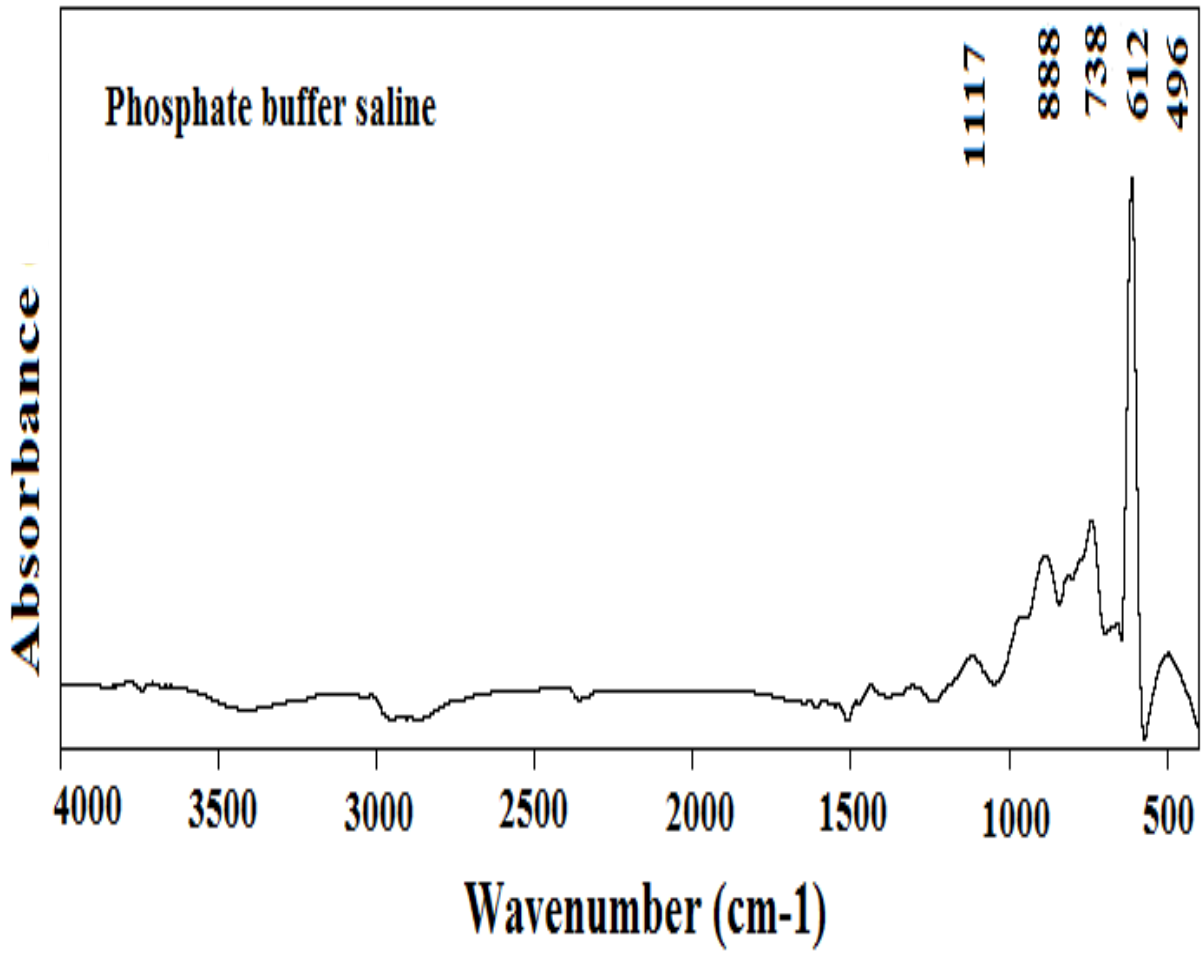

Figure 3.3: FTIR spectra of phosphate buffer saline in the region of 4000-400cm^{-1}.

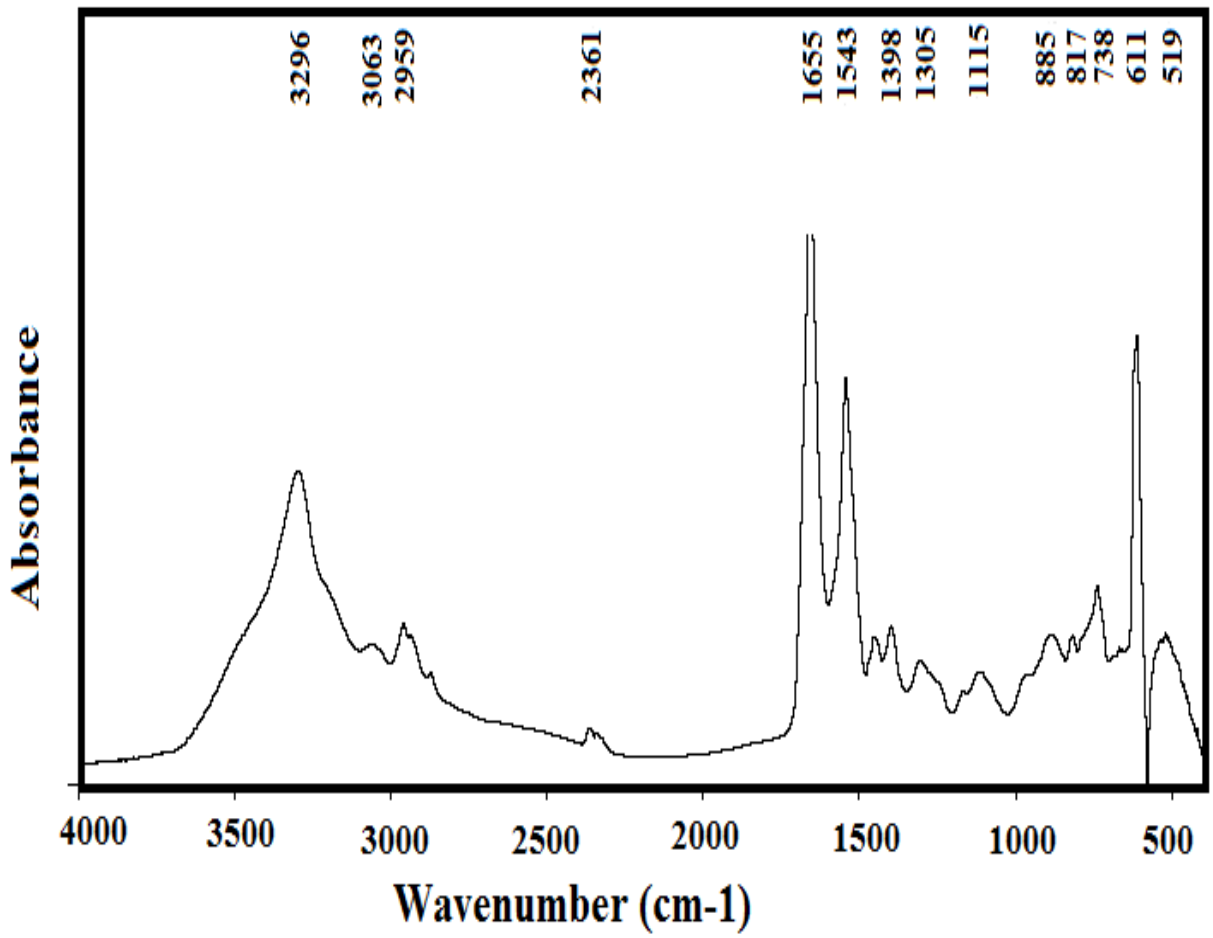

Figure 3.4: FTIR spectra of free HSA in the region of 4000-400cm^{-1}.

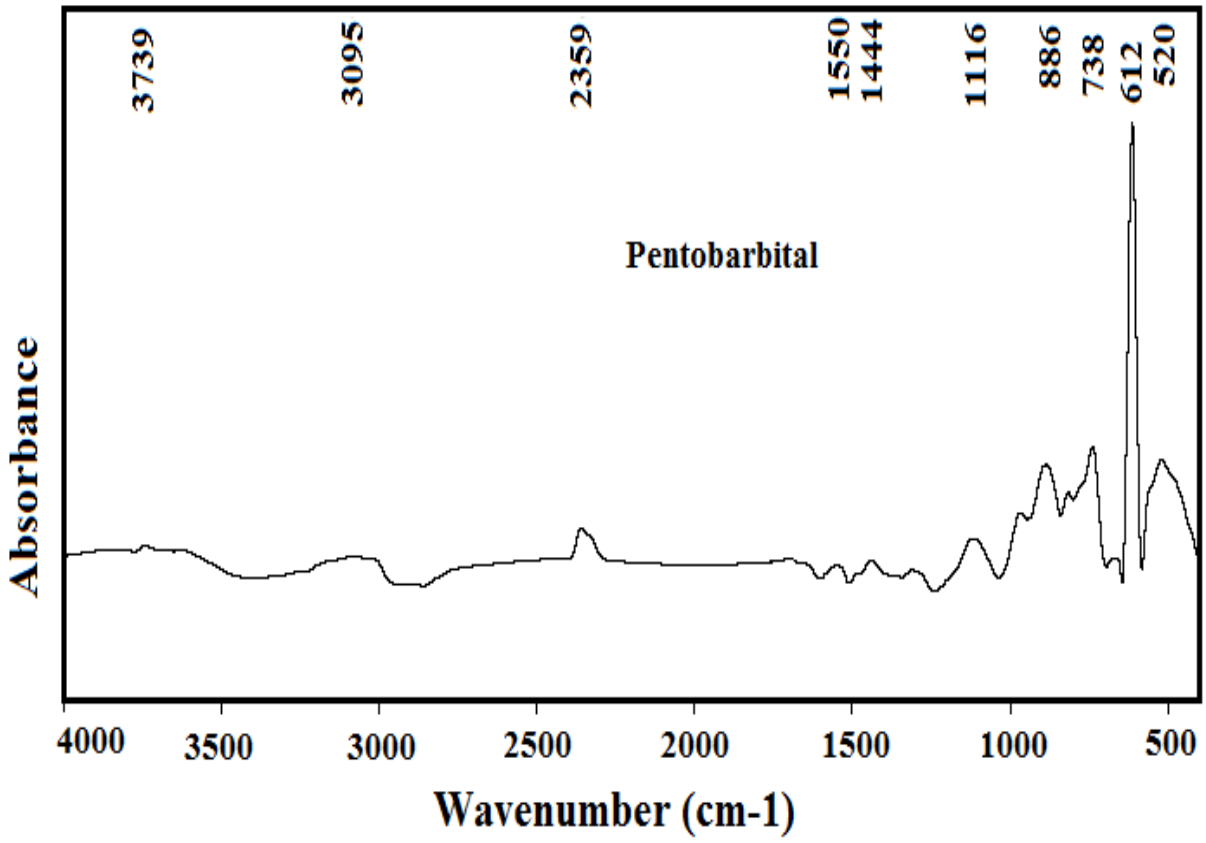

Figure 3.5: FTIR spectra of pentobarbital in the region of 4000-400cm^{-1}.

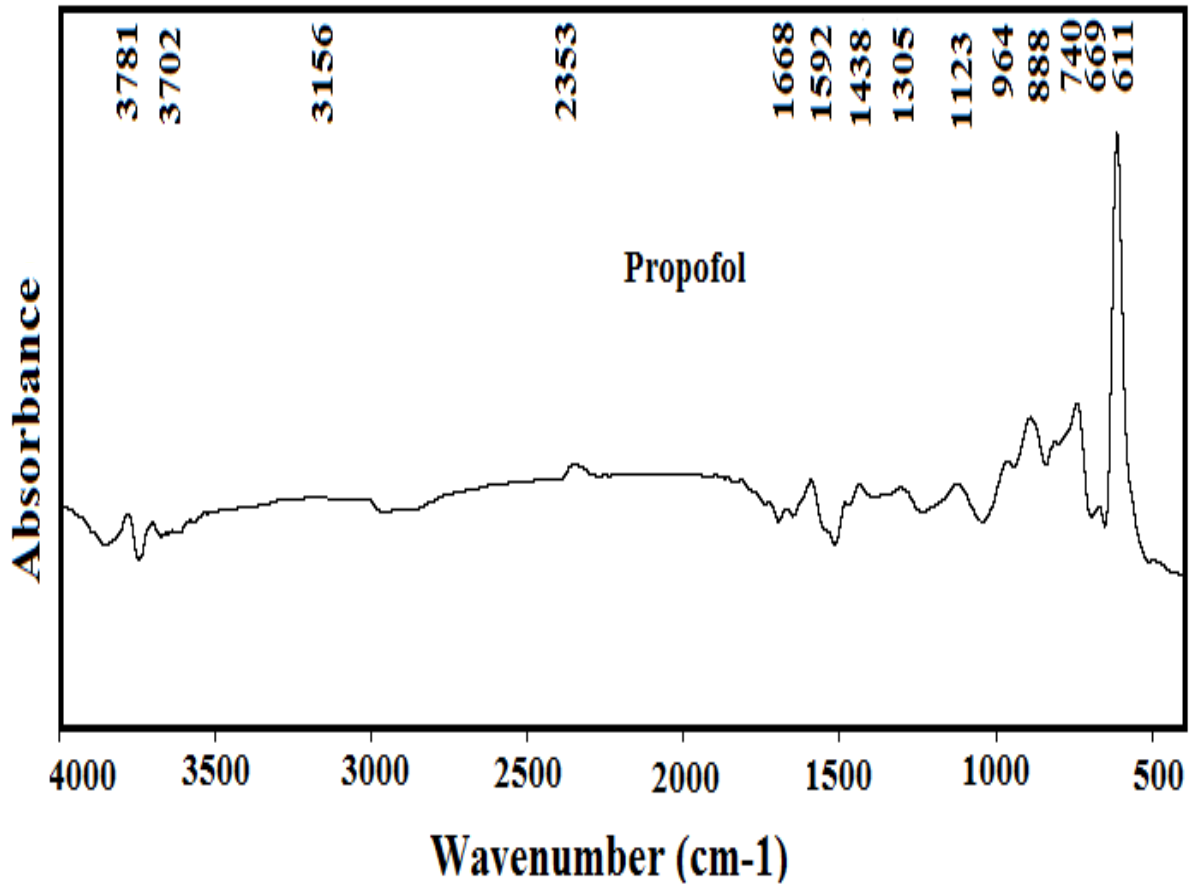

Figure 3.6: FTIR spectra of propofol in the region of 4000-400cm^{-1}.

3.3.3.1 FTIR data processing tasks

The advantage of an FTIR instrument is that high speed and sensitivity, where it acquires the interferogram in less than a second. Modern FTIR spectrometers are usually equipped with a powerful, computerized data system. It can perform a wide variety of data processing tasks such as Fourier transformation, spectral subtraction, baseline correction, smoothing, integration, curve fitting, Fourier self- deconvolution and library searching (Bell, 1972).

In our study several tasks are used to analyze data:

1. Baseline correction

The offset correction is performed by selecting a single point of multiple points on a spectrum and adding or subtracting a y value (intensity value) from the point or points to correct the baseline offset. This preprocessing step is used to align the baseline of two or more spectra causing them to overlap, or it is used to bring the minimum point to zero.

2. Derivatives

Derivatives are used to remove offset and slope due to background differences. In our study the second derivative is used for FTIR spectrum for free HSA, and the spectra for HSA with different concentrations of drugs (Workman, 1998).

3. Fourier self- deconvolution

Fourier self-deconvolution is the most widely used band narrowing technique in infrared spectroscopy of biological materials (Kauppinnen et al, 1981). The goal of Fourier self-deconvolution is to enhance the apparent resolution of a spectrum, or to decrease the line width. Spectral ranges comprising broad and overlapping lines can thus be separated into sharp single lines.

In general, the deconvolution corresponds to a multiplication of the interferogram I(x) using the exp (a*x) deconvolution function for lorentzian and exp (a*x*x) for gaussian shapes, which intensifies the interferogram edges. The deconvolution factor is the maximum value of these functions at the end of the interferogram. Deconvolution factors of 100, 1000 and 5000 correspond to a maximum amplification of 3.4, 12.8, and 40 in case of lorentzian shapes, and 1.06, 3.2 and 16 in case of gaussian shapes. If you work with Lorentzian shapes it is recommended to increase the deconvolution factor in the order 50, 100, 1000, 5000, and to stop if the resultant spectrum shows artificial oscillations (BRUKER, 2004). Successful application of Fourier self deconvolution to overlapping absorption bands can significantly enhance peak separation. The application of deconvolution to the amide I, amide II, amide III regions of proteins reveals the existence of considerable fine structure for most proteins (Workman, 1998).

4. Curve fitting

The curve fitting command allows calculating single components in a system of overlapping bands. A model consisting of an estimated number of bands and a baseline should be generated before the fitting calculation is started. The model can be set up interactively on the display and is optimized during the calculation (BRUKER, 2004).

Chapter Four

Results and Discussion

Chapter Four

Results and Discussion

In this chapter, the major experimental results are presented. The first section deals with UV-absorption spectra. In the second section, the fluorescence spectroscopy results will be shown and discussed. The last section will talk about Fourier transform infrared (FTIR) spectroscopy results.

4.1 UV-absorption spectroscopy

HSA-drug systems with different concentrations of pentobarbital and propofol were recorded and the absorption spectra are shown in (Fig.4.1, and Fig.4.2). The excitation has been done on 210 nm and the absorption is recorded at 280 nm. The UV absorbance intensity of HSA increased with the increasing of pentobarbital and propofol concentration. In addition, the binding of the drugs to HSA resulted in a slight shift of the HSA absorption spectrum. These results clearly indicated that an interaction and some complex formation occurred between HSA and the two drugs separately. It is evident from the spectra of the pure drugs the little or no absorption affect which supports that the resulted peaks are due to the interaction between the drugs and HSA.

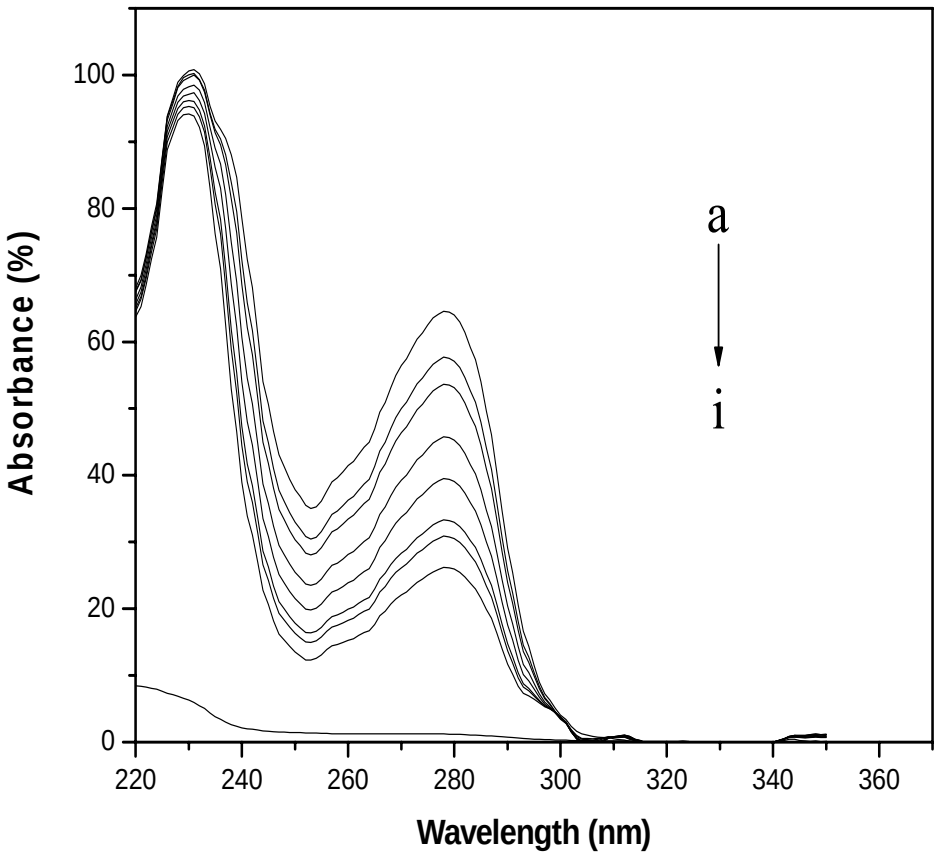

Figure 4.1: UV-absorbance spectra of HSA with different concentrations of pentobarbital (a=0.48 mM, b=0.24 mM, c=0.12mM, d=0.06 mM, e=0.03 mM, f=0.015 mM, g=0.0075 mM, h=0.00 mM and i = pentobarbital).

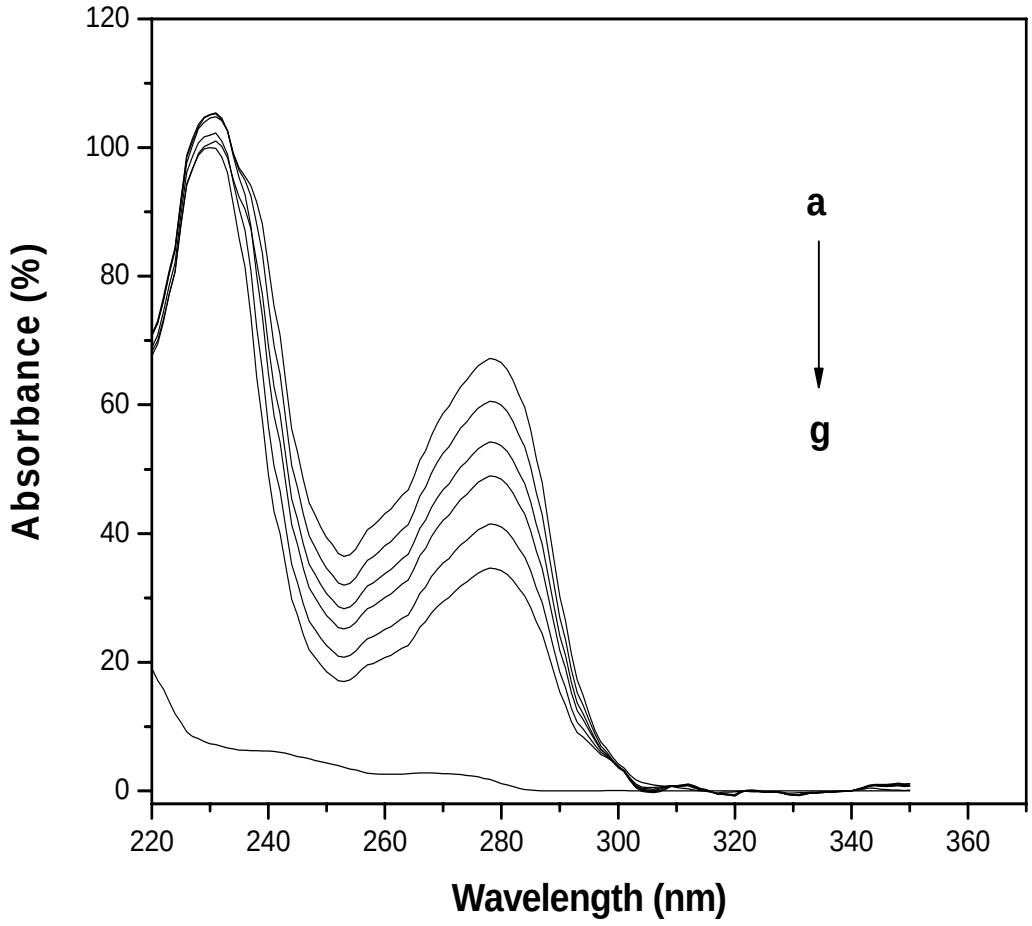

Figure 4.2: UV-absorbance spectra of HSA with different concentrations of propofol (a=1.92 mM, b=1.44 mM, c=0.96 mM, d=0.48 mM, e= 0.24 mM, f=0.00 mM and g= propofol).

4.1.1 Determination of binding constants (K) by UV absorption spectroscopy

The binding constants can be determined using UV absorption spectroscopy as reported for several drug- protein complexes (Stephanos et al, 1996; Klotz et al, 1971; Klotz, 1982; stephanos and farina et al, 1996). By assuming that there is only one type of interaction between pentobarbital or propofol and HSA in aqueous solution, leads to establish equations. (1) and (2) as follows:

HSA + Pentobarbital ↔ Pentobarbital: HSA **(1)**

HSA + Propofol ↔ Propofol: HSA

K = [pentobarbital: HSA]/ [pentobarbital][HSA] **(2)**

K = [propofol: HSA]/ [propofol][HSA]

For the weak-binding cases, the absorption data were treated using linear double reciprocal plots based on the following equation (Kragh-Hansen, 1981).

$$\frac{1}{A - A_0} = \frac{1}{A_\infty - A_0} + \frac{1}{K[A_\infty - A_0]} \cdot \frac{1}{L} \qquad \textbf{(3)}$$

Where A_0 corresponds to the initial absorption of protein at 280 nm in the absence of ligand, A_∞ is the final absorption of the ligated-protein, and A is the recorded absorption at different pentobarbital or propofol concentrations (L).

In order to determine the binding constant (K) by UV-visible spectroscopy we plot 1/ ($A-A_0$) vs. 1/ (L). The double reciprocal plot of 1/ ($A-A_0$) vs. 1/ (L) is linear and the binding constant (K) can be estimated from the ratio of the intercept to the slope (Fig.4.3, and Fig.4.4). The overall binding constant K for pentobarbital-HSA complexes and propofol-HSA complexes are estimated to be 1.812×10^4 M^{-1}, $2.55x10^3$ M^{-1} respectively. The binding constant value obtained are indicative of a relatively weak pentobarbital-HSA and propofol-HSA interaction with respect to the other strong drug-HSA complexes with binding constants in the range of 10^5 and 10^6 M^{-1} (Purcell et al, 2000). The relative weakness of the binding constants may

account for the fast effectiveness of these sedative drugs. It is suggested that the relatively weaker binding drugs such as propofol, might be more effective at competing with the other drugs for binding to HSA. This is due to their availability at sufficiently high concentrations to interact, at least potentially, with a large fraction of the HSA molecules (Bhattacharya et al, 2000). The weak binding of propofol to HSA may contribute to make propofol an ultra–short-acting sedative-hypnotic agent. The reason for the low stability of the pentobarbital-HSA complexes and the propofol-HSA complexes can be attributed to the presence of mainly hydrogen bonding interaction between protein donor atoms and the pentobarbital/propofol polar groups or an indirect drug-protein interaction through water molecules (Sulkowaska et al, 2002).

It has been proposed that anesthetic drugs may exert their effects on proteins at the molecular level by attenuating the movement of the local amino acid side chains, which is in turn postulated to stabilize certain protein conformations and, hence, affect function (stephanos et al, 1996).

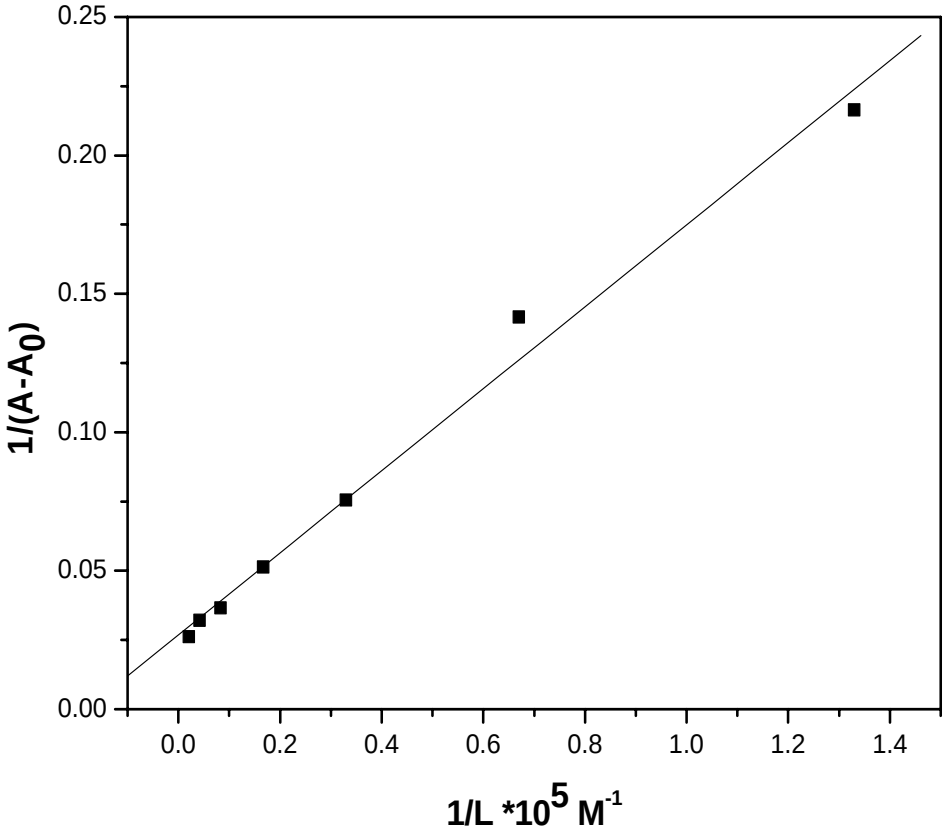

Figure 4.3: The plot of 1/ ($A-A_0$) vs. 1/L for HSA with different concentrations of pentobarbital.

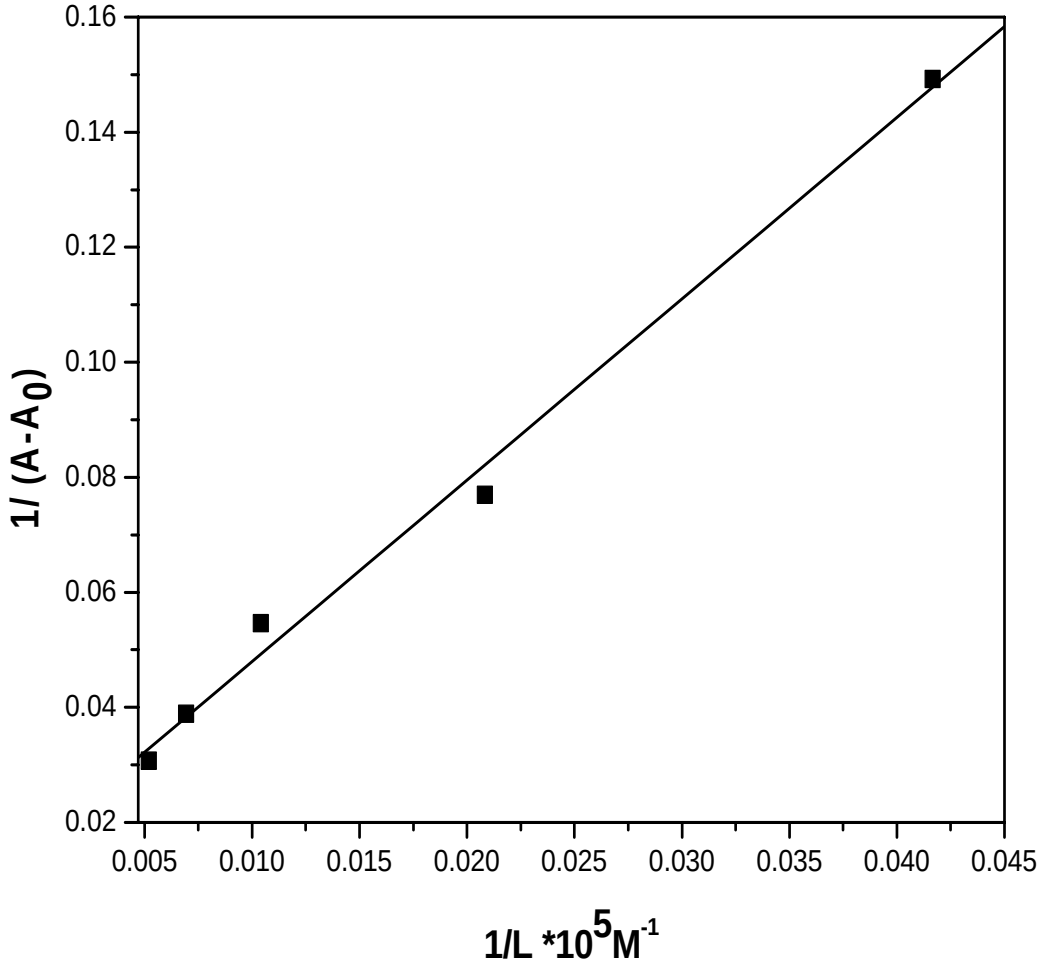

Figure 4.4: The plot of 1/ ($A-A_0$) vs. 1/L for HSA with different concentrations of propofol.

4.2 Fluorescence spectroscopy

Fluorescence spectroscopy methods are widely used to study binding between ligands and proteins. There are three amino acid residues in proteins which are responsible for intrinsic fluorescence of the protein: tyrosine (Tyr), phenylalanine (Phe), and tryptophan (Trp). Actually, the intrinsic fluorescence of HSA is almost contributed by tryptophan alone, because phenylalanine has a very low quantum yield and the fluorescence of tyrosine is almost totally quenched if it is ionized or near an amino group, a carboxyl group, or a tryptophan residue (Gerbanowski et al, 1999).

Fluorescence intensity of a compound can be decreased by a variety of molecular interactions such as molecular rearrangements, excited-state reactions, energy transfer, ground state complex formation, and collisional quenching. Such a decrease in intensity is called quenching (Fang-Ying et al, 2006). In our experiment for HSA-pentobarbital or propofol we have used λ_{ex} at 360nm and the observed λ emission is 439nm, and 443nm respectively. The fluorescence sensor is based on intramolecular charge transfer (ICT), which is highly sensitive to the polarity of microenvironment. Therefore, it is expected to act as fluorescent probe for some biochemical system like proteins (Tian et al, 2003).

The fluorescence emission spectra of HSA at various concentrations of pentobarbital (0.75, 1.5, 3.0, 6.0, 12.0, 24.0, and 48.0) $\times 10^{-5}$ mol L^{-1} are shown in (Fig.4.5). Also the fluorescence emission spectra of HSA at various concentrations of propofol (24, 48, 96, 144, and 192) $\times 10^{-5}$ mol L^{-1} are shown in (Fig.4.6). As we can see in (Fig.4.5, and Fig.4.6), the fluorescence emission spectra of HSA at various concentrations of pentobarbital or propofol showed that HSA had a strong fluorescence emission band at 439 nm, and 443nm respectively. Also it can be seen that the fluorescence emission intensity of HSA decreased regularly with the increase of concentration of pentobarbital or propofol without changing the shape of the peaks. At the same time, a relatively small shift of the maximum emission wavelength occurred. These results indicated that the interaction took place between pentobarbital or propofol and HSA. And the polarity of microenvironment was changed after the addition of pentobarbital or

propofol. The shift in the position of emission peak corresponds to the changes in the polarity around the chromophore molecule.

It is concluded that the changes of the HSA secondary structure is related not only due to the fluorescence quenching extent but also to the shifts of fluorescence emission wavelength when protein interacts with the two drugs. The aromatic ring and the carbonyl groups in the pentobarbital molecule, and the aromatic ring and the hydroxyl group in the propofol molecule can interact with protein's hydrophobic and basic amino acid residues respectively. But the interaction details and distribution of drug molecules for various HSA–drug complexes may be different depending on the structure of the drugs.

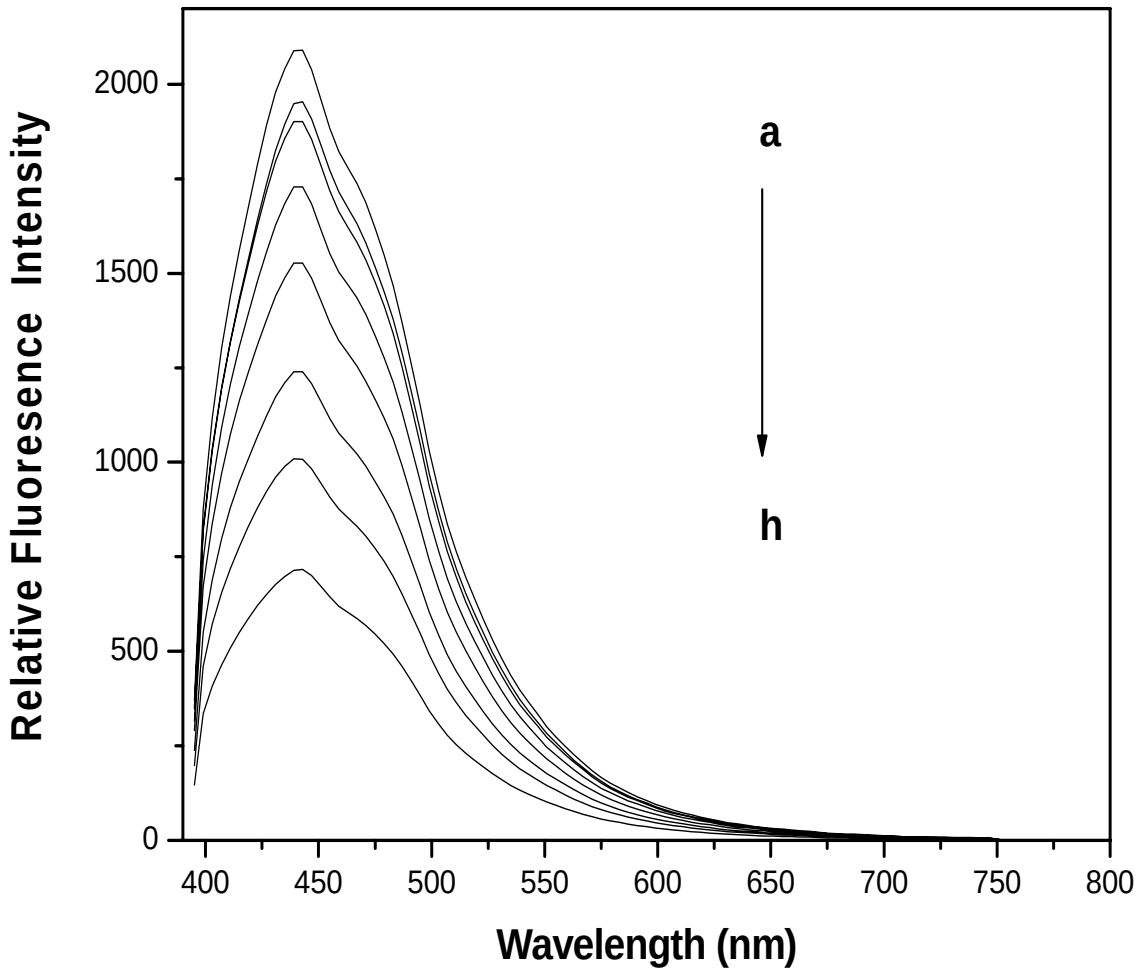

Figure 4.5: Fluorescence emission spectra of HSA in the absence and presence of pentobarbital in these concentrations (a=0.0mM, b=0.0075mM, c=0.015mM, d=0.03mM, e=0.06mM, f=0.12mM, g=0.24mM and h=0.48mM).

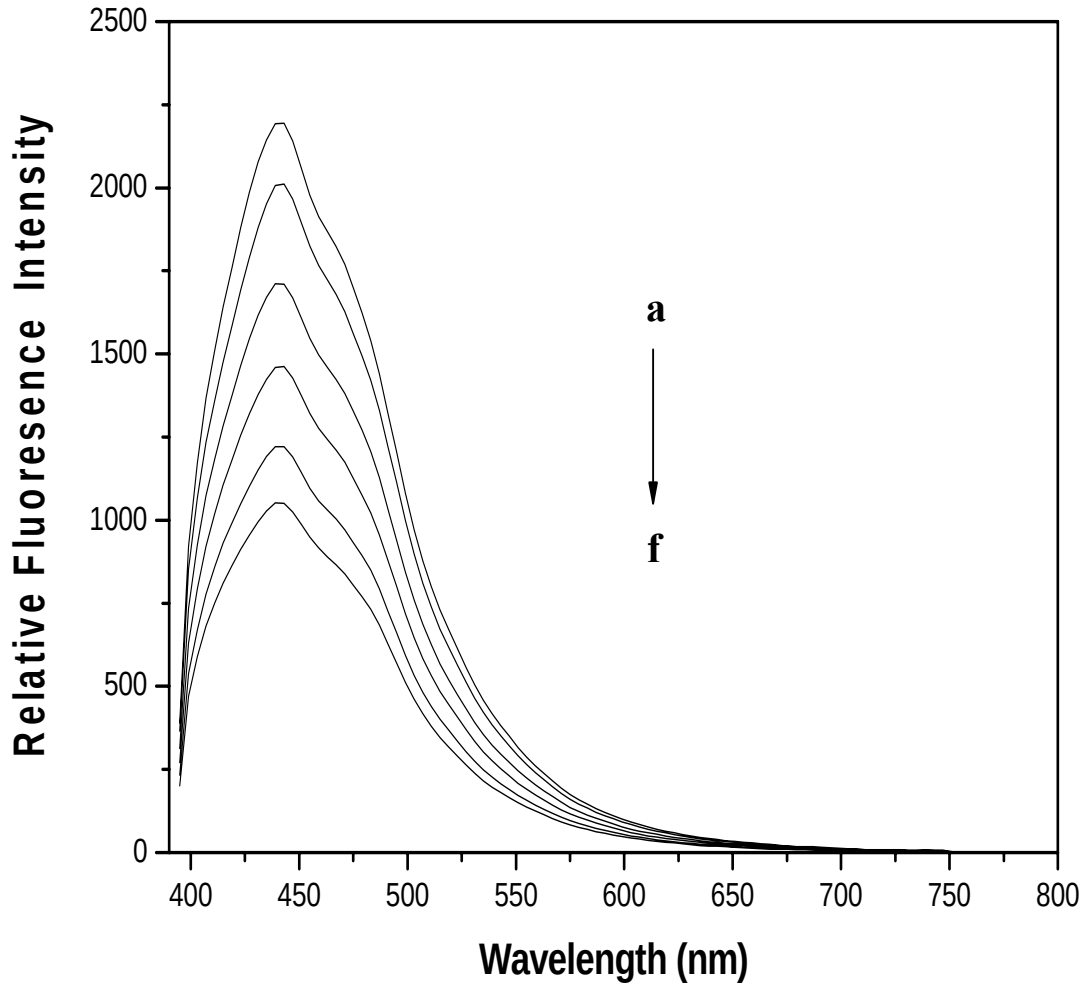

Figure 4.6: Fluorescence emission spectra of HSA in the absence and presence of propofol in these concentrations (a=0.0mM, b=0.24mM, c=0.48mM, d=0.96mM, e=1.44mM and f=1.92).

4.2.1 Determination of Stern-Volmer quenching constants (K_{sv}) and the quenching rate constant of the biomolecule (K_q)

For fluorescence dynamic quenching, the decrease in intensity is described by the well-known Stern–Volmer equation (Chen et al, 1990).

$$\frac{F_0}{F} = 1 + K_q \tau_0 (L) = 1 + K_{sv} (L) \qquad (4)$$

Where F and F_0 are the fluorescence intensities with and without quencher, K_{sv} is the Stern-Volmer quenching constant, and (L) is the concentration of pentobarbital or propofol. The Stern–Volmer quenching constants K_{sv} were obtained by the slope of regression curve according the above Equation (4) at different drug concentrations. As we can see from (Fig. 4.7, Fig.4.8), the Stern-Volmer plots for HSA-pentobarbital or propofol complexes are linear and the slopes are equal to K_{sv} (3.875×10^7 L mol^{-1}, 9.686×10^6 L mol^{-1}), respectively. Three quenching processes are known as static, dynamic and non-radioactive transfer quenching.Fluorescence quenching can be induced by different mechanisms, which were usually classified into dynamic quenching and static quenching. Dynamic quenching arises from collisional encounters between the fluorophore and quencher, and static quenching resulting from the formation of a ground state complex between the fluorophore and the quencher (Lakowicz, 2006).

The linear dependence in Stern–Vollmer coordinates indicates homogeneous quenching (dynamic or static) in this system. By assuming that dynamic quenching occurs, the Stern–Volmer quenching constant can be represented as $\mathbf{K_{SV} = Kq.\tau_0}$, where K_q is the quenching rate constant of the biomolecule and τ_0 is the average lifetime of the biomolecule without quencher. According to the literature, the fluorescence life time τ_0 for HSA is about 10^{-8} s (Lakowicz et al, 1973). The obtained values of quenching rate constants K_q are 3.875×10^{15} L $mol^{-1}s^{-1}$, 9.686×10^{14} L $mol^{-1}s^{-1}$ are much larger than the maximum dynamic quenching constant for various quenchers with biopolymer (2×10^{10} L.mol^{-1}.s^{-1}) (Wang et al, 2008). So these results confirm that the dynamic quenching is not the main mechanism which causes the

fluorescence quenching, and the decrease in fluorescence intensity can be considered as the result of static quenching. This implies that the quenching is initiated by the formation of a complex (Jiang et al, 2003).

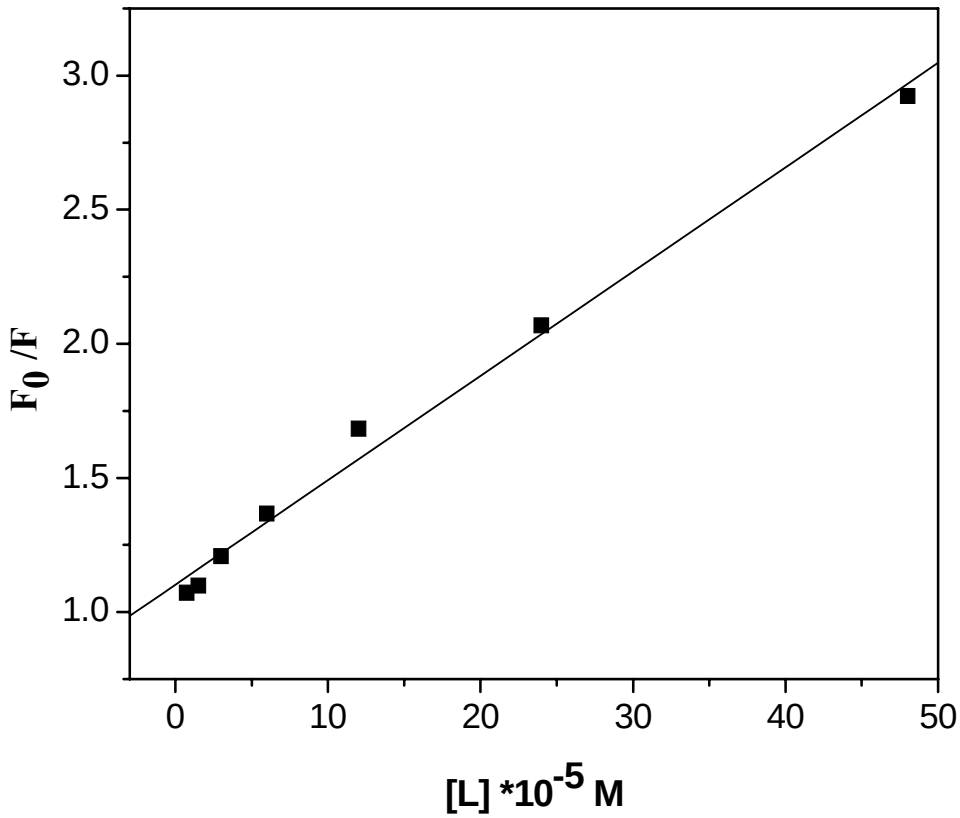

Figure 4.7: The Stern-Volmer plot for pentobarbital-HSA system.

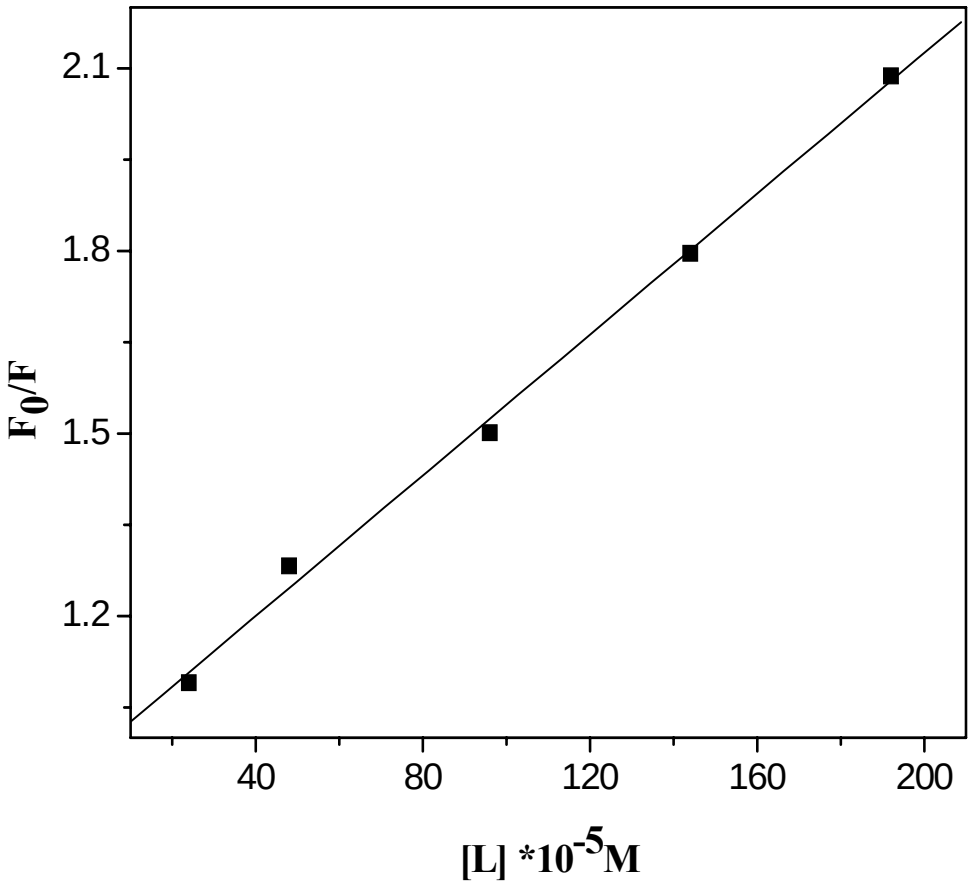

Figure 4.8: The Stern-Volmer plot for propofol-HSA system.

4.2.2 Determination of binding constants (K) by fluorescence spectroscopy

Generally, small molecules interact with macromolecules through four binding modes: hydrogen bond, van der Waals force, electrostatic and hydrophobic interactions (Moreno et al, 1999). The manner in which the fluorescence emission spectra of the bound drug-HSA affected by the presence of ligands which bind specifically on the HSA, leads to use the drug as a fluorescent probe to determine the environment at the drug binding site and the binding constant between drug and HSA (Tuan et al, 2001; Gao et al, 2000).

For the static quenching, we used the following equation (Lakowicz, 2006)

$$\frac{1}{F_0 - F} = \frac{1}{F_0 K(L)} + \frac{1}{F_0} \qquad \textbf{(5)}$$

where K is the binding constant of drug with HSA. In order to determine the binding constants of HSA-pentobarbital and HSA- propofol systems, we plot 1/ (F_0-F) versus 1/ [L] of HSA-drug systems as shown in (Fig.4.9 and Fig.4.10). The plots are linear with ($1/F_0K$) as the slope and 1/ F_0 as the intercept. The binding constant K is a quotient of intercept 1/ F_0 and slope (1/ F_0K). The obtained values of K are $1.809x0^4$ M^{-1}, and $2.55x10^3$ M^{-1} respectively, which agrees well with the value obtained earlier by UV spectroscopy and supports the effective role of static quenching. The interaction between pentobarbital or propofol with HSA includes the hydrophobic interaction between aromatic ring of the two drugs and the hydrophobic amino acid residues, and the static interaction between carbonyl groups of pentobarbital, and hydroxyl group of propofol with the basic residues. The highly effective quenching constants in these cases have lead to a lower value of binding constant between the drug and HSA due to effective hydrogen bonding between drugs pentobarbital and propofol and HSA.

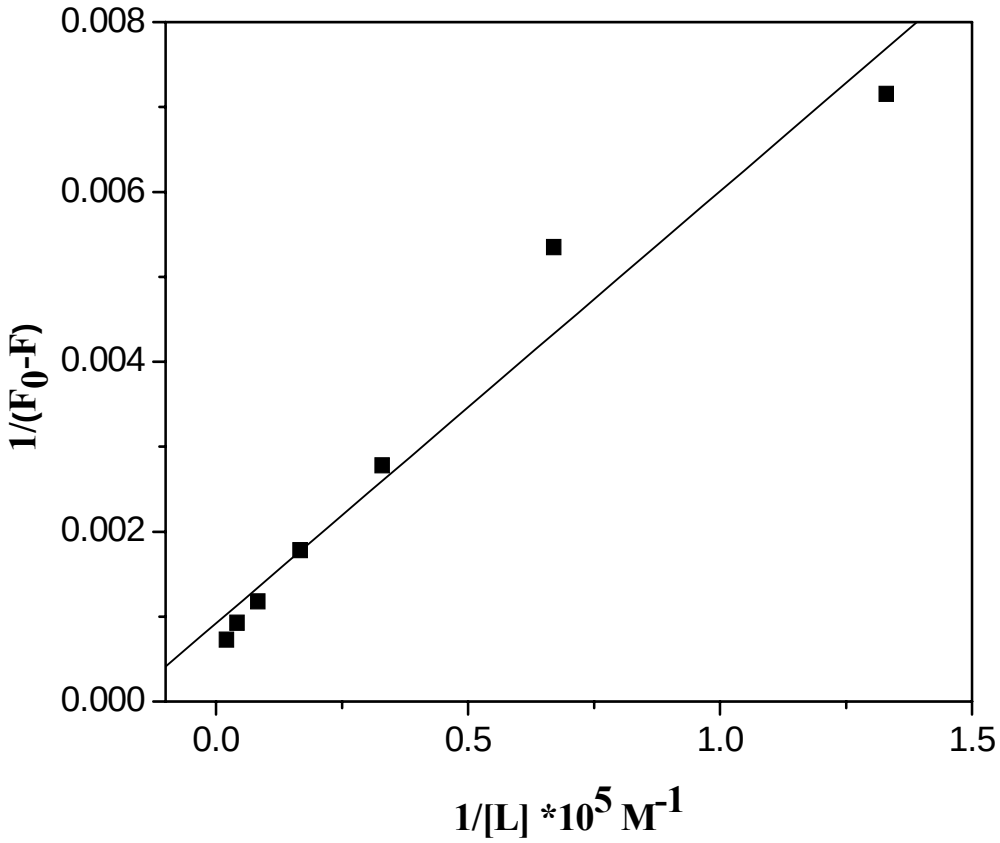

Figure 4.9: The plot of 1/ (F_0-F) vs. 1/ [L*10^5] of HSA-pentobarbital system.

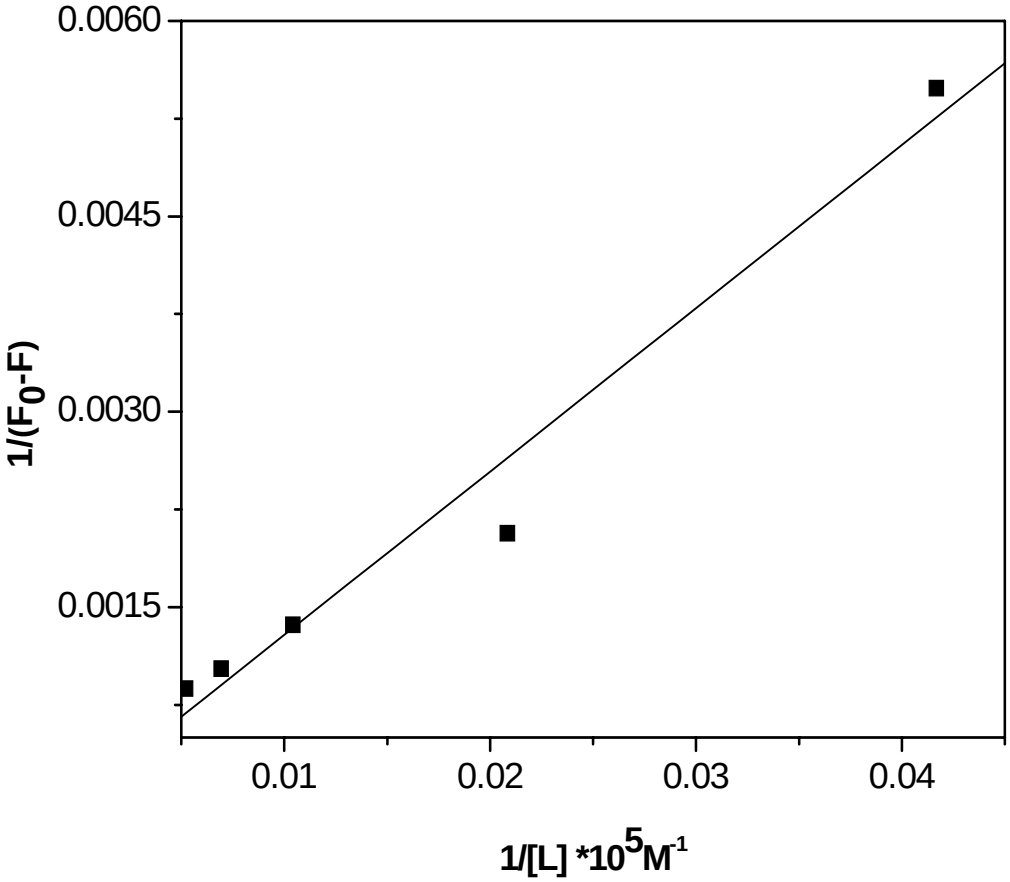

Figure 4.10: The plot of 1/ (F_0-F) vs. 1/ [L*10^5] of HSA-propofol system.

4.3 Fourier transform infrared (FTIR) spectroscopy

FTIR spectroscopy has a unique power for detecting H-bonded components of conformer mixtures. It can provide quantitative analysis of the secondary structure of proteins without the restriction of special amino acids, and its characteristics of high sensitivities, fast analysis and low demanding sample preparation make it suitable to analyze the drug–protein interaction at all kinds of physiological conditions (Sirotkin et al, 2001; Surewicz et al, 1993; Neault et al, 2001). Also the most important advantage of FTIR spectroscopy for biological studies is that spectra of almost any biological system can be obtained in a wide variety of environments. When drugs bind to a globular protein, the intramolecular forces responsible for maintaining the secondary and tertiary structures can be altered, resulting in a conformational change of the protein (Ganim et al, 2006). So the change of three-dimensional structure of HSA includes the transforming of secondary structure in the drug-HSA complex, it can be reflected in the infrared absorption spectra.

In order to investigate the changes of the HSA secondary structure after pentobarbital and propofol binding to HSA, the FTIR spectroscopy was used. Infrared spectra of proteins exhibit a number of so-called amide bands, which represent different vibrations of the peptide moieties. The amide group of proteins and polypeptides presents characteristic vibrational modes (amide modes) that are sensitive to the protein conformation and have largely been constrained to group frequency interpretations (Dukor et al, 2001). Among the amide bands of the protein, amide I band ranging from 1700 to 1600 cm^{-1} is primarily due to the C=O stretching vibration, and has been widely accepted for used (Workman, 1998; Ganim et al, 2006). Amide II band ranging from 1600 to 1480 cm^{-1} is primarily due to the coupling of the N-H in-plane bending and C-N stretching modes. And amide III band ranging from 1330 to 1220 cm^{-1} which is due to the C-N stretching mode coupled to the in-plane N - H bending mode (Surewicz et al, 1993; Chirgadze et al, 1975; Cai et al,1999), so amide III has more characteristics of the protein's secondary structure than amide II (Deleris et al, 2003), but it has not been widely used previously because of its weak intensity and lack of component bands ascription. Furthermore, other bands at 1300-900 cm^{-1} were assigned to C-O bending

modes of saccharides (glucose, lactose and glycerol), the peaks at 1430-1360 cm^{-1} attributed to vibrations of certain amino acids chains and 1480-1430 cm^{-1} is attributed to fatty acids, phospholipids and triglycerides (Bramanti et al 1996; Jackson et al, 1991). In this research work, our emphasis is on analyzing the protein secondary structure after binding with pentobarbital and propofol.

For HSA-pentobarbital interaction and *HSA-propofol interaction* the second derivative of the FT-IR spectrum for free HSA is shown in (Fig.4.11.A, and Fig.4.12.A). From the two figures we can see that there are two dominant peaks, one peak at 1656 cm^{-1} which is related to the amide I band, and the other peak at 1544 cm^{-1} which is related to the amide II band. The spectra of HSA-pentobarbital with concentrations (0.0, 0.015, 0.03, 0.06, 0.12, 0.24, and 0.48 mM), and the spectra of HSA-propofol with concentrations (0.0, 0.24, 0.48, 0.96, 1.44 and 1.92 mM) are shown in (Fig. 4.11.B, and Fig. 4.12.B), respectively. It is evident that, the absorbance intensity of HSA decreased regularly with the increase of concentration of pentobarbital and propofol.

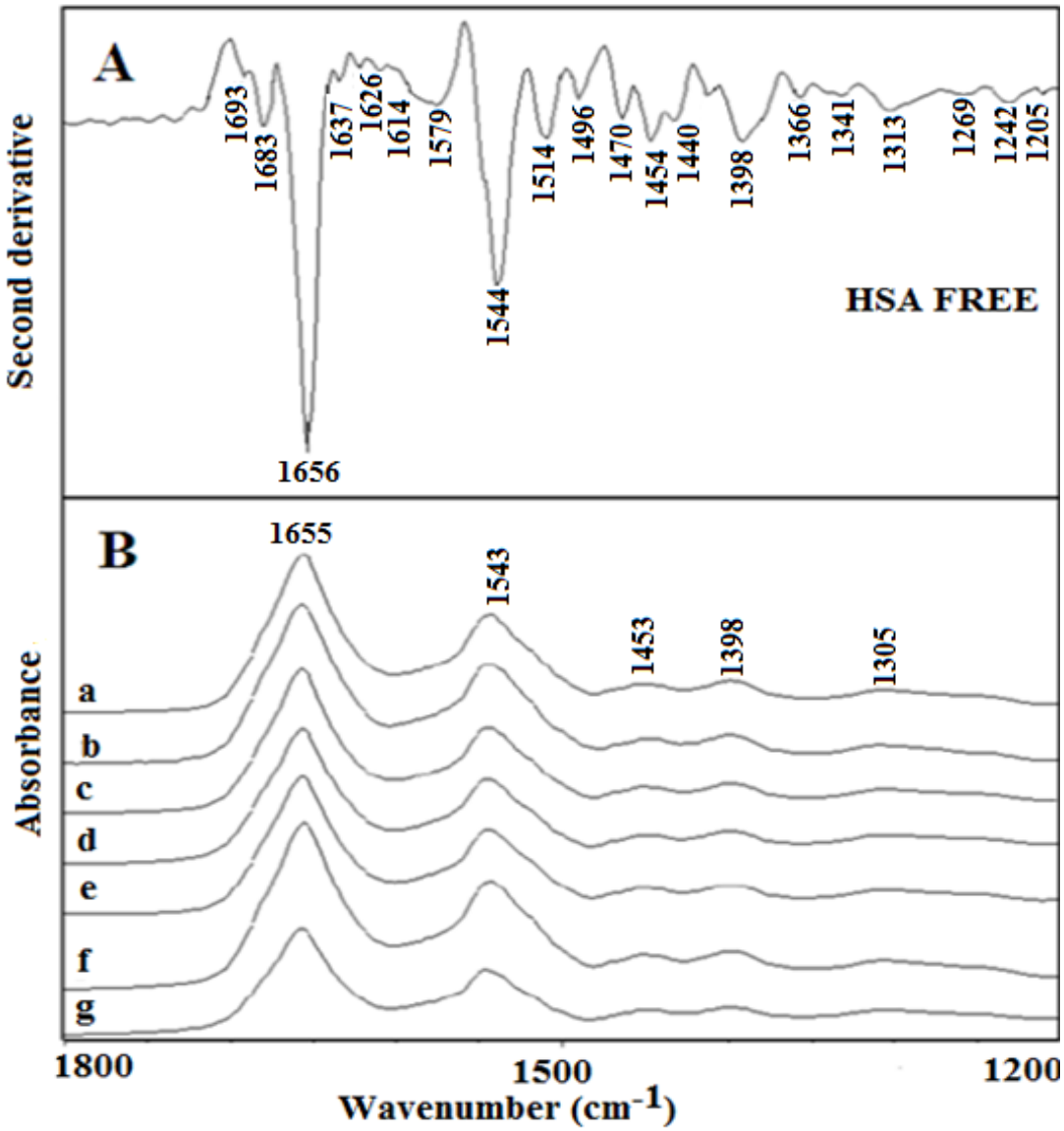

Figure 4.11: The spectra of (A) HSA-free (second derivative) and (B) HSA-pentobarbital with concentrations (a=0.0mM, b=0.015mM, c=0.03mM, d=0.06mM, e=0.12, f=0.24mM, and g=0.48mM).

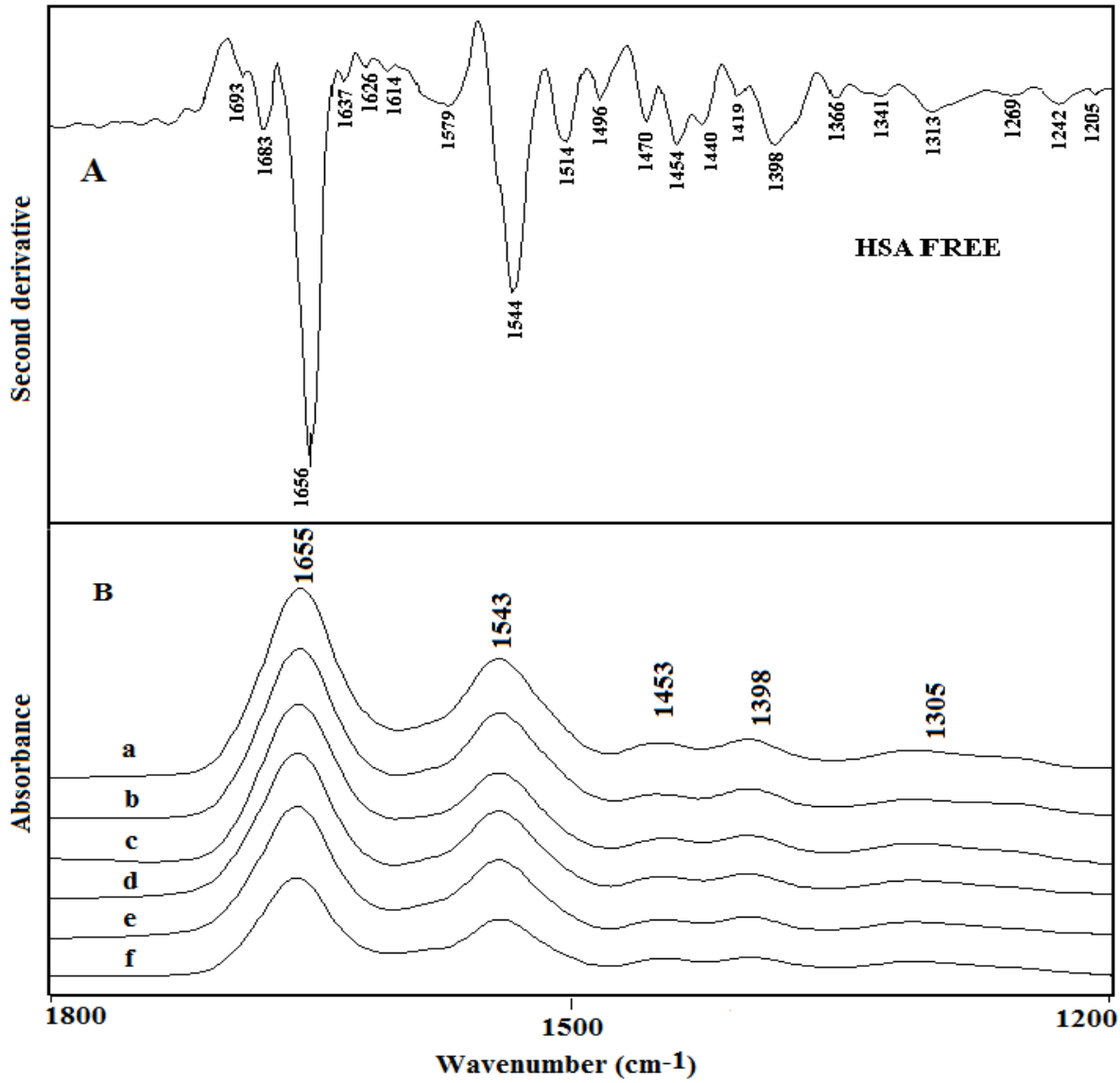

Figure 4.12: The spectra of (A) HSA-free (second derivative) and (B) HSA-propofol with concentrations (a=0.0mM, b=0.24mM, c=0.48mM, d=0.96mM, e=1.44mM, and f=1.92mM).

The peak positions of HSA with different pentobarbital and propofol concentrations for amide I, II and III regions are listed in (Table 4.1, and Table 4.2), respectively. *For HSA-pentobarbital interaction*, the amide I bands of HSA infrared spectrum shifted as listed in table 4.1: 1614 to 1612 cm^{-1}, 1626 to 1627 cm^{-1},1637 to 1639 cm^{-1} , 1656 to 1657 cm^{-1} , 1683 to 1680 cm^{-1}, and 1693 to 1692 cm^{-1} after interaction with pentobarbital. In addition a peak at 1636cm^{-1} has disappeared after the interaction with pentobarbital. The changes of these peak positions and peak shapes demonstrated that the secondary structures of the HSA had been changed by the interaction of pentobarbital with HSA. In amide II region some of the peak positions have shifted in the following order: 1514 to 1515 cm^{-1}, 1544 to 1548cm^{-1}, 1564 to 1568 cm^{-1}, 1579 to 1584 cm^{-1} and 1594 to 1596 cm^{-1}. In addition a peak at 1532 cm^{-1} remains unchanged after the interaction of HSA with pentobarbital. In amide III region little change of the peak positions has been observed in the following order: 1242 to 1243 cm^{-1}, 1269 to 1267 cm^{-1}, 1293 to 1294 cm^{-1}, and 1313 to 1312 cm^{-1}. And the peak at 1226 cm^{-1} remains unchanged after the interaction.

For *HSA-propofol system*, the amide I bands of HSA infrared spectrum shifted as listed in table 4.2: 1615 to 1611 cm^{-1}, 1624 to 1627 cm^{-1}, 1636 to 1642 cm^{-1}, 1655 to 1659 cm^{-1}, 1682 to 1678 cm^{-1}, and 1695 to 1691 cm^{-1} after interaction with propofol. In amide II region the peak positions have shifted in the following order: 1515 to 1514 cm^{-1}, 1532 to 1531 cm^{-1}, 1543 to 1549 cm^{-1}, 1564 to 1567 cm^{-1}, 1577 to 1584 cm^{-1}, and 1594 to 1597 cm^{-1}. In amide III region the change of the peak positions is in the following order: 1243 to 1242 cm^{-1}, and 1314 to 1313 cm^{-1}. There are three peaks at 1226 cm^{-1}, 1268 cm^{-1}, and 1293 do not change after the interaction of HSA- propofol. Also, the peak at (1278-1275) appears as new peak in this interaction. The changes of these peak positions and peak shapes explained that the secondary structures of the HSA had been affected by the interaction of propofol with HSA.

The minor changes in peak positions can be attributed to the effect of the newly imposed H-bonding between the drug molecules and the protein. It is suggested that, the shift to a higher frequency for the major peak in amide I region (1656 to 1657 cm^{-1}) for HSA-pentobarbital system, and (1655 to 1659 cm^{-1}) for HSA-propofol system came as a result of stabilization by

hydrogen bonding by having the C-N bond assuming partial double bond character due to a flow of electrons from the C=O to the C-N bond (Chirgadze et al, 1975).

Table 4.1: Band assignments in the absorbance spectra of HSA with different pentobarbital concentrations for amide I, II and III regions.

Bands	HSA FREE	HSA-Pento. 0.015 mM	HSA-Pento. 0.03 mM	HSA-Pento. 0.06 mM	HSA-Pento. 0.12mM	HSA-Pento. 0.24mM	HSA-Pento. 0.48mM
Amide I (1600-1700)	1614	1615	1614	1613	1613	1614	1612
	1626	1627	1626	1626	1626	1626	1627
	1637	1637	1636	1637	1637	1636	1639
	1656	1657	1656	1656	1656	1654	1657
	1683	1680	1681	1682	1681	1682	1680
	1693	1691	1692	1693	1692	1694	1692
Amide II (1480-1600)	1514	1515	1515	1515	1515	1515	1515
	1532	1532	1532	1531	1531	1531	1532
	1544	1548	1546	1546	1546	1544	1548
	1564	1568	1570	1571	1570	1571	1568
	1579	1579	1582	1581	1581	1585	1584
	1594	1595	1595	1595	1595	1594	1596
Amide III (1220-1330)	1226	1226	1226	1226	1226	1226	1226
	1242	1243	1243	1243	1243	1242	1243
	1269	1267	1269	1268	1268	1268	1267
	1293	1292	1293	1294	1293	1293	1294
	1313	1312	1313	1314	1313	1313	1312

Table 4.2: Band assignments in the absorbance spectra of HSA with different propofol concentrations for amide I, II and III regions.

Bands	HSA FREE	HSA-Prop 0.24 mM	HSA-Prop 0.48 mM	HSA-Prop 0.96 mM	HSA-Prop 1.44mM	HSA-Prop 1.92mM
Amide I (1600-1700)	1615	1612	1611	1616	1617	1611
	1624	1627	1628	1626	1625	1627
	1636	1640	1642	1638	1637	1642
	1655	1657	1658	1657	1656	1659
	1682	1680	1677	1681	1682	1678
	1695	1692	1691	1693	1693	1691
Amide II (1480-1600)	1515	1515	1514	1516	1516	1514
	1532	1532	1531	1532	1532	1531
	1543	1549	1549	1548	1546	1549
	1564	1568	1566	1570	1571	1567
	1577	1583	1583	1590	1578	1584
	1594	1597	1598	1594	1592	1597
Amide III (1220-1330)	1226	1226	1226	1226	1226	1226
	1243	1242	1243	1243	1243	1242
	1268	1267	1269	1268	1268	1268
		1278	1278	1275	1275	1275
	1293	1294	1293	1294	1293	1293
	1314	1311	1313	1314	1313	1313

The difference spectra [(protein + pentobarbital or propofol) – (protein)] were obtained in order to monitor the intensity variations and the results are shown in (Fig.4.13, Fig.4.14, Fig.4.15, and Fig.4.16). *For HSA-pentobarbital interaction,* Fig. (4.13) shows FTIR spectra (top two curves) and difference spectra of HSA and its complexes with different pentobarbital concentrations in the amide I and amide II regions.

In the amide I region, there are one strong negative feature at 1654 cm^{-1} plus one weak negative feature at 1616 cm^{-1} . For the amide II region, there is a strong negative feature at 1543 cm^{-1} plus a weak negative feature at 1575 cm^{-1}. Fig.(4.14) shows that in amide III region there are two strong negative features at 1317 cm^{-1}, and 1242 cm^{-1}. These features were observed at low pentobarbital concentration (0.03mM). *For HSA-propofol interaction*, Fig.(4.15) shows FTIR spectra (top two curves) and difference spectra of HSA and its complexes with different propofol concentrations in the amide I and amide II regions. At low propofol concentration (0.48 mM), one strong negative feature at 1652 cm^{-1} is observed in amide I region, while in amide II region there is a strong negative feature at 1548 cm^{-1} in addition to one weak negative feature at 1513 cm^{-1}. For low propofol concentration (0.48 mM) Fig.(4.16) shows that in amide III region there are two strong negative features at 1242 cm^{-1}, and 1315 cm^{-1}. It is clearly shown that the strong negative features became stronger as pentobarbital or propofol concentration was increased to 0.03, 0.06, and 0.48 mM, and 0.48, 0.96, 1.44, and 1.92 mM respectively with a little shift in their positions.

The observed negative features are attributed to the decrease in the intensity of the amide I band at1655 cm^{-1}, amide II band at 1543 cm^{-1}, and amide III band at 1242 cm^{-1}, and 1313 cm^{-1} as a result of drug interaction (H-bonding) with protein C=O and C-N groups (Purcell et al, 2000). The decrease in the intensity in amide I, II, and III regions is due to the reduction of the α-helix structure in HSA, upon pentobarbital or propofol interactions, which will determine and will be discussed later. The band at 1515 cm^{-1} of the HSA free is due to the tyrosine amino acid side chain vibration (Matsuura et al, 1986; Olinger et al, 1986; Fabian et al, 1994; Yamamoto et al, 1991; Byler et al, 1986) showed no spectral changes upon pentobarbital or propofol complexation (Fig.4.13, Fig.4.15).

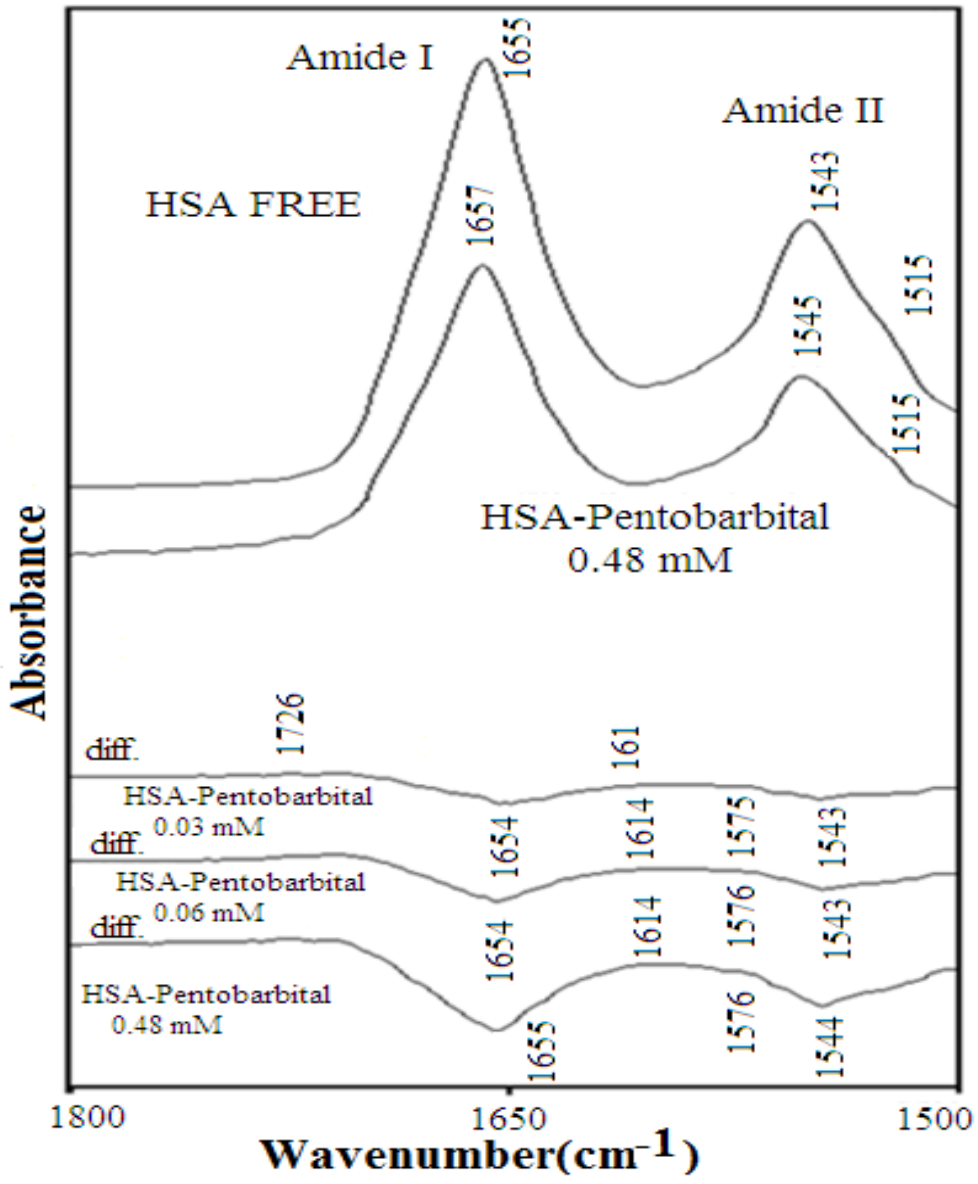

Figure 4.13: FTIR spectra (top two curves) and difference spectra of HSA and its complexes with different pentobarbital concentrations in the region of 1800- 1500 cm^{-1}.

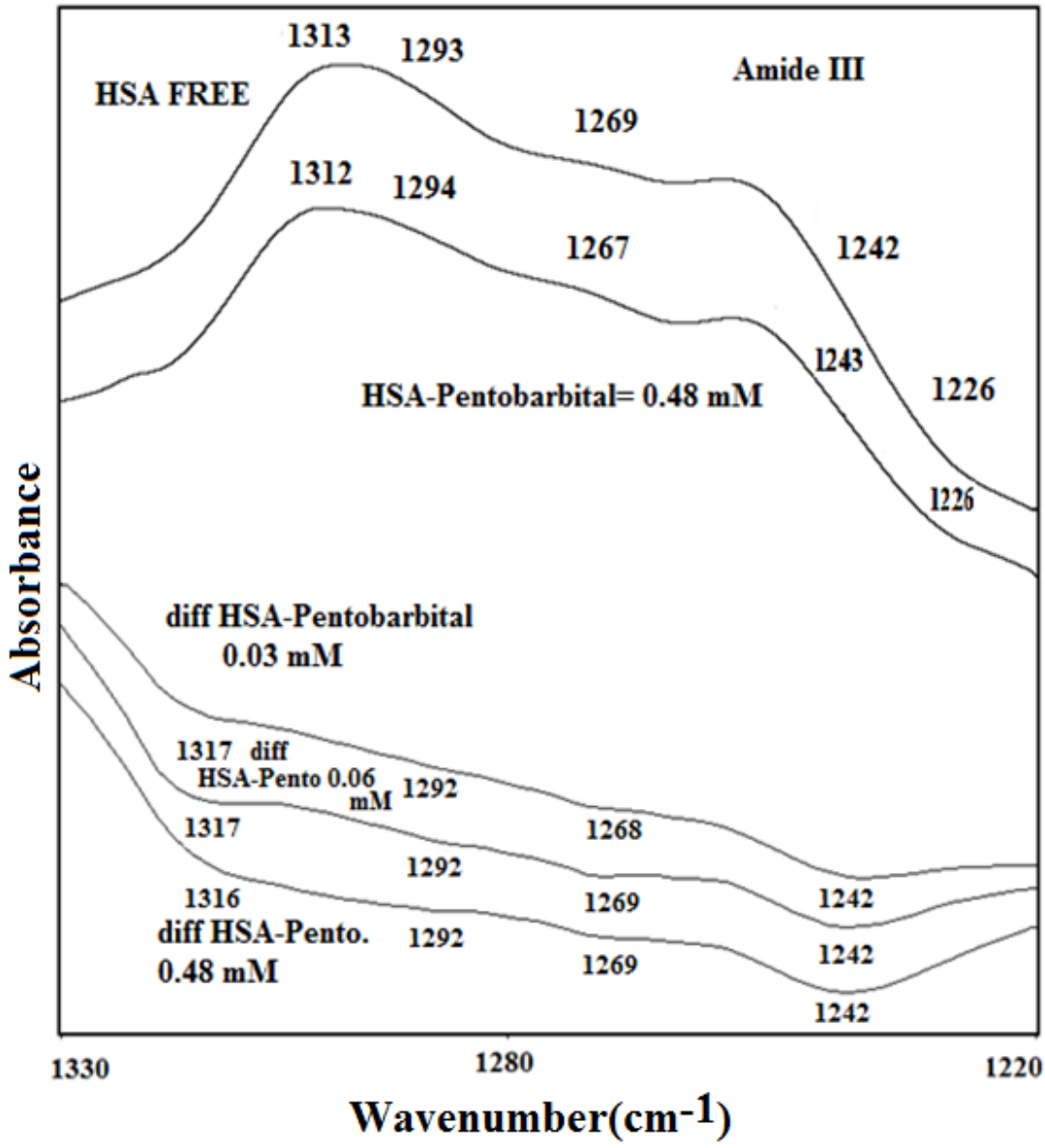

Figure 4.14: FTIR spectra (top two curves) and difference spectra of HSA and its complexes with different pentobarbital concentrations in the region of 1330- 1220 cm^{-1}.

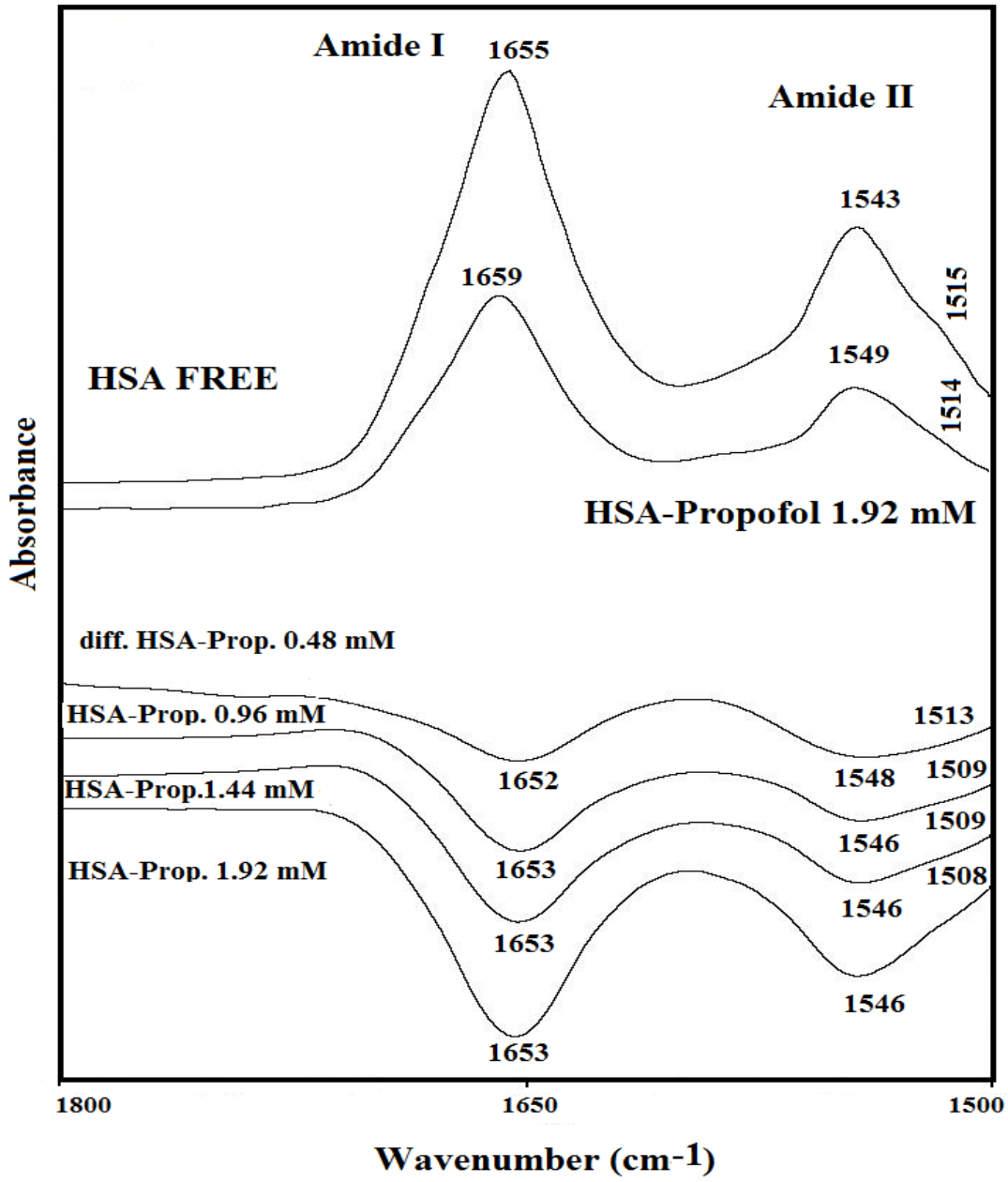

Figure 4.15: FTIR spectra (top two curves) and difference spectra of HSA and its complexes with different propofol concentrations in the region of 1800- 1500 cm^{-1}.

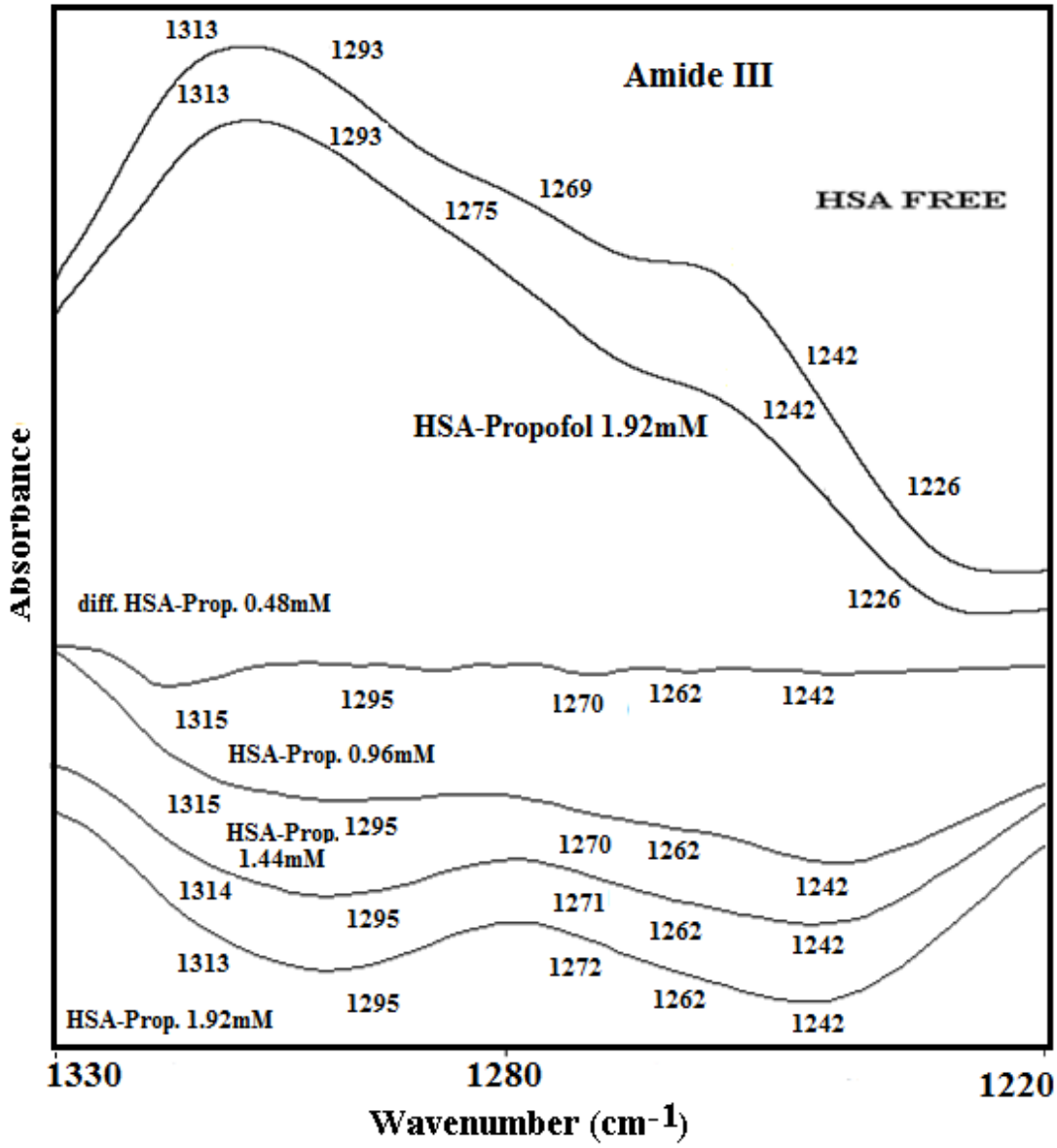

Figure 4.16: FTIR spectra (top two curves) and difference spectra of HSA and its complexes with different propofol concentrations in the region of 1330- 1220 cm^{-1}.

The Determination of the secondary structure of HSA and its pentobarbital or propofol complexes were carried out on the basis of the procedure described by Byler and Susi (Byler et al, 1986). In our work a quantitative analysis of the protein secondary structure for the free HSA, pentobarbital–HSA, and propofol-HSA complexes in dehydrated films are determined from the shape of amide I, II and III bands. Baseline correction was carried out in the range of (1700–1600), (1600-1480), and (1330–1220 cm^{-1}) to get amide I, II, and III bands. Then Fourier self-deconvolution and second derivative were applied to these three ranges respectively to increase spectral resolution and therefore to estimate the number, position and the area of each component bands. Based on these parameters, a curve-fitting process was carried out by Opus software (version 5.5) to obtain the best Lorentzian-shaped curves that fit the original HSA spectrum. The individual bands are identified with its representative secondary structure, and the content of each secondary structure of HSA is calculated by area of their respective component bands. The procedure was in general carried out considering only components detected by second derivatives and the half widths at half height (HWHH) for the component peaks are kept around $5cm^{-1}$.

The component bands of amide I were attributed according to the well-established assignment criterion (Jiang et al, 2004; Ivanov et al, 1994). The amide I bands range 1610–1640 cm^{-1} are generally assigned to β-sheet, 1640–1650 cm^{-1} to random coil, 1650–1658 cm^{-1} to α-helix, and 1660–1700 cm^{-1} to β-turn structure. For amide II, the absorption band consists of four components and assigned in the following order: 1488-1500 cm^{-1} to β-sheets, 1504-1525 cm^{-1} to random coil, 1527-1560 cm^{-1} to α-helix and 1564-1585cm^{-1} to turn structure (Rahmelow et al, 1996). The component bands of amide III have been assigned as follows: α-helix 1330–1290 cm^{-1}, β-turn 1290–1270 cm^{-1}, random coil 1270–1250 cm^{-1} and β-sheet 1250–1220 cm^{-1} (Ivanov et al, 1994). Most investigations have concentrated on amide I band assuming higher sensitivity to the change of protein secondary structure (Erik et al, 2006). However, it has been reported that the amide II band has high information content and could be used alone for prediction of secondary structure in place of amide I (Oberg et al, 2004; Fu et al, 1994). Others have reported that amide III is not directly affected by the strong water band and therefore it has been used for structure determination (Goormaghtigh et al, 1999).

Based on the above assignments, the percentages of each secondary structure of HSA were calculated from the integrated areas of the component bands in amide I, II, and III respectively. Where the area of all the component bands assigned to a given conformation is then summed and divided by the total area. The obtained number is taken as the proportion of the polypeptide chain in that conformation.

The Secondary structure determination for the free HSA and its pentobarbital or propofol complexes with different drug concentrations are given in (Table 4.3, and Table 4.4). The second derivative resolution enhancement and curve – fitted amide I, amide II, and amide III regions and secondary structure determinations of the free human serum albumin (A, B) and its pentobarbital or propofol complexes (C, D) with the highest concentrations in dehydrated films are shown in (Fig. 4.17, Fig.4.18, Fig. 4.19, Fig. 4.20, Fig. 4.21, and Fig.4.22). It is generally accepted that infrared spectra of proteins in films and in solution may display distinct differences, but these differences are due to the presence or absence of the water or buffer molecules that imprint their mark on the spectra. It has been shown that the structural information content is of the same quality in films and in solution with an (error of < 1%) for both systems with respect to amide regions (Ahmed Ouameur et al, 2004).

Table 4.3: Secondary structure determination for amide I, II and III regions in HSA and its pentobarbital complexes.

Bands	HSA FREE	HSA-Pento. 0.015 mM	HSA-Pento. 0.03 mM	HSA-Pento. 0.06 mM	HSA-Pento. 0.12mM	HSA-Pento. 0.24mM	HSA-Pento. 0.48mM
Amide I							
β-sheets(cm^{-1}) (1610-1640) (1680-1700)	**16**	**18**	**16**	**18**	**17**	**17**	**19**
Random(cm^{-1}) (1640-1650)	**15**	**14**	**16**	**16**	**16**	**18**	**13**
α –helix(cm^{-1}) (1650-1660)	**55**	**51**	**51**	**49**	**49**	**49**	**48**
Turn (cm^{-1}) (1660-1680)	**14**	**17**	**17**	**17**	**16**	**16**	**20**
Amide II							
β-sheets(cm^{-1}) (1488-1500) (1587-1598)	**18**	**18**	**17**	**17**	**18**	**17**	**19**
Random(cm^{-1}) (1504-1525)	**14**	**11**	**12**	**14**	**13**	**14**	**10**
α –helix(cm^{-1}) (1527-1560)	**50**	**50**	**51**	**48**	**50**	**50**	**47**
Turn (cm^{-1}) (1564-1585)	**18**	**21**	**20**	**21**	**19**	**19**	**24**
Amide III							
β-sheets(cm^{-1}) (1220-1250)	**17**	**17**	**18**	**19**	**20**	**20**	**21**
Random(cm^{-1}) (1250-1270)	**15**	**16**	**15**	**16**	**15**	**16**	**16**
Turn (cm^{-1}) (1270-1290)	**18**	**18**	**18**	**17**	**17**	**17**	**17**
α –helix(cm^{-1}) (1290-1330)	**50**	**49**	**49**	**48**	**48**	**47**	**46**

Table 4.4: Secondary structure determination for amide I, II and III regions in HSA and its propofol complexes.

Bands	HSA FREE	HSA-Prop. 0.24 mM	HSA-Prop. 0.48 mM	HSA-Prop. 0.96 mM	HSA-Prop. 1.44mM	HSA-Prop. 1.92mM
Amide I						
β-sheets(cm^{-1}) (1603-1635) (1687-1700)	16	32	32	32	36	39
Random(cm^{-1}) (1635-1645)	15	6	6	5	5	5
α –helix(cm^{-1}) (1648-1670)	55	52	52	50	49	46
Turn (cm^{-1}) (1670-1685)	14	10	10	13	10	10
Amide II						
β-sheets(cm^{-1}) (1488-1504) (1585-1600)	18	23	25	27	29	29
Random(cm^{-1}) (1504-1525)	14	15	14	14	15	15
α –helix(cm^{-1}) (1527-1560)	50	47	46	45	43	42
Turn (cm^{-1}) (1564-1585)	18	15	15	14	13	14
Amide III						
β-sheets(cm^{-1}) (1220-1250)	17	22	22	21	20	21
Random(cm^{-1}) (1250-1270)	15	15	16	16	17	17
Turn (cm^{-1}) (1270-1290)	18	18	18	20	21	21
α –helix(cm^{-1}) (1290-1330)	50	45	44	43	42	41

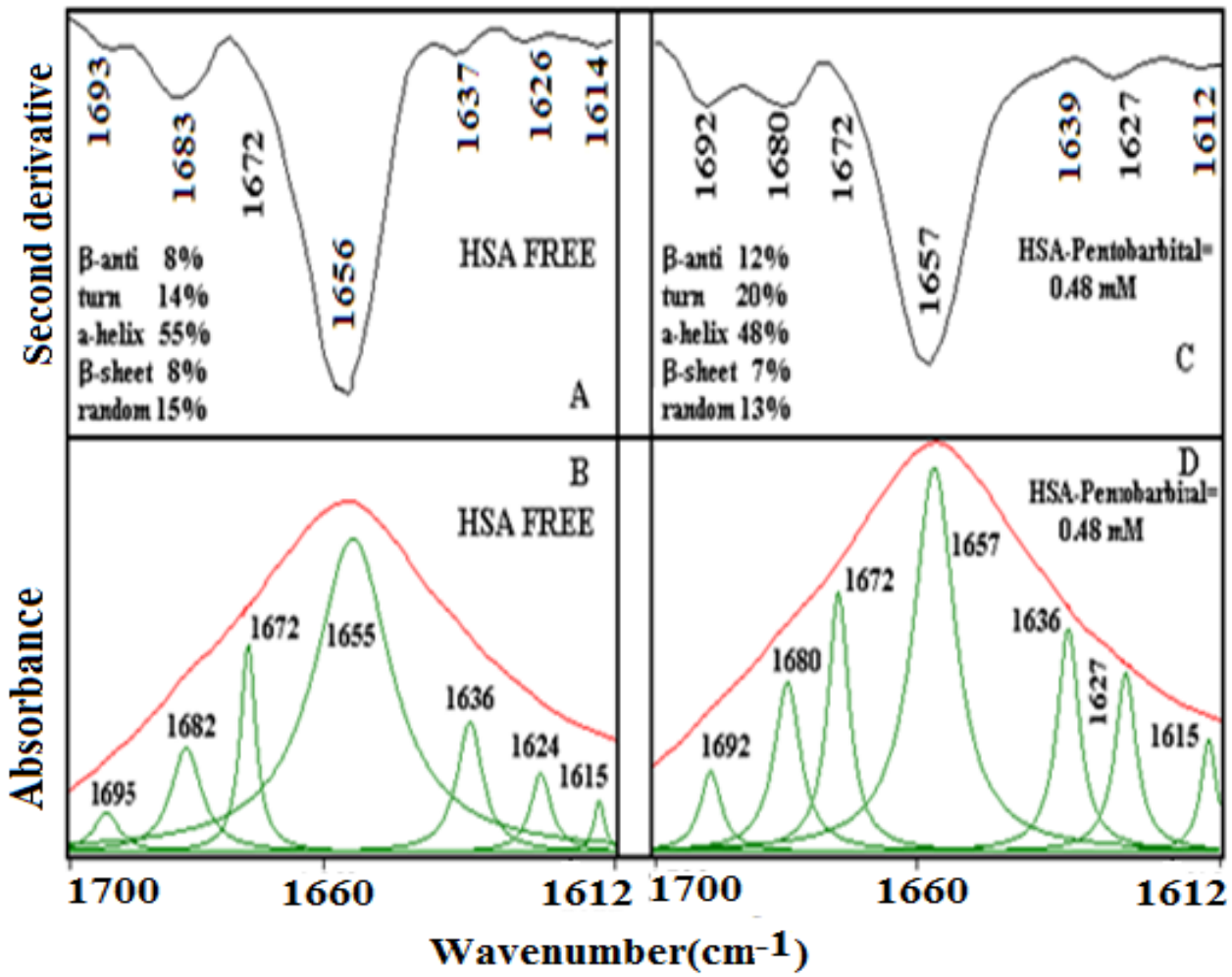

Figure 4.17: Second-derivative resolution enhancement and curve-fitted amide I region (1700-1612 cm^{-1}) and secondary structure determination of the free human serum albumin (A,B) and its pentobarbital complexes (C,D) with 0.48mM drug concentration.

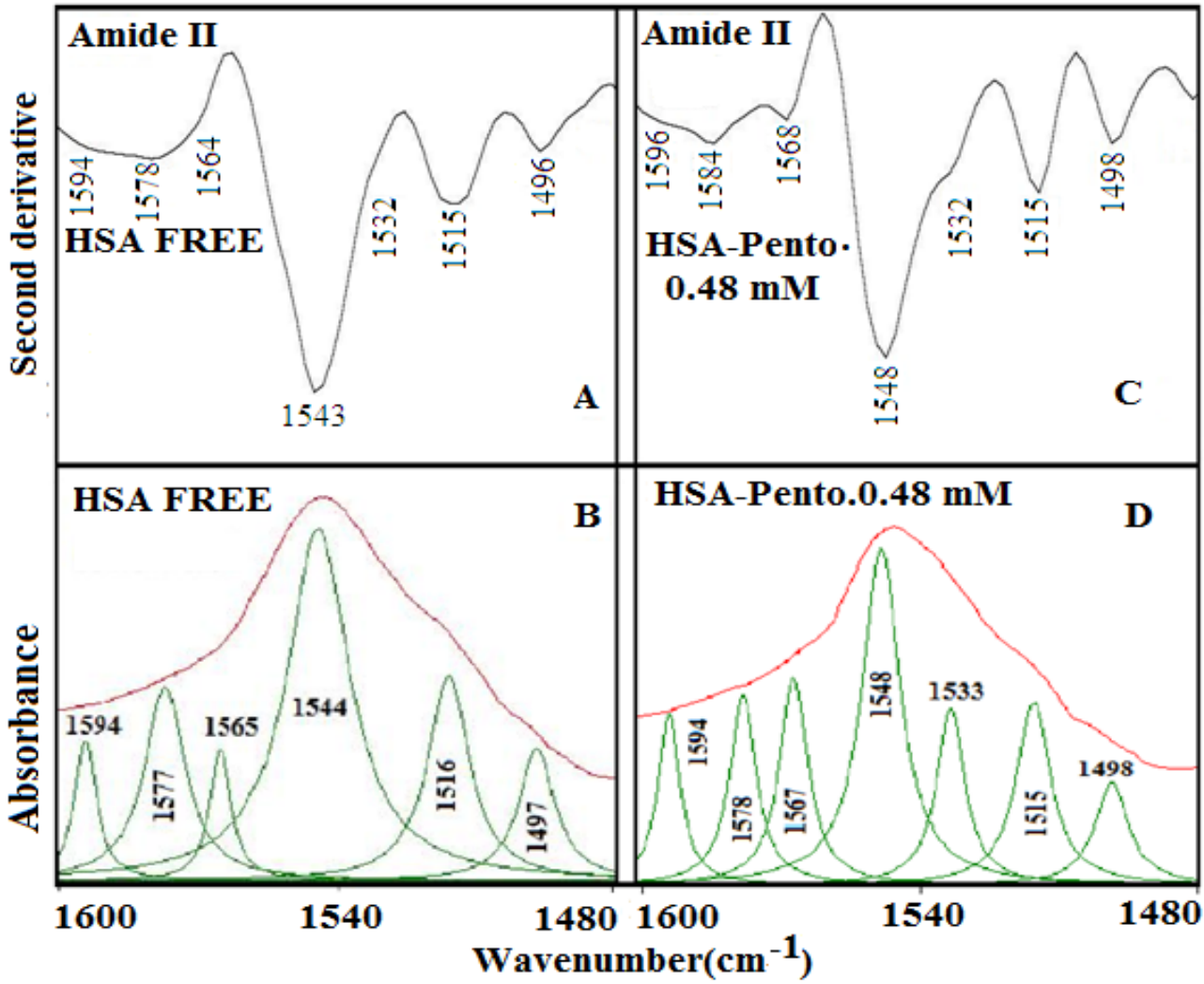

Figure 4.18: Second-derivative resolution enhancement and curve-fitted amide II region (1600-1480 cm^{-1}) and secondary structure determination of the free human serum albumin (A,B) and its pentobarbital complexes (C,D) with 0.48mM drug concentration.

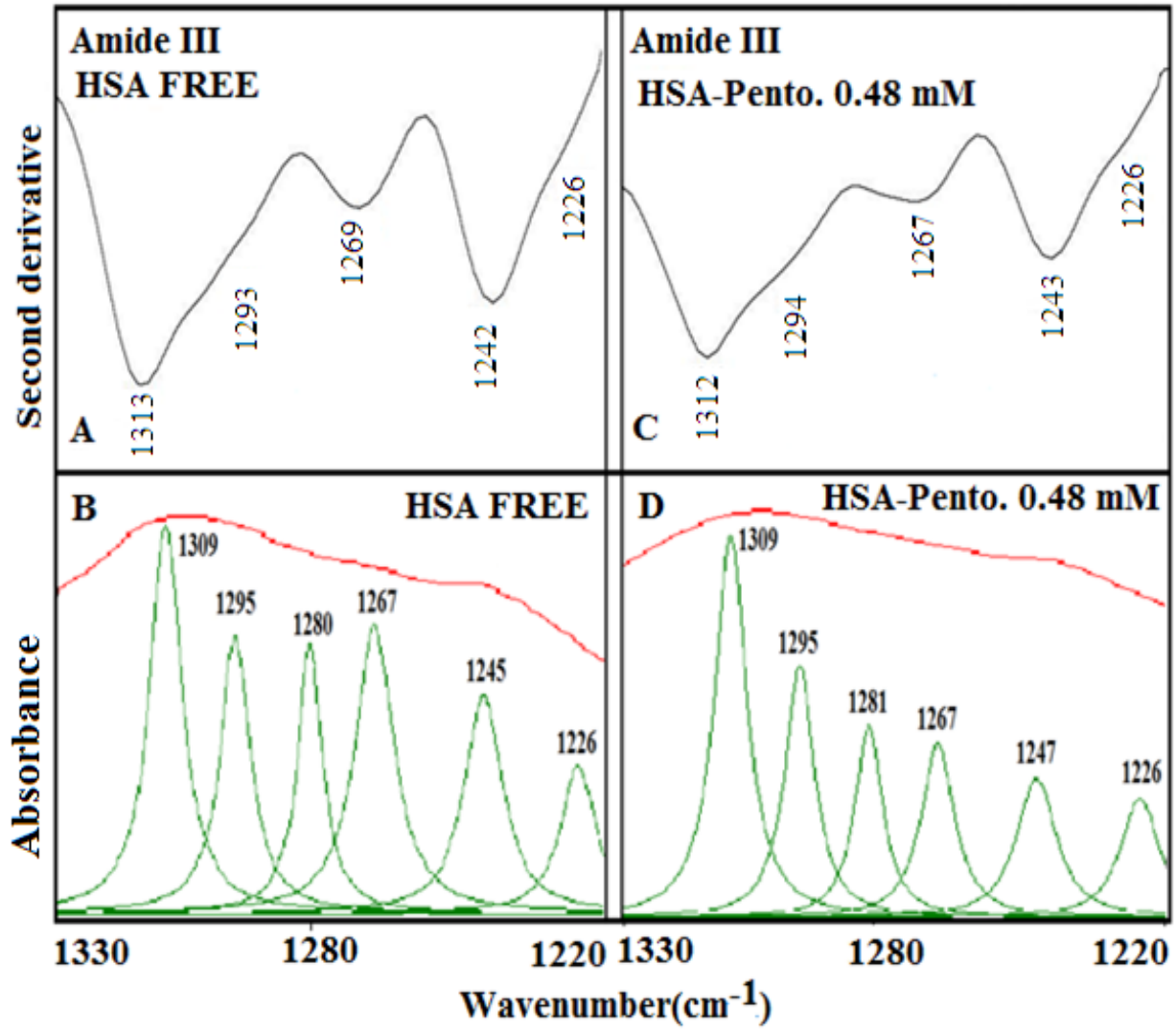

Figure 4.19: Second-derivative resolution enhancement and curve-fitted amide III region (1330-1220 cm^{-1}) and secondary structure determination of the free human serum albumin (A,B) and its pentobarbital complexes (C,D) with 0.48mM drug concentration.

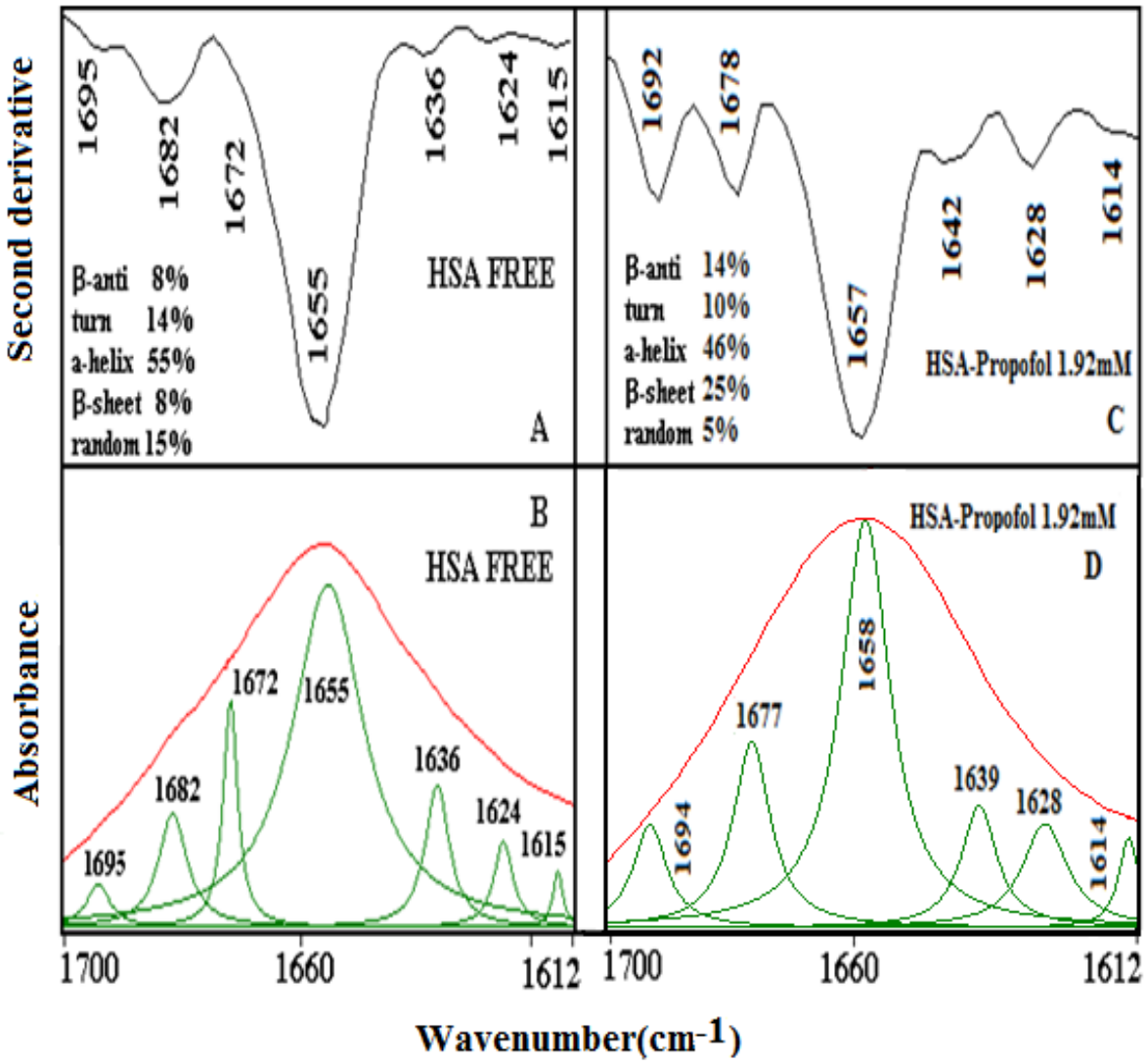

Figure 4.20: Second-derivative resolution enhancement and curve-fitted amide I region (1700-1612 cm^{-1}) and secondary structure determination of the free human serum albumin (A,B) and its propofol complexes (C,D) with 1.92mM drug concentration.

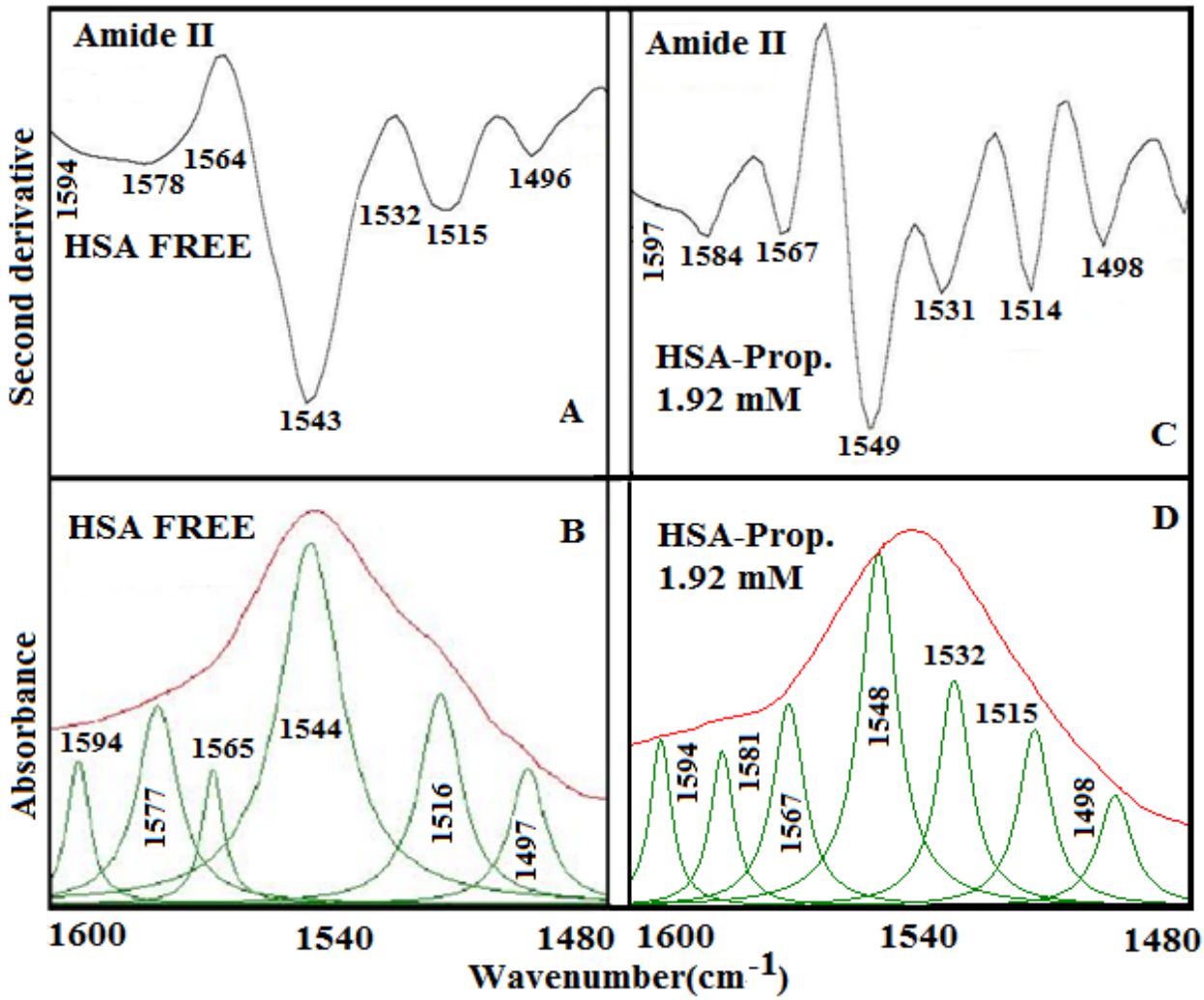

Figure 4.21: Second-derivative resolution enhancement and curve-fitted amide II region (1600-1480 cm^{-1}) and secondary structure determination of the free human serum albumin (A,B) and its propofol complexes (C,D) with 1.92mM drug concentration.

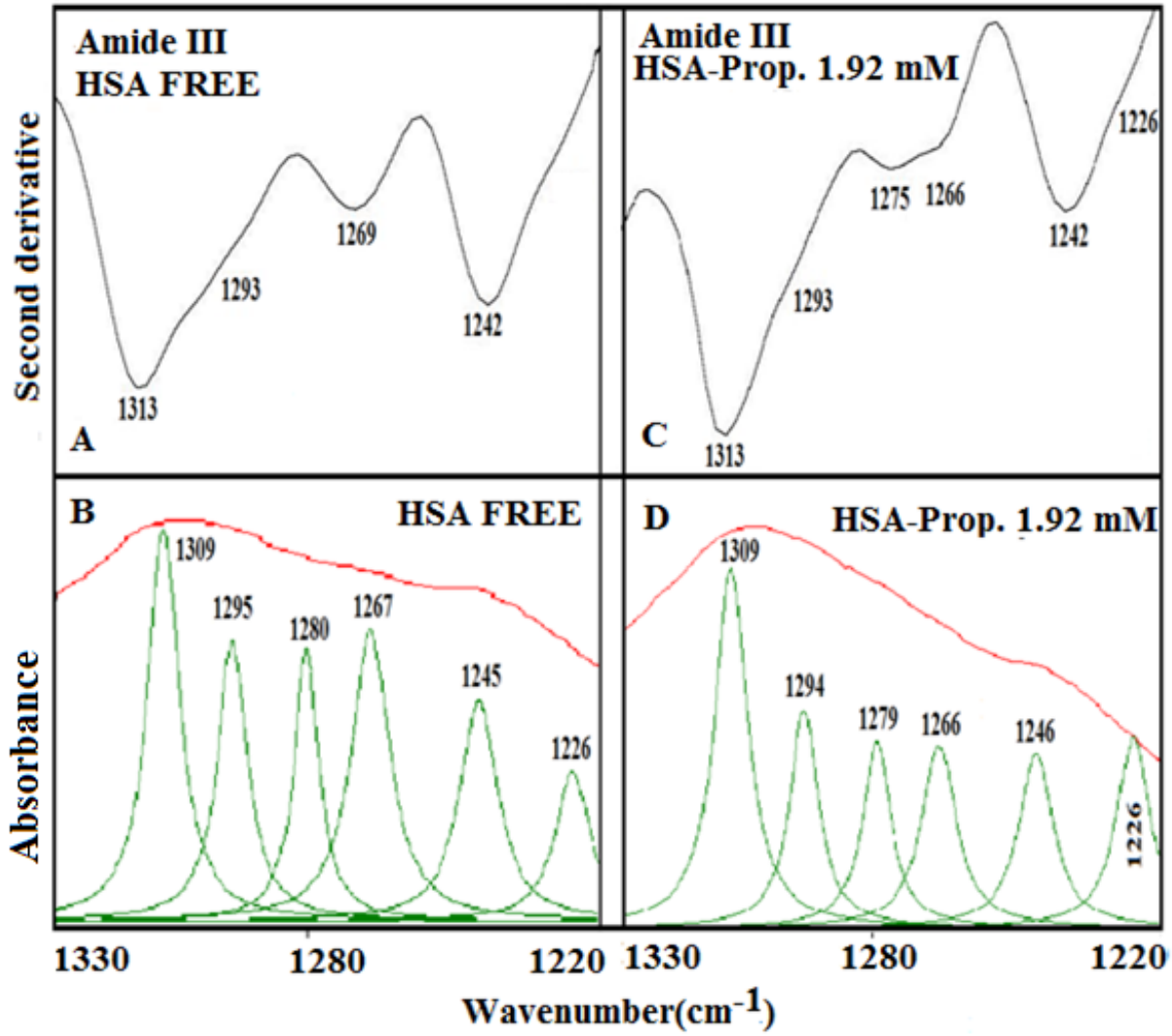

Figure 4.22: Second-derivative resolution enhancement and curve-fitted amide III region (1330-1220 cm^{-1}) and secondary structure determination of the free human serum albumin (A,B) and its propofol complexes (C,D) with 0.48mM drug concentration.

The percentage values for the components of amid I of free HSA are consistent with the results of other recent spectroscopic studies (Beauchemin et al, 2007; Bai et al, 1994). The results of amide II and amide III showed similar trends in their percentage values to that of amide I. In amide I region, the free HSA contained major amounts of α-helical (55%), β-sheet (16%), random coil (15 %), and β-turn structure (14%). We can see from Fig 4.17 and Table 4.3, as a result of HSA-pentobarbital interaction that the α-helical structure reduced from 55% to 48%, β-sheet increased from 16% to 19% , β-turn structure increased from 14% to 20%, and the random coil reduced from 15% to 13%. *For HSA-propofol system*, Fig. (4.20) and Table (4.4) show that the α-helical structure reduced from 55% to 46%, β-sheet increased from 16% to 39%, β-turn structure decreased from 14% to 10%, and the random coil reduced from 15% to 5% after interaction of propofol with HSA.

In amide II region, the free HSA contained α-helical (50%), β-sheet (18%), random coil (14 %), and β-turn structure (18%). With regard to the pentobarbital–HSA complex, the α-helical structure reduced from 50% to 47%, β-sheet increased from 18% to 19%, β-turn structure increased from 18% to 24%, and the random coil reduced from 14% to 10% (Fig.4.18 and Table 4.3). *For HSA-propofol system*, Fig. (4.21) and Table (4.4) show that the α-helical structure reduced from 50% to 42%, β-sheet increased from 18% to 29%, β-turn structure reduced from 18% to 14%, and the random coil increased from 14% to 15% after interaction of propofol with HSA.

In amide III region, HSA free contained α-helical (50%), β-sheet (17%), random coil (15%), and β-turn structure (18%). Upon pentobarbital complexation, the α-helical structure reduced from 50% to 46%, β-sheet increased from 17% to 21%, β-turn structure decreased from 18% to 17%, and the random coil increased from 15% to 16% (Fig4.19, and Table 4.3). *For HSA-propofol system*, the α-helical structure reduced from 50% to 41%, β-sheet increased from 17% to 21%, β-turn structure increased from 18% to 21%, and the random coil increased from 15% to 17% (Fig.4.22 and Table 4.4).

The decrease of α-helix percentage with the increase of pentobarbital and propofol concentrations is evident in the calculations and this trend is consistent in the three amide

regions. However for the β-sheet the relative percentage has increased with increasing pentobarbital and propofol concentrations. The reduction of α-helix intensity percentage in favour of the increase of β-sheets and turn structure are believed to be due to the unfolding of the protein in the presence of pentobarbital and propofol as a result of the formation of H-bonding between HSA and the drug. Similar conformational transitions from an α-helix to β-sheet structure were observed for the protein unfolding upon protonation and heat denaturation (Beauchemin et al, 2007). These results indicate that pentobarbital and propofol interact with HSA through C=O and C-N groups in the HSA polypeptides. The pentobarbital and propofol–HSA complexes caused the rearrangement of the polypeptide carbonyl hydrogen bonding network and finally the reduction of the protein α-helical structure.

The steric blocking effect can contribute an enthalpic stabilization to intra-protein hydrogen bonds and disfavors peptide to catalyst complexation in hydrogen exchange reactions and peptide to peptide H-bonding in the helical main chain conformation but not in β-strands (Kim et al, 1993). The newly formed H-bonding result in the C-N bond assuming partial double bond character due to a flow of electrons from the C=O to the C-N bond which decreases the intensity of the original vibrations (Chirgadze et al, 1975). It seems that the H-bonding affects more of the original bonding in α- helix than in β-sheets depending on the accessibility of the solvent and on propensities of α- helix and β-sheets of the HSA (Parker, 1983). The hydrogen bonds in α- helix are formed inside the helix and parallel to the helix axis, while for β-sheet the hydrogen bonds take position in the planes of β-sheets as the preferred orientations especially in the anti-parallel sheets. The restrictions on the formation of hydrogen bonds in β-sheet relative to the case in α- helix explains the larger effect on reducing the intensity percentage of α- helix to that of β-sheet (Holzbaur et al, 1996; Zhang et al, 1999).

Pentobarbital and propofol complexes mainly induce changes in protein conformation of HSA from α-helix to β- turn, which indicates a partial unfolding of the HSA molecular upon pentobarbital and propofol interaction. The HSA–pentobarbital interaction was the strongest among the two drugs, since the pentobarbital binding to HSA is greater than propofol binding

to HSA. Depending on the chemical structures of the two drugs; there are more side interactions in presence of pentobarbital (Heterocyclic aromatic side and three different locations of carbonyl group) to interact with HSA, while in the presence of propofol there is one side group (hydroxyl group) that has the ability to interact with the HSA protein. Therefore, the binding constant of pentobarbital with HSA is greater than the binding constant of propofol with HSA molecule. Hence from my study, I can say that the pentobarbital binds with HSA more strongly than propofol, so it has the more deposition time in human plasma to release its function (Zhang et al, 1999). And propofol has a faster sedation than pentobarbital.
The obtained results of pentobarbital and propofol in our study are similar to those previously reported (Pershad et al, 2007) they showed that propofol offered significantly shorter sedation induction time, recovery time, total sedation time, time to return to baseline functional status, and permits faster onset recovery than pentobarbital with comparable efficacy for sedation (Bassett et al, 2003).

Chapter Five

Conclusions and Future work

Chapter Five

Conclusions and Future work

5.1 Conclusions

Pentobarbital and propofol are anesthetic drugs and their interaction with serum albumin is of prime significance. I have studied the interaction of anesthetic drugs pentobarbital and propofol with HSA using UV-absorption spectroscopy, fluorescence spectroscopy and by FTIR spectroscopy. I have determined the binding parameters for the binding of pentobarbital or propofol with HSA: For HSA-pentobarbital and HSA-propofol complexes, the binding constants by using UV-absorption spectroscopy are estimated to be K= 1.812×10^{4} M^{-1}, $2.55x10^{3}$ M^{-1} respectively, also the obtained values of K by using fluorescence spectroscopy are $1.809x0^{4}$ M^{-1}, and $2.55x10^{3}$ M^{-1} respectively, which agree well with the value obtained earlier by UV spectroscopy. In addition, the values of Stern–Volmer quenching constants and quenching rate constants for both pentobarbital and propofol are estimated to be ($3.875x10^{7}$ L mol^{-1}, 3.875x 10^{15} L $mol^{-1}s^{-1}$), and ($9.686x10^{6}$ L mol^{-1}, $9.686x10^{14}$ L $mol^{-1}s^{-1}$) respectively.

These experimental results confirm that the dynamic process is not the main mechanism which causes the fluorescence quenching, and the decrease in fluorescence intensity can be considered as a result of static quenching, which is indicative of a complex formation between the protein and the drug molecule. Also the lower value of binding constant between the drug and HSA is due to the effective hydrogen bonding between drugs (pentobarbital and propofol) and HSA.

Analysis of the FTIR spectra reveals that HSA–pentobarbital and HSA-propofol interactions induce intensity reduction in the absorption bands of α-helix and β-sheets components with different proportionality due to the different accessibility of H-bond formation in these components. This means that the drug–HSA combination caused the rearrangement of the

protein polypeptide chain and changes of the protein's secondary structure. We inferred that the binding forces that involve in the binding process besides hydrophobic interaction are electrostatic attraction and hydrogen bonding.

The conclusion can be drawn that the (carbonyl groups and N-H groups) and the hydroxyl group which are substituted on aromatic ring of pentobarbital and propofol respectively play an important role for reduction of percentage content of α-helix structure in drug–HSA interaction. When pentobarbital and propofol interact with hydrophobic pockets of HSA, their carbonyl groups and hydroxyl group can interact with the C=O and C–N groups in the protein polypeptides chain forming hydrogen bonding. The interactions caused the rearrangement of the polypeptide carbonyl hydrogen bonding network, then the reduction of HSA α-helix structure.

Drug interactions will in most cases significantly affect the apparent distribution volume of the drugs and also affect the elimination rate and determine the therapeutic affectivity of drugs. These experimental data may be a useful guide for pentobarbital and propofol efficient drug design, and provide some important data for clinical study of these two drugs.

5.2 Future work

The binding study of pentobarbital or propofol with HSA is of great importance in pharmacology and biochemistry. Our research can supply some important information to clinical research and provide the theoretical basis for the new drug design. Therefore, this research needs further studies to be a useful guide for synthesis of efficient pentobarbital and propofol drugs such as the determinations of binding sites, binding location, and thermodynamic parameters (enthalpy, free energy, entropy) at different temperatures to deduce the type of the acting force for the binding reaction between pentobarbital or propofol and HSA.

Furthermore, effects of ions on the binding constants need to be investigated, because the existence of metal ions can directly influence the binding force of drug with protein, thus affecting the storage time of the drug in blood plasma and enhancing the maximum effectiveness of the drug.

References

Ahmed Quamour, A., et al. (2004). Biopolymers, 73, p503.

Bryson, H. M., Fulton, B. R., Faulds, D. (1995). Drugs, 50, p513.

Bhattacharya, A., Gruene, T., Curry, S. (2000). Journal of Molecular Biology. 303, p721.

Bertucci, C., Ascoli, G., Barretta, G. U., Bari, L. D., Salvadori, P. (1995). Journal of Pharmaceutical and Biomedical Analysis, 13, p1087.

Bellamy, L. J. (1954). The Infrared Spectra of Complex Molecules. Methuen, London.

Britlain, E. F. H., George, W. O., Wells, C. H. J. (1970): Introduction to Molecular Spectroscopy, Academic Press, London.

Barrow. G. M. (1962): Introduction to Molecular Spectroscopy, McGraw-Hill, New York.

Blitz, J. P. and Augustine, S. M. (1994). Spectroscopy, 9, p28.

Bellamy, L. J. (1975): The Infrared Spectra of Complex Molecules, 3rd ed., John Wiley, New York.

Berlman, I.B. (1971). Handbook of fluorescence spectra of aromatic molecules, 2nd ed. Academic Press, New York.

Byler, D.M. and Susi, H. (1986). Biopolymers 25, p469.

Bell, R. J. (1972): Introduction Fourier Transform Spectroscopy. Academic Press, New York.

Bhattacharya, A. A. Curry, S., Franks, N. P. (2000). Journal of Biological Chemistry, 275, 49, p38738.

Bramanti, E. and Benedetti, E. (1996). Biopolymers 38, p639.

Byler, D. M., Brouilette, J. N., Susi, H. (1986). Spectroscopy 1, p39.

Beauchemin, R., et al. (2007). Biomacromolecules 8, p3177.

Bai, Y. and Englander, S. W. (1994). Proteins 18, p262.

Bassett, K. E, Anderson, J. L., Pribble, C. G, Guenther, E. (2003). Journal Annals of Emergency Medicine, 42, p773.

Curry, S., Mandelkow, H., Brick, P., Franks, N. (1998). Natural Structural Biology, 5, p827.

Curry, S., Brick P., Franks, N. P. (1999). Biochimica et Biophysica Acta, 1441, p131.

Cui, F. L., Fan, J., Li, J. P., Hu, Z. D. (2004). Bioorganic and Medicinal Chemistry, 12, p151.

Cui, F. L., et al. (2006). Biopolymers 83, p170.

Cui, F. L., Wang, J. L., Cui, Y. R., Li, J. P. (2006). Analytica Chimica Acta, 571, p175.

Coblentz, W. W. (1951): From the Life of a Researcher, Philosophical Library, New York.

Chang, R. (1971): Basic Principles of Spectroscopy, McGraw-Hill, New York.

Colthrup, N., Daly, L. Wiberley, S. (1990): Introduction to Infrared and Raman pectroscopy. 3rd ed. Academic Press, New York.

Clark, B. G., Frost, T., Russell, M. A. (1993): UV Spectroscopy: techniques, nstrumentation, data handing. 1st ed., Chapman Hall, London.

Chen, G. Z., Huang, X. Z., Xu, J. G., Zheng, Z. Z., Wang, Z. B. (1990): Method of Fluorescence Analysis, Science Press, Beijing.

Chirgadze, Y. N., Fedorov, O. V., Trushina, N. P. (1975). Biopolymers 14, p679.

Cai, S. W. and Snghl, B. R. (1999). Biophysical Chemistry 80, p7.

Deepa, S. and Mishra, A. K. (2005). Journal of Pharmaceutical and Biomedical Analysis, 38, p556.

Duxbury, G. (1999): Infrared Vibration–Rotation Spectroscopy, John Wiley, Chichester.

Donald P. (2001): Introduction to spectroscopy. 4th ed. Cengage learning. USA.

Dukor, R. K., Chalmers, J. M., Griffiths, P. R. (Eds). (2001): Vibrational Spectroscopy in the Detection of Cancer, in Handbook of Vibrational Spectroscopy, vol. 5, John Wiley and Sons, Chichester.

Donald, C. (2003): Essentials of pharmaceutical chemistry, 3rd ed., Pharmaceutical Press, London.

Deleris, G. and Petibios, C. (2003). Vibrational Spectroscopy, 32, p129.

Edward M, G., Maged, S. M., Michael, J. M (1995): Clinical anaesthesiology, 4th ed.Mc Graw Hill, US.

Elliott, A. and Ambrose. E. (1950). Nature 165, p921.

Erik, G., Jean-Marie, R., Vincent, R. (2006). Biophysical Journal, 90, p2946.

Fu, F. N., DeOliveira, D. B., Trumble, W. R., Sarkar, H. K., Singh, P. R. (1994). Applied Spectroscopy, 48, p1432.

Fabian, H. et al. (1994). Biochemistry 33, p10725.

Fang-Ying, W., Zhao-Jun, J, Yu-Mei, W., Xiao-Fen, W. (2006). Chemical Physics Letters 424, p387.

Ferraro, J, R. And Basilo, L. J. (1979): Fourier Transform Infrared Spectroscopy. Applications to Chemical Systems, Academic Press, New York.

Filyasova, A. I., Kudelina, I. A., Feofanov, A. V. (2001). Journal of Molecular Structure, 173, p565.

Fulton, B. and Sorkin, E.M. (1995). Drugs. 50, p636.

Goormaghtigh, E., Raussens, V., Ruysschaert, J. M. (1999). Biochimica et Biophysica Acta 1422, p105.

Ganim, Z. and Tokmakoff, A. (2006). Biophysical Journal, 91, p2636.

Gao, T., Ci, Y. X., Jian, H. Y., An, C. (2000). Vibrational Spectroscopy 24, p225.

Gerbanowski, A. Malabat, C. Rabiller, C. Gueguen, J. (1999). Journal of Agricultural and Food Chemistry, 47, p5218.

Griffiths, P. R. and Hareth, J. D. (1986): Fourier Transform Infrared Spectroscopy, Wiley, New York.

Gans, P. (1971): Vibrational Molecules: an Introduction to the Interpretation of Infrared and Raman Spectra, Chapman and Hall, London.

Gordon, G. H. (2005): Spectroscopy for the biological Sciences. John Wiley & Sons. Canada.

Holzbaur, I. E., English, A. M., Ismail, A. A. (1996). Biochemistry 35, p5488.

Houck, M. S. (2006): Fundamentals of forensic science, Elsevier Academic Press, Burlington, MA.

Herzberg, G. (1989): Molecular Spectra and Molecular Structure I. Spectra of Diatomic Molecules, 2nd ed., Krieger, Florida.

Herzberg, G. (1991): Molecular Spectra and Molecular Structure.II. Infrared and Raman Spectra of Polyatomic Molecules, Krieger, Florida.

Herschel, F. W. (1800). Philos. Trans. R. Soc. London.

Howarth, O. (1973): Theory of Spectroscopy, Thomas Nelson and Sons, London.

Herzberg, G. (1945): Infrared and Raman Spectra of Polyatomic Molecules, Van Nostrand Reinhold, New York.

He, W. Y., Li, Y., Tian, J. N., Liu, H. X., Hu, Z. D., Chen, X. G. (2005). Journal of Photochemistry and Photobiology A: Chemistry, 174, p53.

Herve, F., Urien, S., Albengres, E., Duche, J.C., Tillement, J. (1994). Clinical Pharmacokinetics, 26, p44.

Hannallah, R.S. et al. (1991). Anesthesiology,74, p217.

Hetzer, B. E., and Krekow, L. K. (1999). Neurotoxicol Teratol, 21, p181.

Hodes, J. E., Soncrant, T. T., Larson, D. M., Carlson, S. G., Rapoport,S. I. (1985). Anesthesiology 63, p633.

Il'ichev, Y. V., Perry, J. L., Simon, J. D. (2002). Journal of Physical Chemistry B, 106, p460.

Ivanov, A. I. et al. (1994). Journal of Applied Spectroscopy, 60, p305.

Jiang, C. Q., Gao, M. X., Meng, X. Z.(2003). Spectrochimica Acta Part A: Molecular and Biomolecular Spectroscopy, 59, p1605.

Jones, R. N. and Sandorfy, C. (1956): The application of Infrared and Raman Spectrometry to the Elucidation of Molecular Structure. In: W. West, (Ed.) Chemical Applications of Spectroscopy. Interscience, New York.

Jackson, M. and Mantsch, H. H. (1991). Journal of Biological Chemistry, 69, p639.

Jiang, M., Xie, M. X., Zheng, D., Liu, Y., Li, X. Y., Chen, X. (2004). Journal of Molecular Structure, p692.

Kragh-Hansen, U. (1981). Pharmacological Reviews, 33, p17.

Kragh-Hansen, U., Chuang, V.T.G., Otagiri, M. (2002). Biological and Pharmaceutical Bulletin, 25, 695.

Krishnakumar, S. S. and Panda, D. (2002). Biochemistry 41**,** p7443.

Kragh-Hansen, U. (1990). Danish Medical Bulletin, 37, p57.

Kandagal, P. B. et al. (2006). Journal of Pharmaceutical and Biomedical Analysis, 41, p393.

Krimm, S., Bandekar, J. (1986). Advances in Protein Chemistry, 38, p181.

Kalsi. P. S. (2004): Spectroscopy of Organic Compounds. 6th ed. New Age International (P) Ltd., New Delhi.

Kim, C. A. and Berg, J. M. (1993). Nature 362, p267.

Klotz, M. I. And Hunston, L. D. (1971). Biochemistry 10, 3065.

Kendrew, J. C. et al. (1958). Nature 18, 662-666.

Kauppinnen, J. K., Moffatt, D. J., Mantsch, H. H., Cameron, D. G. (1981). Applied Spectroscopy, 18, p35.

Klotz, M. I. (1982). Science 217, p1247.

Leslie, S. and Richard, D. (1993): The Focal encyclopaedia of photography. 3rd ed, Elsevier group.

Lakowicz, J. R. (2006): Principles of Fluorescence Spectroscopy, 3rd ed., Springer science. Maryland, USA.

Lakowicz, J. R. (1991): Topics in Fluorescence Spectroscopy: Principles, Plenum Press. New York.

Lakowicz, J. R. and Weber, G. (1973). Biochemistry, 12, p4161.

Lehninger, A.L. (1975): Biochemistry, 2ed ed., Worth Publishers, New York.

Mandsager, R. E., Clarke, C. R., Shawley, R. V., Hague, C. M. (1995). American Journal of Veterinary Research, 56, p95.

Mansel Davies, M. (Ed). (1963): Infra-Red Spectroscopy and Molecular Structure. An outline of the principles. Elsevier, New York.

Michael Hollas. J. (2004): MODERN SPECTROSCOPY. 4th Ed. *John* Wiley & Sons, Chichester, England.

Muñoz-Cuevas, J., Cruz-Paz, M., Olivero-Vásquez, Y. (2005). Revista Mexicana Anestesia, 28, p148.

Matsuura, H., Hasegawa, K., Miyazawa, T. (1986). Spectrochim. Acta A 42, p1181.

Moreno, F., Jose, J. G.(1999). Chemico-Biological Interactions 121, p237.

Neault, J. F., Benkirane, A., Malonga, H., Tajmir-Riahi, H. A. (2001). Journal of Inorganic Biochemistry 86, p603.

Nahar, S., Carpentier, R., Tajmir-Riahi, H. A. (2001). J. Inorg. Biochem. 65, p245.

Nakanishi, K. and Solomon, P. H. (1977): Infrared Spectroscopy, Holden-Day, San Francisco.

Oettl, K. and Stauber, R. E. (2007). British Journal of Pharmacology, 151, p580.

Oberg, K. A., Ruysschaert, J. M., Goormaghtigh, E. (2004). Eur. J. Biochem., 271, p2937.

Olinger J. M., Hill, D. M., Jakobsen, R. J., Brody, R. S. (1986). Biochim. Biophys. Acta 869, p89.

Owen, T. Fundamentals of modern UV-visible spectroscopy, Primer, Agilent Technologies.

Purcell, M., Neault, J. F., Tajmir-Riahi, H. A. (2000). Biochim. Biophys. Acta., 1478, p61.

Parker, S. F. (1983): Applications of infrared, raman, and resonance raman spectroscopy in biochemistry, Plenum Press, New York.

Pershad, J., Wan, J., Doralina, L. (2007). Pediatrics, 120, p629.

Pershad, J., Gilmore, B. (2006). Pediatrics,117, p413.

Padrid, P. (2000). Vet Clin North Am, 30, p1390.

Peters, T. (1995): All about albumin, Academic Press, San Diego.

Peter, R. Griffiths, A., James, A. (2007): Fourier Transform Infrared Spectrometry, 2nd ed., John Wiley & Sons.

Ruhl, T. et al. (2003). Bioorg. Med. Chem. 11, p2965.

Robinson, J. W., Skelly, E. M., Frame, G. M. (2005): Undergraduate Instrumental Analysis. 6th ed. Marcel Dekker New York.

Richardson, J. S. (1981). Adv. Protein Chem., 34, p167.

Rahmelow, K. and Hubner, W. (1996). Anal. Biochem., 241, p5.

Reves, J.G. and Lubarsky, D.A. (2000): Nonbarbiturate intravenous anesthetics. In: R. Miller (Ed). Anesthesia. (251-254). 5th ed., Churchill Livingstone, Philadelphia, PA.

Smith, I., White P. F., Nathanson, M., Gouldson, R. (1994). Anesthesiology, 81, p1005.

Schuttler, J.,and Ihmsen, H. (2000). Anesthesia, 92, p727.

Schaller, J., Gerber, S., Kämpfer, U., Lejon, S., Trachsel, C. (2008): Human Blood Plasma Proteins: Structure and Function, John Wiley & Sons,

Sudlow, G., Birkett, D. J., Wade, D. N. (1975). Mol Pharmacol 11, p824.

Shin-ichi, F., Takashi, A. (2008). Biophys J, 94, p95.

Simard, J. R., Zunszain, P. A., Hamilton, J. A., Curry, S. (2006): Location of High and Low Affinity Fatty Acid Binding Sites on Human Serum Albumin Revealed by NMR Drug-competition , J. Mol. Biol. 361, 336-351.

Susi, H. and Byler, D. M. (1983). Biophys Biochem Res Com 115, p391.

Sathyanarayana. D. N. (1004): Vibrational spectroscopy :Theory and applications. 1st ed., New Age International (P) Ltd., New Delhi.

Schermann, J. (2008): Spectroscopy and modelling of biomolecular building bloks. 1st ed., Elsevier, UK.

Siebert, F. and Hildebrandt, P. (2008): Vibrational Spectroscopy in Life Science. WILEY-VCH Verlag GmbH & Co. KGaA, Weinheim, Germany.

Shaw, T. I., et al. (1993). Spectroscopy, 8, p45.

Szudy, J. (Ed). (1998):, Uniwersytet Mikolaja Kopernika, Torun, Poland.8. Acta Physica Polonica. 1978. Polska Akademia Nauk Instytut Fizyki. Europhys J, Vol.A65(6).

Stokes, G.G. (1852). Phil Trans R Soc. 142, p463.

Surewicz, W.K. and Mantsch, H.H. (1988). Biochim. Biophys. Acta 952, p115.

Surewicz, W. K., Mantsch, H. H., Chapman, D. (1993). Biochemistry 32, p389.

Stephanos, J. J.(1996). Inorg. Biochem., 62, p155.

Sulkowaska, A. (2002). J. Mol. Strurct., 614, p227.

Stephanos, J. farina, S., Addison. A.(1996). Biochemica. Biophysica. Acta., 1295, p209.

Sirotkin, V. A., Zinatullin, A. N., Solomonov, B. N., Faizullin, D. A., Fedotov, V. D. (2001). Biochimica et Biophysica Acta 1547, p359.

Spectroscopic Software Reference Manual. BRUKER OPTIK GmbH, Rudolf-Plank 2004 Ettlingen.

Surewicz, W. K., Mantsch, H. H., Chapman, D. (1993). Biochemistry 32, p389.

Theophanides, T. (Ed.) (1984): FT-IR Spectroscopy: Industrial Chemical and Biochemical Applications. Netherlands: Reidel, Dordrecht.

Tian, J. N., Liu, J. Q., Zhang, J. Y., Hu, Z. D., Chen, X. G.(2003). Chem. Pharm. Bull., 51, p579.

Tuan, V., Chuang, G., Otagiri, M. (2001). Biochimica et Biophysica Acta, 1546, p337.

Upton, R.N., Ludrook, G.I., Grant, C. (1999). Anesthesia Analgesia, 89, p545.

Uversky, V. N. and. Permyakov. E. A. (2007): Vibrational Spectroscopy: Methods in Protein Structure and Stability Analysis. Nova Science, New York.

Ulrich, K. H. Hiroshi, W., Keisuke, N. Yasunori, I., Masaki, O. (2006). J. Mol. Biol. 363, p702.

Whitlock F.A. (1975). Med J Aust 1, 24, p737.

Wright, M. (1982). Journal of the American Veterinary Medical Association,180, p1462.

Whiffen, D. H. (1972): Spectroscopy, 2nd, ongmans, London.

Wetlaufer, D. (1962). Adv. Protein Chem. 17, p303.

Workman, J. R. (1998): Applied Spectroscopy: Optical Spectrometers. Academic Press.

Wang, T., Xiang, B., Wang, Y., Chen, C., Dong, Y., Fang, H., Wang, M. (2008). Colloids Surf. B 65, p113.

Xie, M. X., Xu, X. Y., Wang, Y. D. (2005). Biochim. Biophys. Acta 1724, p215.

Yamamoto, T. and Tasumi, M. (1991). J. Mol. Struct. 242, p235.

Zsila, F., Bik´adi, Z., Simonyi, M. (2003). Biochem. Pharmacol. 65, p447.

Zhao, B. Z., Song, L. M., Liu, X., Xie, J., Zhao, J. Q. (2006). Bioorg. Med. Chem. 14, p2428.

Zhang, W. S., Li, A. L. (1999): Medical Chemistry, Higher Education Press.

الملخص

تم دراسة التفاعل بين كل من الأدوية المخدرة (بنتوباربيتال و البروبوفول) مع بروتين الدم البشري (Human Serum Albumin) باستخدام جهاز مطياف الأشعة فوق البنفسجية (UV-visible spectroscopy) ، جهاز انبعاث الاشعاع (Fluorescence spectroscopy) وجهاز مطياف تحويل فوريير للأشعة تحت الحمراء (Fourier transform Infrared spectroscopy) حيث تم حساب ثابت الترابط (binding constant) للبنتوباربيتال والبروبوفول عن طريف جهاز مطياف الأشعة فوق البنفسجية وجهاز مطياف انبعاث الاشعاع عند درجة حرارة (293K) والقيم هي ($1.812x10^4$ M^{-1}) للبنتوباربيتال و ($2.55x10^3$ M^{-1}) للبروبوفول. بالإضافة الى ذلك تم حساب ثابت (Sten-Volmer constant) وهي للبنتوباربيتال ($3.875x10^7$ L mol^{-1}) و ($9.686x10^6$ L mol^{-1}) للبروبوفول.

ومن النتائج التي تم التوصل اليها هي أن شدة امتصاص الإشعة فوق البنفسجية (Maximum Intensity) لبروتين الدم مع الأدوية المخدرة (البنتوباربيتال واليروبوفول) تزداد بزيادة تركيز هذه المواد مع بقاء تركيز البروتين ثابت.

ومن خلال استخدام جهاز إنبعاث الإشعاع وجد أن النتائج تكشف عن انخفاض شدة (Intensity) الإشعاع المنبعث جراء تفاعل كل من البنتوباربيتال والبروبوفول من بروتين الدم (HSA) مع زيادة تركيز الدوائين وبقاء تركيز البروتين ثابت. حيث أن هذا الإنخفاض في شدة الإشعاع المنبعث يشير الى أن كل من البنتوباربيتال والبروبوفول لديها قدرة قوية على خفض أو التقليل من الإشعاع المنبعث ذاتياً من البروتين (HSA) من خلال الية (Static quenching).

بإستخدام جهاز مطياف تحويل فوريير للأشعة تحت الحمراء (FTIR) مع تطبيق عدد من التقنيات الموجود في هذا الجهاز مثل تقنية (Fourier-self deconvolution) و (Second derivative resolution) بالإضافة الى تقنية (Curve fitting procedure) تم تحليل منطقة الأميد الاول والأميد الثاني والأميد الثالث الموجودة في بروتين الدم (HSA) من أجل تحديد بنية البروتين الثانوية (Secondary structure) والية ارتباط الأدوية المخدرة معه حيث أن

جميع مواقع القمم (Peaks) تم تحديدها في مناطق الاميد الثلاث، بالإضافة الى تحديد وتفسير التغيرات في مواقع القمم (Peaks) نتيجة تغيير تركيز الأدوية المضافة.

يشير الطيف المقاس بواسطة جهاز (FTIR) الى تغيير في شدة حزم الامتصاص (Absorption bands) نتيجة تغيير في تركيز الأدوية المضافة (البنتوباربيتال والبروبوفول). إضافة الى ذلك ظهر من خلال هذه النتائج أن هناك انخفاض أكبر في شدة حزم الإمتصاص التابعة ل (α-helix) بالمقارنة مع حزم الامتصاص التابعة (β-sheets).

هذا التباين والإختلاف في الشدة (The intensity) يرجع على تكوين الروابط الهيدروجينية (H-bonding) في الجزيئات المعقدة، وهو ما يفسر الميول الذاتي لكل من (α-helix) و (β-sheets) لتكوين هذه الروابط.

من خلال هذا البحث وجد أن (مجموعات الكاربونيل (C=O) ومجموعات الامين(N-H)) و (مجموعات الهيدروكسيل (-OH)) الموجود في البناء الجزيئي لكل من البنتوباربيتال والبروبوفول على التوالي تلعب دوراً هاماً في تغيير البنية الثانوية (Secondary structure) للبروتين (HSA) عند ارتباطها معه. ويدعم هذا التحليل تلك النتائج التي تم التوصل اليها حيث أن الانخفاض في قيمة ثابت الترابط (binding constant) للبروبوفول بالمقارنة من البنتوباربيتال يشير الى أن البروبوفول يعطي تخدير في وقت أقل من البنتوباربيتال وهذا يتفق مع كل ما تم التوصل اليه مسبقاً.